

COMPUTATIONAL MODELLING AND ENTROPY GENERATION ANALYSIS OF NANOFLUIDS IN A CHANNEL

Michael H. Mkwizu

**FOR REFERENCE
ONLY**

**A Dissertation Submitted in Partial Fulfilment of the Requirements for the Degree of
Doctor of Philosophy in Mathematical and Computer Sciences and Engineering of the
Nelson Mandela African Institution of Science and Technology**



Arusha, Tanzania

April, 2016



ABSTRACT

Nanofluid is a fluid containing nanometre- sized particles, called nanoparticles. These fluids are engineered colloidal suspension nanoparticles in a based fluid. The commonly used fluids are water, ethylene, oil and lubricant. Entropy is an extensive thermodynamic property that is the measure of a system's thermal energy per unit temperature that is unavailable for doing useful work. That is it destroys the available energy in any flow process and thermal system.

This study consists of six chapters. Chapter one is an introduction, in this chapter useful terms have been defined, objectives of the study, statement of the problem, significance of the study were stated. The method used for analysis in all chapters is a semi discretization finite difference method together with Runge-Kutta Fehlberg integration scheme. The nanoparticles used was Copper (Cu) and Alumina (Al_2O_3).

In chapter two, the analysis of the entropy generation in a variable viscosity channel flow of nanofluids with convective cooling was numerically investigated. The results revealed that Entropy generation rate generally increases with time t , Eckert number Ec , viscosity variation parameter β , pressure gradient A , thermophoresis parameter Nt . Increase in Biot Bi increase entropy generation at the walls but decreases entropy generation within the channel. The paper was prepared and published in Comptes Rendus Mecanique.

In chapter three, the combined effect of buoyancy force and convective cooling on the unsteady flow, heat transfer and entropy generation rate in water based nanofluids was investigated. Al_2O_3 -water nanofluid observed to produces higher entropy than Cu-water nanofluid. Fluid friction irreversibility dominants the channel centreline region while the effects of heat transfer irreversibility near the walls increases with Grashof number Gr , Ec , A , but decreases with nanoparticles volume fraction ϕ and Bi . Prepared paper was published in applied and computational mathematics journal.

In chapter four, the flow structure, heat transfer and entropy generation in unsteady generalized Couette flow of a water-based nanofluid with convective cooling was numerically investigated. It was found that the entropy generation increases with ϕ and Ec , it decreases with A . With an increase in Bi the entropy generation rate decreases and reverse its behaviour near the upper wall. The Bejan number increases with an increase in ϕ .

One paper from this chapter was prepared and published in Sadhana - Academy Proceedings in Engineering Science.

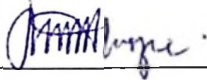
In chapter five, computational model and thermodynamic analysis of the effects of Navier slip and wall permeability on entropy generation in unsteady generalized Couette flow was investigated. An increase in an entropy generation rate was observed with an increase in ϕ and slip parameter f , the paper was published at University Politehnica of Bucharest (U.P.B) Scientific Bulletin, Series D. Chapter six consist of general discussion, conclusion, recommendation and future work.

General observation was that entropy can be reduced by mixture of nanoparticles and base fluid with careful combination of parameters controlling the flow and geometry in consideration. Alumina- water nanofluid produces more entropy compared to Copper- water nanofluid.

DECLARATION

I, **MICHAEL H. MKWIZU** do hereby declare to the Senate of Nelson Mandela African Institution of Science and Technology that this dissertation is my own original work and that it has neither been submitted nor being concurrently submitted for degree award in any other institution.

Michael H. Mkwizu



Name and signature of candidate

13th April 2016

Date

The above declaration is confirmed

Prof. Oluwole D. Makinde



Name and signature of supervisor 1

14th April 2016

Date

Dr. Yaw Nkansah-Gyekye



Name and signature of supervisor 2

14th April 2016

Date

COPYRIGHT

This dissertation is copyright material protected under the Berne Convention, the Copyright Act of 1999 and other international and national enactments, in that behalf, on intellectual property. It must not be reproduced by any means, in full or in part, except for short extracts in fair dealing; for researcher private study, critical scholarly review or discourse with an acknowledgement, without the written permission of the office of Deputy Vice Chancellor for Academics, Research and Innovations, on behalf of both the author and the Nelson Mandela African Institution of Science and Technology.

CERTIFICATION

The undersigned certify that have read and found the dissertation acceptable by the Nelson Mandela African Institution of Science and Technology.

Prof. Oluwole D. Makinde



Name and signature of supervisor 1

14th April 2016

Date

Dr. Yaw Nkansah-Gyekye



Name and signature of supervisor 2

14th April 2016

Date

ACKNOWLEDGEMENT

I would like to thank the Almighty God since is the source of my strength, faith and health that enabled me to complete this study successfully. My deepest thanks go to my research supervisors Prof. O. D. Makinde and Dr Yaw Nkansah-Gyekye for providing me valuable guidance, without which this research would not have been a success.

Special thanks to the Nelson Mandela African Institution of Science and Technology for offering me a scholarship and Sokoine University of Agriculture for granting me a three years study leave.

I would like to express my deep appreciation to my family for their support in prayers, love and encouragement during all the time of my studies.

Finally, I express my warm appreciation to everybody who has contributed in one way or the other towards the success of this work. I know they are many, this makes difficult to mention one after the other.

DEDICATION

This research work is dedicated to my lovely wife Anna, my children Alexander, Tajiel, Yoeza and Japhety. Furthermore, it is dedicated to my parents Yoeza Mkwizu, Catherine and Ernestina and all my family. All together was the source of happiness during challenges in my study life.

TABLE OF CONTENTS

ABSTRACT.....	ii
DECLARATION.....	iv
COPYRIGHT.....	v
CERTIFICATION.....	vi
ACKNOWLEDGEMENT.....	vii
DEDICATION.....	viii
TABLE OF CONTENTS	ix
LIST OF TABLES.....	xii
LIST OF FIGURES	xiii
LIST OF APPENDICES.....	xviii
LIST OF ABBREVIATIONS AND SYMBOLS.....	xix
CHAPTER ONE	1
General Introduction and Background.....	1
Introduction	1
1.1 Background Information	1
1.1.1 Channel flow.....	1
1.1.2 Nanofluid	2
1.1.3 Entropy	3
1.1.4. Engineering and industrial applications	5
1.1.5. Viscosity	5
1.1.6. Buoyancy	6
1.1.7. Governing equations.....	6
1.1.8. Mathematical methods.....	7
1.2 Statement of the Research Problem	7
1.4 Significance of the Study	8
1.5 Dissertation Outline.....	8

CHAPTER TWO	10
2.1 Introduction	10
2.2 Mathematical Model	12
2.3 Entropy Analysis	15
2.4 Numerical Procedure.....	16
2.5 Results and Discussion.....	17
2.5.1 Effects of parameter variation on velocity profiles	17
2.5.2 Effects of parameter variation of temperature profiles.....	19
2.5.3 Effects of parameter variation on nanoparticles concentration	21
2.5.4 Effects of parameter variation on skin friction and Nusselt number	24
2.5.5 Effects of parameter variation on entropy generation rate	26
2.5.6 Effects of parameter variation on Bejan number.....	29
2.6 Conclusions	32
CHAPTER THREE.....	34
3.1 Introduction	34
3.2 Mathematical Model	36
3.3 Entropy Analysis	39
3.4 Numerical Procedure.....	40
3.5 Results and Discussions	41
3.5.1 Effects of parameter variation on velocity profiles	41
3.5.2 Effects of parameter variation on temperature profiles	44
3.5.3 Skin friction and Nusselt number	47
3.5.4 Effects of parameter variation on entropy generation rate	50
3.5.5 Effects of parameter variation on Bejan number	52
3.6 Conclusions	55
CHAPTER FOUR.....	56
4.1 Introduction	56
4.2 Mathematical Model	59
4.3 Entropy Analysis	62
4.4 Numerical Procedure.....	63
4.5 Results and Discussions	63
4.5.1 Effects of parameter variation on velocity profiles	64

4.5.2	Effects of parameter variation on temperature profiles	67
4.5.3	Skin friction and Nusselt number	71
4.5.4	Effects of parameter variation on entropy generation rate	74
4.5.5	Effects of parameter variation on Bejan number	77
4.6	Conclusions	80
CHAPTER FIVE		81
5.1	Introduction	81
5.2	Mathematical Model	84
5.3	Entropy Analysis	87
5.4	Numerical Procedure.....	89
5.5	Results and Discussions	89
5.5.1	Effects of parameter variation on velocity profiles	90
5.5.2	Effects of parameter variation on temperature profiles	93
5.5.3	Skin friction and Nusselt number	96
5.5.4	Effects of parameter variation on entropy generation rate	98
5.5.5	Effects of parameter variation on Bejan number.....	100
5.6	Conclusion.....	103
CHAPTER SIX		105
6.1	General Discussion.....	105
6.2	Conclusion.....	105
6.3	Recommendations	108
REFERENCES.....		109
APPENDIX.....		114

LIST OF TABLES

Table 2.1: Computation showing the skin friction $Pr = 6.2$, $Sc = 1$	25
Table 3.1: Thermophysical properties of the fluid phase (water) and nanoparticles	38
Table 4.1: Thermophysical properties of the fluid phase (water) and nanoparticles	60
Table 5.1: Thermophysical properties of the fluid phase (water) and nanoparticles	86

LIST OF FIGURES

Figure 1.1: Couette flow	1
Figure 1.2: Poiseuille flow.....	2
Figure 1.3: Copper-Water nanofluid	3
Figure 1.4: Entropy increase with temperature.....	4
Figure 1.5: Engine cooling system	5
Figure 1.6: Heat exchange device.....	5
Figure 2.1: Schematic diagram of the problem under consideration	12
Figure 2.2: Velocity profiles across the channel with increasing time	18
Figure 2.3: Velocity profiles with increasing time	18
Figure 2.4: Velocity profiles with increasing Bi	18
Figure 2.5: Velocity profiles with increasing β	19
Figure 2.6: Velocity profiles with increasing Ec	19
Figure 2.7: Temperature profiles with increasing time.....	20
Figure 2.8: Temperature profiles with increasing time.....	20
Figure 2.9: Temperature profiles with increasing Bi	20
Figure 2.10: Temperature profiles with increasing β	21
Figure 2.11: Temperature profiles with increasing Ec	21
Figure 2.12: Nanoparticles distribution with increasing time.....	22
Figure 2.13: Nanoparticles distribution with increasing time.....	22
Figure 2.14: Nanoparticles distribution with increasing Bi	23
Figure 2.15: Nanoparticles distribution with increasing β	23
Figure 2.16: Nanoparticles distribution with increasing Ec	23
Figure 2.17: Nanoparticles distribution with increasing Nt	24
Figure 2.18: Nanoparticles distribution with increasing Nb	24
Figure 2.19: Nusselt number profiles	25

Figure 2.20: Entropy generation with increasing time	26
Figure 2.21: Entropy generation with increasing time	27
Figure 2.22: Entropy generation with increasing Bi	27
Figure 2.23: Entropy generation with increasing Ec	27
Figure 2.24: Entropy generation with increasing β	28
Figure 2.25: Entropy generation with increasing A	28
Figure 2.26: Entropy generation with increasing Nt	28
Figure 2.27: Bejan number with increasing time	29
Figure 2.28: Bejan number with increasing time	30
Figure 2.29: Bejan number with increasing Bi	30
Figure 2.30: Bejan number with increasing β	30
Figure 2.31: Bejan number with increasing Ec	31
Figure 2.32: Bejan number with increasing λ	31
Figure 2.33: Bejan number with increasing Nt	31
Figure 2.34: Bejan number with increasing A	32
Figure 2.35: Bejan number with increasing Nb	32
Figure 3.1: Schematic diagram of the problem under consideration	36
Figure 3.2: Nanofluids velocity profiles with increasing time	42
Figure 3.3: Nanofluids velocity profiles across the channel with increasing time	42
Figure 3.4: Nanofluid velocity profiles with increasing ϕ	43
Figure 3.5: Nanofluid velocity profiles with increasing Gr	43
Figure 3.6: Nanofluid velocity profiles with increasing Ec	43
Figure 3.7: Nanofluid velocity profiles with increasing A	44
Figure 3.8: Nanofluids temperature profiles with increasing time	45
Figure 3.9: Nanofluids temperature profiles across the channel with increasing time	45
Figure 3.10: Nanofluid temperature profiles with increasing ϕ	46
Figure 3.11: Nanofluid temperature profiles with increasing Bi	46

Figure 3.12: Nanofluid temperature profiles with increasing Gr.....	46
Figure 3.13: Nanofluid temperature profiles with increasing Ec.....	47
Figure 3.14: Nanofluid temperature profiles with increasing A	47
Figure 3.15: Skin friction with increasing ϕ	48
Figure 3.16: Skin friction with increasing Gr, Ec, Bi	49
Figure 3.17: Nusselt number with increasing ϕ	49
Figure 3.18: Nusselt number with increasing Gr, Ec, Bi	49
Figure 3.19: Entropy generation rate with increasing time	50
Figure 3.20: Entropy generation rate with increasing ϕ	51
Figure 3.21: Entropy generation rate with increasing Bi	51
Figure 3.22: Entropy generation rate with increasing Gr	51
Figure 3.23: Entropy generation rate with increasing Ec	52
Figure 3.24: Entropy generation rate with increasing A.....	52
Figure 3.25: Bejan number with increasing time.....	53
Figure 3.26: Bejan number with increasing ϕ	53
Figure 3.27: Bejan number with increasing Bi	54
Figure 3.28: Bejan number with increasing Gr.....	54
Figure 3.29: Bejan number with increasing Ec.....	54
Figure 3.30: Bejan number with increasing A	55
Figure 4.1: Schematic diagram of the problem under consideration	59
Figure 4.2: Nanofluids velocity profiles with increasing time	64
Figure 4.3: Nanofluids velocity profiles across the channel with increasing time	65
Figure 4.4: Nanofluid velocity profiles with increasing ϕ	65
Figure 4.5: Nanofluid velocity profiles with increasing A	66
Figure 4.6: Nanofluid velocity profiles with increasing Re.....	66
Figure 4.7: Nanofluids temperature profiles with increasing time	68
Figure 4.8: Nanofluids temperature profiles across the channel with increasing time	68

Figure 4.9: Nanofluid temperature profiles with increasing ϕ	69
Figure 4.10: Nanofluid temperature profiles with increasing Bi	69
Figure 4.11: Nanofluid temperature profiles with increasing Ec.....	70
Figure 4.12: Nanofluid temperature profiles with increasing A	70
Figure 4.13: Nanofluid temperature profiles with increasing Re	71
Figure 4.14: Skin friction with increasing ϕ	72
Figure 4.15: Skin friction with increasing ϕ , A and Re	72
Figure 4.16: Nusselt number with increasing ϕ	73
Figure 4.17: Nusselt number with increasing ϕ , A and Re.....	73
Figure 4.18: Entropy generation rate with increasing time	74
Figure 4.19: Entropy generation rate with increasing ϕ	75
Figure 4.20: Entropy generation rate with increasing Bi.....	75
Figure 4.21: Entropy generation rate with increasing Ec	76
Figure 4.22: Entropy generation rate with increasing A.....	76
Figure 4.23: Bejan number with increasing time.....	77
Figure 4.24: Bejan number with increasing ϕ	78
Figure 4.25: Bejan number with increasing Bi.....	78
Figure 4.26: Bejan number with increasing Ec.....	79
Figure 4.27: Bejan number with increasing A.....	79
Figure 5.1: Schematic diagram of the problem under consideration	84
Figure 5.2: Nanofluids velocity profiles with increasing time	90
Figure 5.3: Nanofluids velocity profiles across the channel with increasing time	91
Figure 5.4: Nanofluid velocity profiles with increasing ϕ	91
Figure 5.5: Nanofluid velocity profiles with increasing A	92
Figure 5.6: Nanofluid velocity profiles with increasing Re.....	92
Figure 5.7: Nanofluids temperature profiles with increasing time	93
Figure 5.8: Nanofluids temperature profiles across the channel with increasing time	94

Figure 5.9: Nanofluid temperature profiles with increasing ϕ	94
Figure 5.10: Nanofluid temperature profiles with increasing f	95
Figure 5.11: Nanofluid temperature profiles with increasing Bi	95
Figure 5.12: Nanofluid temperature profiles with increasing Ec	96
Figure 5.13: Skin friction with increasing ϕ , A , Re and f	97
Figure 5.14: Nusselt number with increasing ϕ , A , Re and f	97
Figure 5.15: Entropy generation rate with increasing time	98
Figure 5.16: Entropy generation rate with increasing ϕ	99
Figure 5.17: Entropy generation rate with increasing f	99
Figure 5.18: Entropy generation rate with increasing Bi	100
Figure 5.19: Bejan number with increasing time.....	101
Figure 5.20: Bejan number with increasing ϕ	101
Figure 5.21: Bejan number with increasing Bi	102
Figure 5.22: Bejan number with increasing Ec	102
Figure 5.23: Bejan number with increasing A	103

LIST OF APPENDICES

Matlab Codes.....	114
-------------------	-----

LIST OF ABBREVIATIONS AND SYMBOLS

D_B	Brownian diffusion coefficient
D_T	Thermophoretic diffusion coefficients
u	Nanofluid velocity in the x -direction
T	Temperature of the nanofluid
P	Nanofluid pressure
t	Time
T_a	Ambient temperature which also correspond to the nanofluid initial temperature
φ	Concentration of nanoparticles
τ	Ratio of solid particles heat capacitance to that of the nanofluid heat capacitance
Nb	Brownian motion parameter
Bi	Local Biot number
Nt	Thermophoresis parameter
Sc	Schmidt number
Pr	Prandtl number
Ec	Eckert number
Gr	Grashof number
Br	Brinkman number
Ns	Entropy generation
Be	Bejan number
A	Pressure gradient parameter
C_f	Skin friction coefficient
Nu	Local Nusselt number
ϕ	Nanoparticles volume fraction
ρ_f	Density of the fluid
μ_f	Viscosity of the fluid fraction
α_f	Thermal diffusivity of the fluid
ρ_s	Density of the nanoparticle
β_f	Thermal expansion coefficients of the base fluid
β_s	Thermal expansion coefficients of the nanoparticle
k_s	Thermal conductivity of the nanoparticles
k_f	Thermal conductivity of the fluid fraction

μ_{nf}	Dynamic viscosity of the nanofluid
k_{nf}	Nanofluid thermal conductivity
ρ_{nf}	Density of the nanofluid
β_{nf}	Volumetric expansion coefficient of the nanofluids
$(\rho c_p)_f$	Heat capacitance of the base fluid
$(\rho c_p)_s$	Heat capacitance of the nanoparticle
β	Coefficient of sliding friction and viscosity variation parameter
f	Slip parameter
τ_w	Wall shear stress
q_w	Heat flux at the channel walls
λ	Nanoparticles mass transfer parameter

CHAPTER ONE

General Introduction and Background

Introduction

This chapter describes the general introduction of the study. It mainly focuses on the background information of the study, the flow terminologies and governing mathematical equations have been defined. The statements of the research problem, objectives of the study, significance of the study, applications and dissertation outline are also stated.

1.1 Background Information

1.1.1 Channel flow

Couette flow is the laminar flow of a viscous fluid in the space between two parallel plates, one of which is moving relative to the other. The flow is driven by virtue of viscous drag force acting on the fluid and the applied pressure gradient parallel to the plates. Steady viscous fluid flow driven by an effective pressure gradient established between the two ends of a long straight pipe of uniform circular cross-section is generally known as Poiseuille flow.

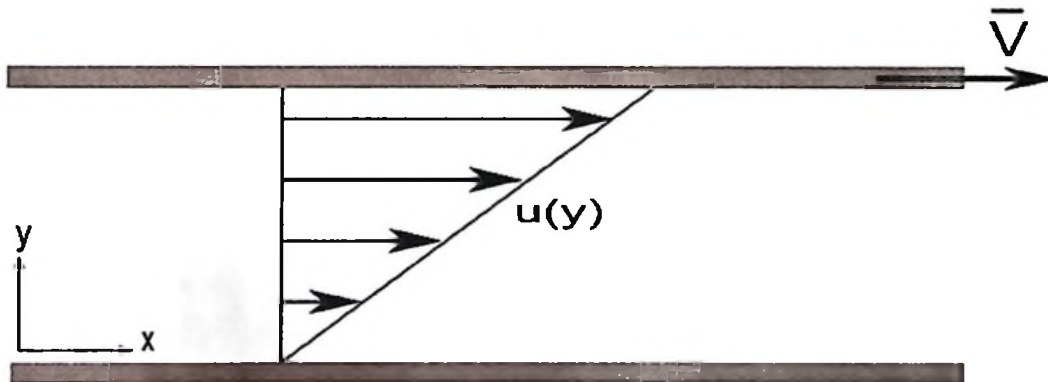


Figure 1.1: Couette flow: *Source; Department of Applied Mathematics
University of Waterloo*

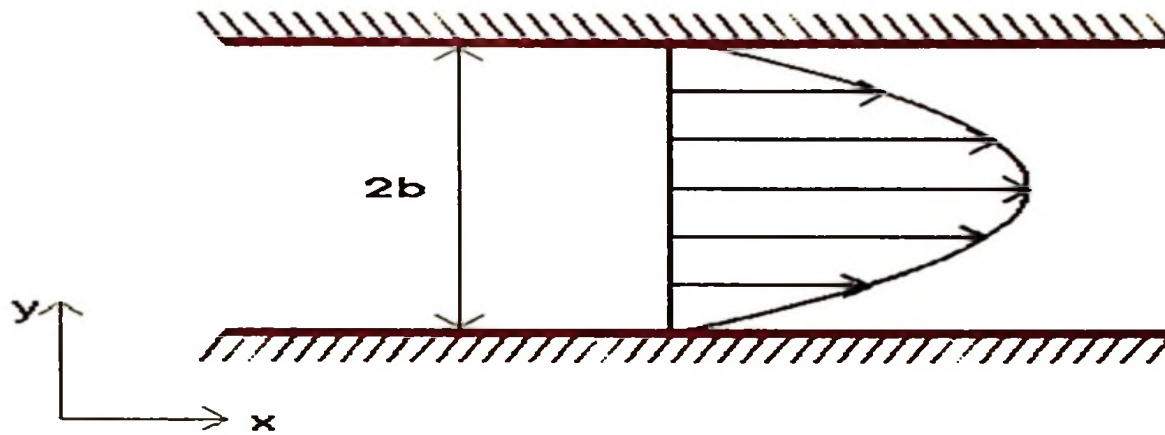


Figure 1.2: Poiseuille flow: *Source; Department of Applied Mathematics
University of Waterloo*

1.1.2 Nanofluid

Nanofluid is a fluid containing nanometre-sized particles, called nanoparticle. These fluids are engineered colloidal suspension nanoparticles in a based fluid. The commonly used fluids are water, ethylene, oil and lubricant. The terms nanofluid was first introduced by Choi (1995) who was working with the group at the Argonne National Laboratory (ANL), USA. Investigations have shown that nanofluids possess enhanced thermophysical properties such as thermal conductivity, thermal diffusivity, viscosity and convective heat transfer coefficients compared to those of base fluids like oil or water (Choi, 2009).

Examples of nanoparticle are pure metals (Au, Ag, Cu, and Fe), metal oxides (CuO , SiO_2 , Al_2O_3 , TiO_2 , ZnO , and Fe_3O_4), Carbides (SiC , TiC), Nitrides (AlN , SiN) and different types of carbon (diamond, graphite, single/multi wall carbon nanotubes) (Zhen-Hua Lui, and Yuan-Yang Li, 2012).

There are two techniques used in nanofluids production; the single-step method in which nanoparticles are evaporated directly into the base fluid and the two-step method in which nanoparticles are first prepared by either the inert gas-condensation technique or chemical vapor deposition method and then dispersed into the base fluid. See Figure 1.3 below of Cu-water nanofluid.

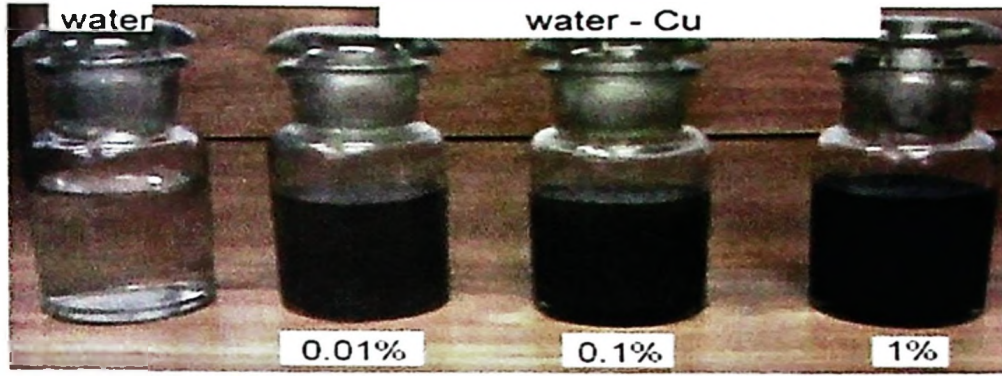


Figure 1.3: Copper-Water nanofluid: *Source; Krauthammer Lab 2008, Yale University*

1.1.3 Entropy

Entropy is a measure of how energy and other extensive quantities distribute within available constraints in a thermodynamic system. The entropy generation is always a positive quantity or zero (reversible process). Its value depends on the process, thus it is not a property of a system. That is it destroys the available energy in any flow process and thermal system. It has the dimension of energy divided by temperature which has a unit of Joules per Kelvin (J/K) in the International System of Units. As entropy-generation takes place the quality of energy decreases, so to preserve the quality of energy entropy generation in fluid flow should be reduced. According to Woods (1975), the local volumetric rate of entropy generation is given by

$$S'' = \frac{k_f}{T_a^2} \left(\frac{\partial T}{\partial y} \right)^2 + \frac{\mu_f(T)}{T_a} \left(\frac{\partial u}{\partial y} \right)^2 + \frac{D_B}{\phi_0} \left(\frac{\partial \phi}{\partial y} \right)^2 + \frac{D_B}{T_a} \frac{\partial T}{\partial y} \frac{\partial \phi}{\partial y} \quad (1.1)$$

The first term in Eq. (1.1) is the irreversibility due to heat transfer; the second term is the entropy generation due to viscous dissipation, while the third and the fourth terms are the local entropy generation due to nanoparticles mass transfer and complex interaction with the base fluid.

The study of laminar falling viscous incompressible liquid film along an inclined porous heated plate has many significant applications in thermal engineering and industries. Starting from petroleum drilling equipment to various industrial exchanger systems, this type of geometry can be observed. Meanwhile, the improvement in thermal systems as well as energy utilization during the convection in any fluid is one of the fundamental problems of the engineering processes, since improved thermal systems will provide better material processing, energy conservation and environmental effects, (Makinde, 2004).

One of the methods used for predicting the performance of the engineering processes is the second law analysis. The second law of thermodynamics is applied to investigate the irreversibility in terms of the entropy generation rate. Natural convection in trapezoidal enclosures has been the subject of interest for many studies due to its important application in various fields such as electronic components and solar collectors. Although, there are some valuable studies on natural convection in trapezoidal enclosures using pure fluid only few studies considered the effect of nanofluid, (Natarajan *et al*, 2008). No attempt was made to optimize the problem. This can be done by using the Entropy Generation Minimization technique as introduced, (Bejan, 1982). However, there are only a few studies that consider the second thermodynamic laws in the presence of nanofluids. Mahmoudi *et al* (2012) numerically studied the entropy generation and natural convection in a square cavity with a vertical heat source which is filled with copper–water nanofluid. They have considered entropy generation and heat transfer for a wide range of the Rayleigh number, solid volume fraction parameter and different positions of the heat source. It has been found that the entropy generation decreases with the solid volume fraction.

Figure 1.4 depicts how entropy increases with an increase of temperature. The figure shows that, vapour state has high entropy compared to the liquid and solid states. This is because as temperature increases, solid state become liquid and finally vapour state, molecules are free to move in vapour state compared to other states. The second law of thermodynamics states that in an isolated system the entropy will increase.

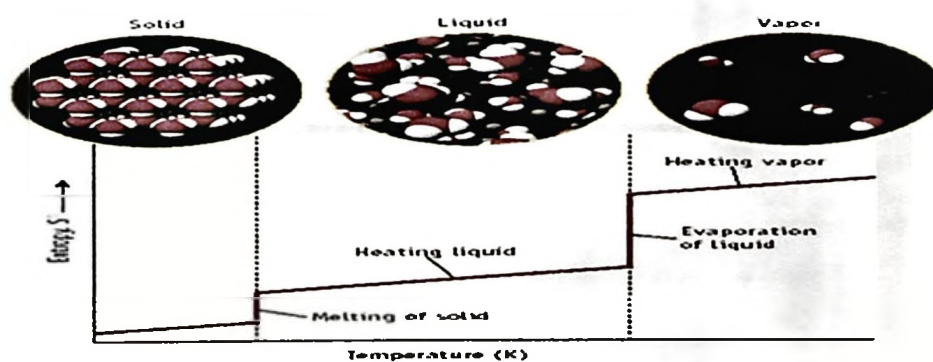


Figure 1.4: Entropy increase with temperature: *Source; Science aid.co.uk*

Factors that influence the entropy of the system are volume change, temperature change, phase change, molar mass, chemical reaction and molecular complexity.

1.1.4. Engineering and industrial applications

The study has useful applications in industries and engineering, some of these useful applications are cooling process, heat exchangers, nuclear reactors, electronics, automotive, transportation, electronics, geothermal system, drainage system, and petroleum refinery. where crude oil is transform into useful products such as liquefied petroleum gas, gasoline or petrol, kerosene, jet fuel, diesel oil and fuel oils. Figure 1.5 and Figure 1.6 below show the engine cooling system and Heat exchange device respectively.

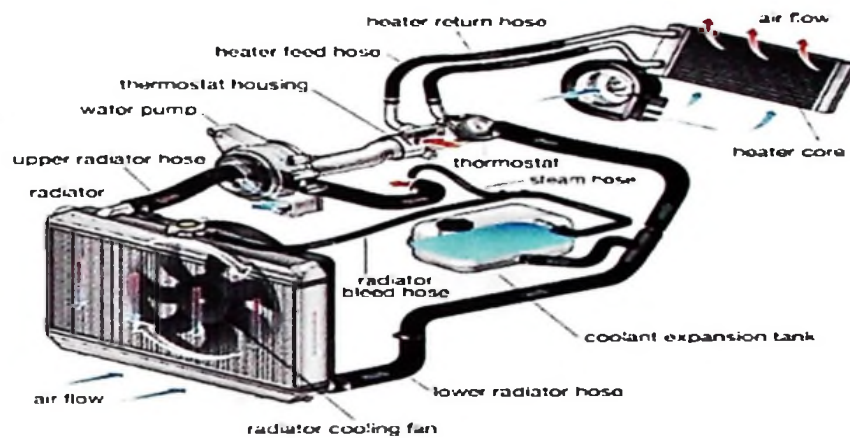


Figure 1.5: Engine cooling system: *Source; www.stforeignauto.com/service-repair/engine-cooling-system*

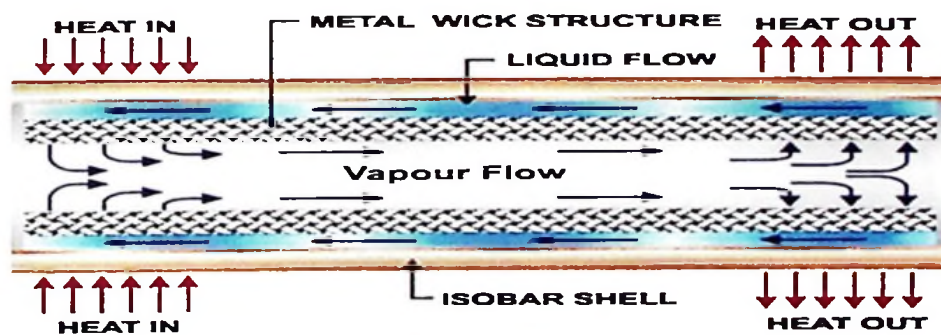


Figure 1.6: Heat exchange device: *Source; Scientific & Academic Publishing Co*

1.1.5. Viscosity

The viscosity of a fluid is a measure of its resistance to gradual deformation by shear stress or tensile stress. For liquids, it corresponds to the informal concept of "thickness". For example, honey has a much higher viscosity than water. It is a property arising from collisions between

neighboring particles in a fluid that are moving at different velocities. When the fluid is forced through a tube, the particles which comprise the fluid generally move more quickly near the tube's axis and more slowly near its walls: therefore some stress, (such as a pressure difference between the two ends of the tube), is needed to overcome the friction between particle layers to keep the fluid moving. For the same velocity pattern, the stress required is proportional to the fluid's viscosity.

A fluid that has no resistance to shear stress is known as an ideal or inviscid fluid. Zero viscosity is observed only at very low temperatures in super fluids. Otherwise, all fluids have positive viscosity, and are technically said to be viscous or viscid. In common parlance however, a liquid is said to be viscous if its viscosity is substantially greater than that of water; and may be described as mobile, if the viscosity is noticeably less than water. A fluid with a relatively high viscosity, for example, pitch, may appear to be a solid.

1.1.6. Buoyancy

Buoyancy also known as upthrust is an upward force exerted by a fluid that opposes the weight of an immersed object. In a column of fluid, pressure increases with depth as a result of the weight of the overlying fluid. Thus a column of fluid, or an object submerged in the fluid, experiences greater pressure at the bottom of the column than at the top. This difference in pressure results in a net force that tends to accelerate an object upwards. The magnitude of that force is proportional to the difference in the pressure between the top and the bottom of the column, and (as explained by Archimedes' principle) is also equivalent to the weight of the fluid that would otherwise occupy the column, i.e. the displaced fluid.

For this reason, an object whose density is greater than that of the fluid in which it is submerged tends to sink. If the object is either less dense than the fluid or is shaped appropriately (as in a boat), the force can keep the object afloat. This can occur only in a reference frame which either has a gravitational field or is accelerating due to a force other than gravity defining a "downward" direction. In a situation of fluid statics, the net upward buoyancy force is equal to the magnitude of the weight of fluid displaced by the body.

1.1.7. Governing equations

This study will be governed by basic equations, which are continuity equation, nanofluid Navier Stokes equation, nanofluid energy equation as listed below respectively.

$$\frac{\partial u}{\partial x} + \frac{\partial v}{\partial y} = 0 \quad (1.2)$$

$$\frac{\partial u}{\partial t} + u \frac{\partial u}{\partial x} + v \frac{\partial u}{\partial y} = -\frac{1}{\rho_{nf}} \frac{\partial p}{\partial x} + \frac{\mu_{nf}}{\rho_{nf}} \nabla^2 u \quad (1.3)$$

$$\frac{\partial v}{\partial t} + u \frac{\partial v}{\partial x} + v \frac{\partial v}{\partial y} = -\frac{1}{\rho_{nf}} \frac{\partial p}{\partial y} + \frac{\mu_{nf}}{\rho_{nf}} \nabla^2 v \quad (1.4)$$

$$\frac{\partial T}{\partial t} + u \frac{\partial T}{\partial x} + v \frac{\partial T}{\partial y} = -\frac{K_{nf}}{(\rho C_p)_{nf}} \nabla^2 T + \mu_{nf} \phi \quad (1.5)$$

1.1.8. Mathematical methods

Numerical approach will be to solve formulated differential equations. In this study the finite difference method, shooting technique as well as the fourth order Runge-Kutta integration scheme will be used. Shooting technique is an iterative algorithm which attempt to identify appropriate initial conditions for a relative initial value problem (IVP) that provide the solution to the original boundary value problem (BVP). Runge-Kutta methods are among the most popular classes of formulas for the approximate numerical integration of non-stiff, initial value problems. However, high-order Runge-Kutta methods require more function evaluations per integration step.

1.2 Statement of the Research Problem

Several studies on nanofluid and entropy generation have been done in different geometry like pipes, channels, plates and others. The study on, effect of variable viscosity and convective cooling in the unsteady channel flow, analysis of the second law of Buoyancy driven unsteady channel flow of nanofluids with convective cooling, entropy generation in a transient Couette flow of nanofluids with convective cooling and analysis of the entropy generation of an unsteady nanofluids Couette flow channel with permeable walls have never reported. Specifically effects of different types of nanoparticles on the flow and temperature profile, entropy generation, skin friction and Nusselt number, thermophoresis and Brownian motion, temperature and concentration of nanofluid, entropy generation, Bejan number, Nusselt number and skin friction. In this research it is intended to formulate models which will be used to analyse the nanofluid flow and entropy- generation in a channel by incorporating parameters controlling the flow.

1.3 Objectives of the Study

The general objective of this study is to investigate a channel flow model for nanofluids and heat transfer under various physical situations as well as thermodynamic analysis of the entropy generation and their minimization for efficient operation of the flow and thermal systems. This will be achieved through implementation of the following specific objectives:-

1. To obtain a mathematical model for entropy generation rate in nanofluid flow with heat transfer under different flow geometry.
2. To determine the effect of variable viscosity, thermophoresis and Brownian motion on the flow, temperature and concentration of nanofluid, entropy generation, Nusselt number and skin friction.
3. To analyse the second law of thermodynamics driven unsteady channel flow of nanofluids with convective cooling
4. To investigate and analyse the entropy generation of an unsteady nanofluids in a Transient Couette flow with convective cooling and permeable wall

1.4 Significance of the Study

This research will be useful in industries, engineering and medicine. Specifically in cooling process, nuclear reactors, transportation, electronics, automotive, geothermal system, as a viscometer, drainage system, biomedicine and food. Moreover it may have an application in petroleum refining processes where crude oil is transform into useful products such as liquefied petroleum gas, gasoline or petrol, kerosene, jet fuel, diesel oil and fuel oils. Reducing entropy-generation in a nanofluid flow system will make the fluid to be much more effective in cooling machines, engines such as automobile engines, welding equipment, high heat flux devices.

1.5 Dissertation Outline

The dissertation is organised as follows:

Chapter one presents the general introduction, background of the research, the problem statement, justification, research objectives, research questions and the significance of the research.

Chapter two presents the entropy generation in a variable viscosity channel flow of nanofluids with convective cooling. Their first and second objectives are achieved in this chapter.

Chapter three presents a second law analysis of buoyancy driven unsteady channel flow of nanofluids with convective cooling. The third specific objective of the research is achieved through chapter three.

Chapter four presents a numerical investigation into entropy generation in a transient generalized Couette flow of nanofluids with convective cooling. This chapter summarizes the findings of the part of fourth specific objective.

Chapter five present effects of Navier slip and wall permeability on entropy generation in unsteady generalized Couette flow of nanofluids with convective cooling. The fourth specific objective is also achieved through this chapter.

Chapter six presents the general discussion, conclusion, recommendations and future work.

CHAPTER TWO

Entropy Generation in a Variable Viscosity Channel Flow of Nanofluids with Convective Cooling¹

Abstract

This chapter investigates the combined effects of thermophoresis, Brownian motion and variable viscosity on entropy generation in unsteady flow of water based nanofluids confined between two parallel plates with convective heat exchange with the ambient surrounding at the walls. Both first and second laws of thermodynamics are applied to analyse the problem. The nonlinear governing equations of continuity, momentum, energy and nanoparticles concentration are tackled numerically using a semi discretization finite difference method together with Runge-Kutta-Fehlberg integration scheme. Numerical results for velocity, temperature, and nanoparticles concentration profiles are obtained and utilised to compute the skin friction, Nusselt number, entropy generation rate, irreversibility ratio and Bejan number. Pertinent results are displayed graphically and discussed quantitatively.

2.1 Introduction

Heat transfer enhancement in engineering and industrial systems is one of the hottest topics in research today. With the growing demand for efficient cooling systems, more effective coolants are required to keep the temperature of heat generating engines and engineering devices such as electronic components below safe limits. In recent time, the use of nanofluids has provided an innovative technique to enhance heat transfer. Nanotechnology has been widely used in engineering and industry since nanometer size materials possess unique physical and chemical properties. The addition of nanoscale particles into the conventional fluids like water, engine oil, ethylene glycol, etc., is known as nanofluid and was firstly introduced by Choi (1995). Moreover, the effective thermal conductivity of conventional fluids increases remarkably with the addition of metallic nanoparticles with high thermal conductivity. Nanofluid may be considered as a single phase flow in low solid concentration

¹This chapter is based on the paper:

Mkwizu, M.H and Makinde, O. D (2015). Entropy Generation in a Variable Viscosity Channel Flow of Nanofluids with Convective Cooling, *Comptes Rendus Mecanique*, Vol 343, 38–56, ISSN 1631-072.

because of very small sized solid particles. There are many experimental and theoretical studies on flow of nanofluids in different geometries (Choi *et al.*, 2001).

Numerical study of buoyancy driven flow and heat transfer of Alumina (Al_2O_3)–water based nanofluid in a rectangular cavity was done by Hwang *et al.* (2007). The nanofluid in the enclosure was assumed to be in single phase. The result revealed that for any given Grashof number, the average Nusselt number increased with the solid volume concentration parameter. Nield and Kuznetsov (2009) investigated numerically the Cheng–Minkowycz problem for natural convective boundary-layer flow in a porous medium saturated by a nanofluid. Oztop and Abu-Nada (2008) considered natural convection in partially heated enclosures having different aspect ratio and filled with nanofluid. The results showed that the heat transfer was more pronounced at low aspect ratio and high volume fraction of nanoparticles. Ibrahim and Makinde (2013) studied the effect of double stratification on boundary-layer flow and heat transfer of nanofluid over a vertical plate. The buoyancy effects stretching/shrinking sheet with or without magnetic field were considered by Makinde *et al.* (2013) and Makinde (2013). Wang and Mujumdar (2007) presented a comprehensive review of heat transfer characteristics of nanofluids. Detail reports on convective transport in nanofluids can be found in Buongiorno (2006), Mutuku-Njane and Makinde (2014), Tiwari and Das (2007), etc.

Meanwhile, in the nanofluids flows, the improvement of the heat transfer properties causes the reduction in entropy generation. The foundation of knowledge of entropy production goes back to Clausius and Kelvin's studies on the irreversible aspects of the second law of thermodynamics. Since then the theories based on these foundations have rapidly developed, see Bejan (1982) and Bejan (1996). However, the entropy production resulting from heat and mass transfer coupled with viscous dissipation in nanofluids has remained untreated by classical thermodynamics, which motivates many researchers to conduct analyses of fundamental and applied engineering problems based on second law analysis with respect to nanofluid. Based on the concept of efficient energy use and the minimal entropy generation principle, optimal designs of thermodynamic systems have been widely proposed by the thermodynamic second law Woods (1975). It is possible to improve the efficiency and overall performance of all kinds of flow and thermal systems through entropy minimization techniques. The analysis of energy utilization and entropy generation has become one of the primary objectives in designing a thermal system. This has become the main concern in many fields such as heat exchangers, turbo machinery, electronic cooling, porous media and

combustion. Several studies have thoroughly dealt with conventional fluid flow irreversibility due to viscous effect and heat transfer by conduction Narusawa (1998).

Makinde *et al* (2013) performed numerous investigations to calculate entropy production and irreversibility due to flow and heat transfer of nanofluids over a moving flat surface. They found that the entropy generation in the flow system can be minimized by appropriate combination of parameter values together with nanoparticles volume fraction.

In the present study, we analyse the combined effects of thermophoresis, Brownian motion and variable viscosity on entropy generation rate in unsteady channel flow of water base nanofluid under the influence of convective heat exchange with the ambient surrounding. Such flows are very important in engine cooling, solar water heating, cooling of electronics, cooling of transformer oil, improving diesel generator efficiency, cooling of heat exchanging devices, improving heat transfer efficiency of chillers, domestic refrigerator-freezers, cooling in machining and in nuclear reactor. In the following sections the problem is formulated, numerically analysed and solved. Pertinent results are displayed graphically and discussed.

2.2 Mathematical Model

Consider the unsteady flow of an incompressible variable viscosity nanofluid between two parallel plates channel under the combined action of a constant pressure gradient and convective heat exchange with the ambient surrounding. It is assumed that the channel width is $2a$ and the flow is symmetrical with no slip at the walls as depicted in Figure 2.1 below;

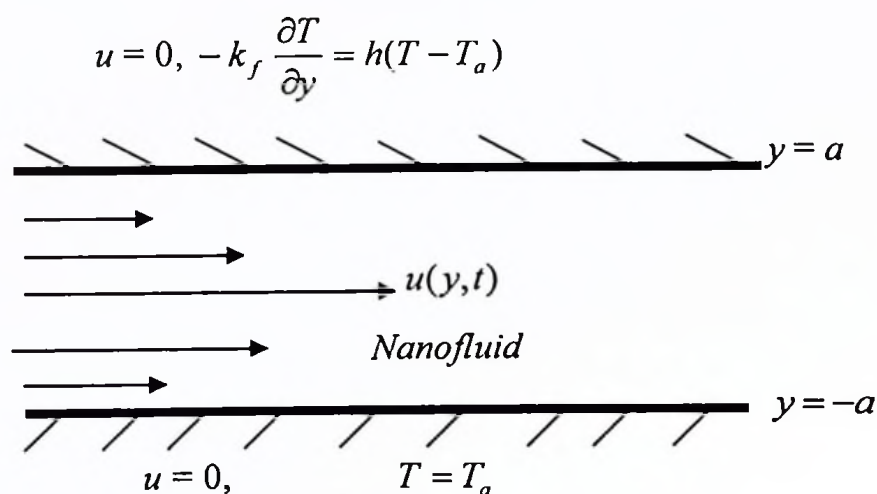


Figure 2.1: Schematic diagram of the problem under consideration

Using the Buongiorno nanofluid model with the Brownian motion, thermophoresis and nanoparticle volume fraction distributions, the governing equations for continuity, momentum, energy and nanoparticle concentration are

$$\frac{\partial u}{\partial x} = 0, \quad (2.1)$$

$$\rho_f \frac{\partial u}{\partial \bar{t}} = -\frac{\partial P}{\partial x} + \frac{\partial}{\partial y} \left(\mu_f(T) \frac{\partial u}{\partial y} \right), \quad (2.2)$$

$$\frac{\partial T}{\partial \bar{t}} = \alpha_f \frac{\partial^2 T}{\partial y^2} + \tau \left\{ D_B \frac{\partial T}{\partial y} \frac{\partial \varphi}{\partial y} + \frac{D_T}{T_a} \left(\frac{\partial T}{\partial y} \right)^2 \right\} + \frac{\alpha_f \mu_f(T)}{k_f} \left(\frac{\partial u}{\partial y} \right)^2, \quad (2.3)$$

$$\frac{\partial \varphi}{\partial \bar{t}} = D_B \frac{\partial^2 \varphi}{\partial y^2} + \left(\frac{D_T}{T_a} \right) \left(\frac{\partial^2 T}{\partial y^2} \right), \quad (2.4)$$

where D_B and D_T are the Brownian and thermophoretic diffusion coefficients respectively, u is the nanofluid velocity in the x -direction, T is the temperature of the nanofluid, P is the nanofluid pressure, \bar{t} is the time, T_a is the ambient temperature which also correspond to the nanofluid initial temperature, φ is the concentration of nanoparticles, ρ_f is the density of the nanofluid, μ_f is the viscosity of the fluid fraction, α_f is the thermal diffusivity of the nanofluid, k_f is the thermal conductivity of the fluid fraction and τ is the ratio of solid particles heat capacitance to that of the nanofluid heat capacitance. The dynamic viscosity of nanofluid is assumed to be temperature dependent as follows:

$$\mu_f(T) = \mu_0 e^{-m(T-T_a)}, \quad (2.5)$$

where μ_0 is the nanofluid viscosity at the ambient temperature T_a , $\beta = mT_a$ is a viscosity variation parameter which depends on the particular fluid. The initial and boundary conditions are given as follows:

$$u(y,0) = 0, \quad T(y,0) = T_a, \quad \varphi(y,0) = \varphi_0, \quad (2.6)$$

$$\frac{\partial u}{\partial y}(0,\bar{t}) = \frac{\partial T}{\partial y}(0,\bar{t}) = \frac{\partial \varphi}{\partial y}(0,\bar{t}), \quad (\text{axial-symmetric conditions}) \quad (2.7)$$

$$u(a,\bar{t}) = 0, \quad -k_f \frac{\partial T}{\partial y}(a,\bar{t}) = h(T(a,\bar{t}) - T_a), \quad D_B \frac{\partial \varphi}{\partial y}(a,\bar{t}) = -\frac{D_T}{T_a} \frac{\partial T}{\partial y}(a,\bar{t}), \quad (2.8)$$

where h is the heat transfer coefficient and φ_0 is the nanoparticles initial concentration. We introduce the non dimensionless variables and parameters as follows:

$$\left. \begin{aligned} \theta &= \frac{T - T_a}{T_a}, W = \frac{ua}{v_f}, \eta = \frac{y}{a}, t = \frac{\bar{t} v_f}{a^2}, Bi = \frac{ha}{k_f}, \\ \bar{P} &= \frac{\rho_f a^2 P}{\mu_0^2}, Nb = \frac{\tau D_B \phi_0}{\alpha_f}, A = -\frac{\partial \bar{P}}{\partial X}, X = \frac{x}{a}, Pr = \frac{\mu_0 c_{pf}}{k_f}, Sc = \frac{v_f}{D_B}, \\ Ec &= \frac{v_f^2}{c_{pf} T_a a^2}, H = \frac{\phi}{\phi_0}, Nt = \frac{\tau D_T}{\alpha_f}, \tau = \frac{(\rho c_p)_s}{(\rho c_p)_f}, \beta = m T_a \end{aligned} \right\} \quad (2.9)$$

The dimensionless governing equations together with the appropriate initial and boundary conditions can be written as:

$$\frac{\partial W}{\partial t} = A + e^{-\beta\theta} \frac{\partial^2 W}{\partial \eta^2} - \beta e^{-\beta\theta} \frac{\partial \theta}{\partial \eta} \frac{\partial W}{\partial \eta}, \quad (2.10)$$

$$Pr \frac{\partial \theta}{\partial t} = \frac{\partial^2 \theta}{\partial \eta^2} + \left\{ Nb \frac{\partial \theta}{\partial \eta} \frac{\partial H}{\partial \eta} + Nt \left(\frac{\partial \theta}{\partial \eta} \right)^2 \right\} + Ec Pr e^{-\beta\theta} \left(\frac{\partial W}{\partial \eta} \right)^2, \quad (2.11)$$

$$Sc \frac{\partial H}{\partial t} = \frac{\partial^2 H}{\partial \eta^2} + \frac{Nt}{Nb} \frac{\partial^2 \theta}{\partial \eta^2}, \quad (2.12)$$

with

$$W(\eta, 0) = 0, \quad \theta(\eta, 0) = 0, \quad H(\eta, 0) = 1, \quad (2.13)$$

$$\frac{\partial W}{\partial \eta}(0, t) = \frac{\partial \theta}{\partial \eta}(0, t) = \frac{\partial H}{\partial \eta}(0, t) = 0 \quad (2.14)$$

$$W(1, t) = 0, \quad \frac{\partial \theta}{\partial \eta}(1, t) = -Bi \theta(1, t), \quad \frac{\partial H}{\partial \eta}(1, t) = -\frac{Nt}{Nb} \frac{\partial \theta}{\partial \eta}(1, t), \quad (2.15)$$

where Nb is the Brownian motion parameter, Bi is the Biot number, Nt is the thermophoresis parameter, Sc is the Schmidt number, Pr is the Prandtl number, Ec is the Eckert number and A is the pressure gradient parameter. The quantities of practical interest in this study are the skin friction coefficient C_f and the local Nusselt number Nu which are defined as

$$C_f = \frac{a^2 \tau_w}{\rho_f v_f^2}, \quad Nu = \frac{a q_w}{k_f T_a}, \quad (2.16)$$

where τ_w is the wall shear stress and q_w is the heat flux at the channel walls given by

$$\tau_w = \mu_f \left. \frac{\partial u}{\partial y} \right|_{y=a}, \quad q_w = -k_f \left. \frac{\partial T}{\partial y} \right|_{y=a}. \quad (2.17)$$

Substituting equation (2.17) into (2.16), we obtain

$$\left. \begin{aligned} C_f &= e^{-\beta\theta} \frac{\partial W}{\partial \eta}, \\ Nu &= -\frac{\partial \theta}{\partial \eta}, \end{aligned} \right\} \text{at } \eta = 1. \quad (2.18)$$

2.3 Entropy Analysis

In the nanofluids flows, the improvement of the heat transfer properties causes the reduction in entropy generation. However, convection process involving channel flow of nanofluids is inherently irreversible. The non-equilibrium conditions due to the exchange of energy and momentum, within the nanofluid and at solid boundaries, cause continuous entropy generation. One part of this entropy production results from heat transfer in the direction of finite temperature gradients, while other part arises due to the fluid friction, nanoparticle concentration and complex interaction between the base fluid and the nanoparticles. According to Woods (1975), the local volumetric rate of entropy generation is given by

$$S'' = \frac{k_f}{T_a^2} \left(\frac{\partial T}{\partial y} \right)^2 + \frac{\mu_f(T)}{T_a} \left(\frac{\partial u}{\partial y} \right)^2 + \frac{D_B}{\phi_0} \left(\frac{\partial \phi}{\partial y} \right)^2 + \frac{D_B}{T_a} \frac{\partial T}{\partial y} \frac{\partial \phi}{\partial y}. \quad (2.19)$$

The first term in Eq. (2.19) is the irreversibility due to heat transfer; the second term is the entropy generation due to viscous dissipation, while the third and the fourth terms are the local entropy generation due to nanoparticles mass transfer and complex interaction with the base fluid. Using equation (2.9), we express the entropy generation number in dimensionless form as,

$$N_s = \frac{a^2 S''}{k_f} = \left(\frac{\partial \theta}{\partial \eta} \right)^2 + Bre^{-\beta\theta} \left(\frac{\partial W}{\partial \eta} \right)^2 + \lambda \left[\left(\frac{\partial H}{\partial \eta} \right)^2 + \frac{\partial H}{\partial \eta} \frac{\partial \theta}{\partial \eta} \right], \quad (2.20)$$

where $Br = Ec Pr$ is the Brinkmann number, $\lambda = \phi_0 D_B / k_f$ is the nanoparticles mass transfer parameter. Let

$$N_1 = \left(\frac{\partial \theta}{\partial \eta} \right)^2, \quad N_2 = Bre^{-\beta\theta} \left(\frac{\partial W}{\partial \eta} \right)^2, \quad N_3 = \lambda \left[\left(\frac{\partial H}{\partial \eta} \right)^2 + \frac{\partial H}{\partial \eta} \frac{\partial \theta}{\partial \eta} \right], \quad (2.21)$$

The irreversibility distribution ratio is define as $\Phi = N_2/(N_1+N_3)$. Heat and nanoparticles mass transfer irreversibility dominates for $0 \leq \Phi < 1$ and fluid friction irreversibility dominates when $\Phi > 1$. The contribution of both irreversibilities to entropy generation are equal when $\Phi = 1$. We define the Bejan numbers (Be) mathematically as

$$Be = \frac{N_1 + N_3}{Ns} = \frac{1}{1 + \Phi}. \quad (2.22)$$

From equation (2.22), it is very obvious that the Bejan number ranges from 0 to 1. The zero value of the Bejan number corresponds to the limit where the irreversibility is dominated by the effect of fluid friction while $Be = 1$ is the limit where the irreversibility due to heat and nanoparticles mass transfer dominates the flow system. Heat and mass transfer together with fluid friction irreversibilities are the same when the Bejan number equals 0.5.

2.4 Numerical Procedure

Equations (2.10)-(2.15) constitute a system of nonlinear Initial Boundary Value Problem (IBVP) and are solved numerically using a semi-discretization finite difference method known as method of lines. A partition of the spatial interval $0 \leq \eta \leq 1$ into N equal parts is introduced such that the grid size $\Delta\eta = 1/N$ and grid points $\eta_i = (i-1)\Delta\eta$, $1 \leq i \leq N+1$. The semi-discretization finite difference technique known as method of line is employed to tackle the model nonlinear initial boundary value problem in equations (2.10)-(2.15). The discretization is based on a linear Cartesian mesh and uniform grid on which finite-differences are taken. The first and second spatial derivatives in equations (2.10)-(2.12) are approximated with second-order central finite differences. Let $W_i(t)$, $\theta_i(t)$ and $H_i(t)$ be approximation of $W(\eta_i, t)$, $\theta(\eta_i, t)$ and $H(\eta_i, t)$, then the semi-discrete system for the problem becomes

$$\frac{dW_i}{dt} = A + e^{-\beta\theta_i} \frac{(W_{i+1} - 2W_i + W_{i-1}))}{(\Delta\eta)^2} - \beta e^{-\beta\theta_i} \frac{(\theta_{i+1} - \theta_{i-1})(W_{i+1} - W_{i-1}))}{4(\Delta\eta)^2}, \quad (2.23)$$

$$\begin{aligned} \text{Pr} \frac{d\theta_i}{dt} = & \frac{(\theta_{i+1} - 2\theta_i + \theta_{i-1}))}{(\Delta\eta)^2} + Nb \frac{(\theta_{i+1} - \theta_{i-1})(H_{i+1} - H_{i-1}))}{4(\Delta\eta)^2} \\ & + Nt \left(\frac{\theta_{i+1} - \theta_{i-1}}{2\Delta\eta} \right)^2 + Ec \text{Pr} e^{-\beta\theta_i} \left(\frac{W_{i+1} - W_{i-1}}{2\Delta\eta} \right)^2, \end{aligned} \quad (2.24)$$

$$Sc \frac{dH_i}{dt} = \frac{(H_{i+1} - 2H_i + H_{i-1}))}{(\Delta\eta)^2} + \frac{Nt}{Nb} \frac{(\theta_{i+1} - 2\theta_i + \theta_{i-1}))}{(\Delta\eta)^2}, \quad (2.25)$$

with initial conditions

$$W_i(0) = \theta_i(0) = 0, \quad H_i(0) = 1, \quad 1 \leq i \leq N+1. \quad (2.26)$$

The equations corresponding to the first and last grid points are modified to incorporate the boundary conditions as follows

$$\begin{aligned}
W_2 &= W_1, \theta_2 = \theta_1, H_2 = H_1, w_{N+1} = 0, \\
\theta_{N+1} &= \theta_N (1 - Bi \Delta \eta), H_{N+1} = H_N - Nt \frac{(\theta_{N+1} - \theta_N)}{Nb},
\end{aligned} \tag{2.27}$$

There is only one independent variable in equations (2.23)-(2.27), so they are first order Ordinary Differential Equations (ODE) with known initial conditions. The resulting initial value problem can be easily solved iteratively using Runge-Kutta-Fehlberg integration technique using MATLAB, see Na, (1979) for example. From the process of numerical computation, the skin-friction coefficient and the Nusselt number in equation (2.18) are also worked out and their numerical values are presented.

2.5 Results and Discussion

Numerical solution for the representative velocity field, temperature field, nanoparticles concentration, skin friction, Nusselt number, Entropy generation rate and Bejan number have been carried out by assigning some arbitrary chosen specific values to various thermophysical parameters controlling the flow system (see Figures 2.2-2.35). Following Hwang et al (2007), the Prandtl number (Pr) of the pure water base nanofluid under consideration is assigned the value 6.2.

2.5.1 Effects of parameter variation on velocity profiles

Figures 2.1-2.6 depict the effects of various physical parameters on the nanofluid velocity profiles. Generally, the velocity profile is maximum along the channel centreline and minimum at the walls. This can be attributed to the strong boundary layer effects at the walls due to the nanofluid viscosity and the impose no-slip condition at the walls. It is noted in Figures 2.2-2.3 that as time t increases the velocity increases across the channel until it attains a steady state profile for a given set of parameter values. Figure 2.4 shows that the nanofluid velocity profile decreases with increasing convective cooling at the walls as the Biot number Bi increases. This may be attributed to increasing rate of heat loss at the channel walls leading to an increase in the nanofluid thickness and a decrease in the flow speed. In Figure 2.5, we observed that the nanofluid velocity increases with a decrease in the viscosity due to an increase in the temperature. This is expected, since as β increases, the fluid viscosity decreases due to a rise in temperature, consequently, the fluid becomes lighter and flow faster. Similar trend is observed in Figure 2.6 with an increase Eckert number Ec due to viscous dissipation. The nanofluid kinetic energy increases with viscous heating; this invariably leads to a decrease in the fluid viscosity and an increase in velocity profile.

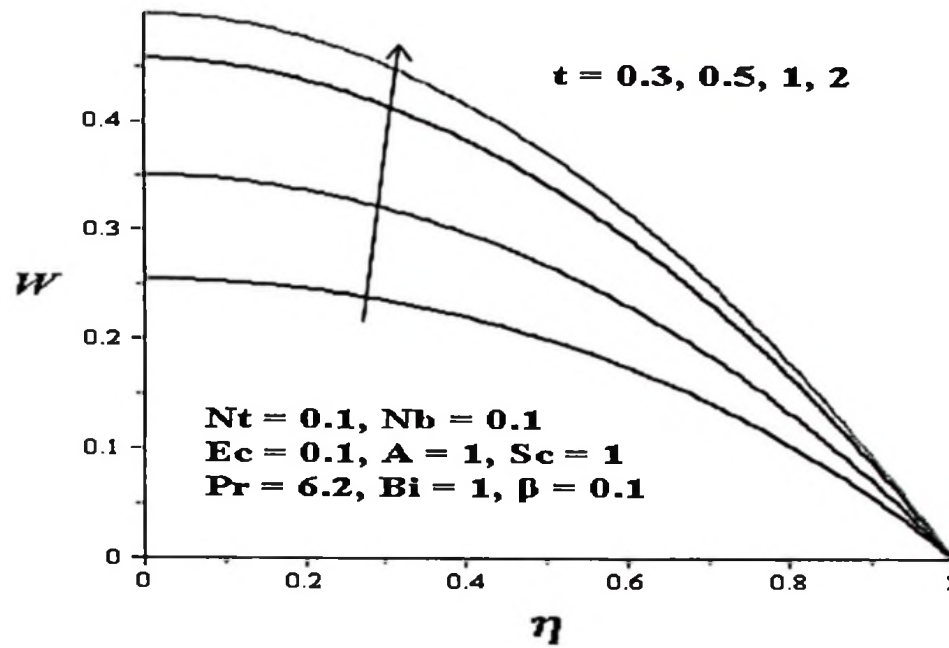


Figure 2.2: Velocity profiles across the channel with increasing time

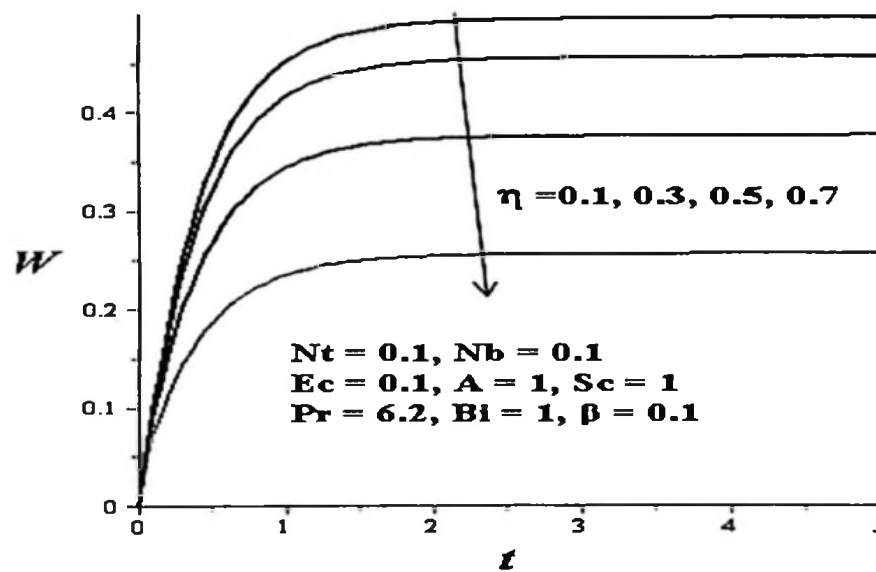


Figure 2.3: Velocity profiles with increasing time

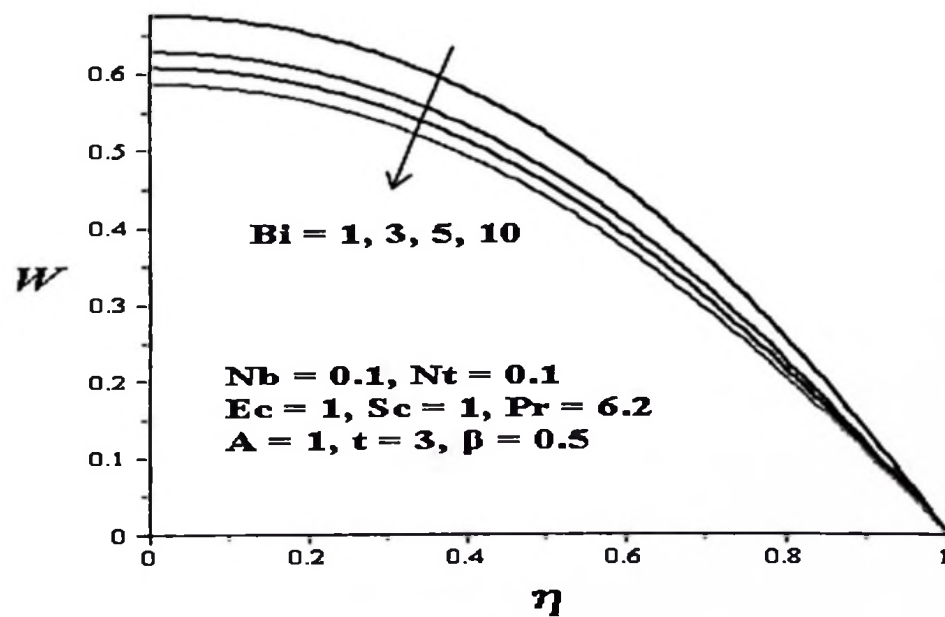


Figure 2.4: Velocity profiles with increasing Bi

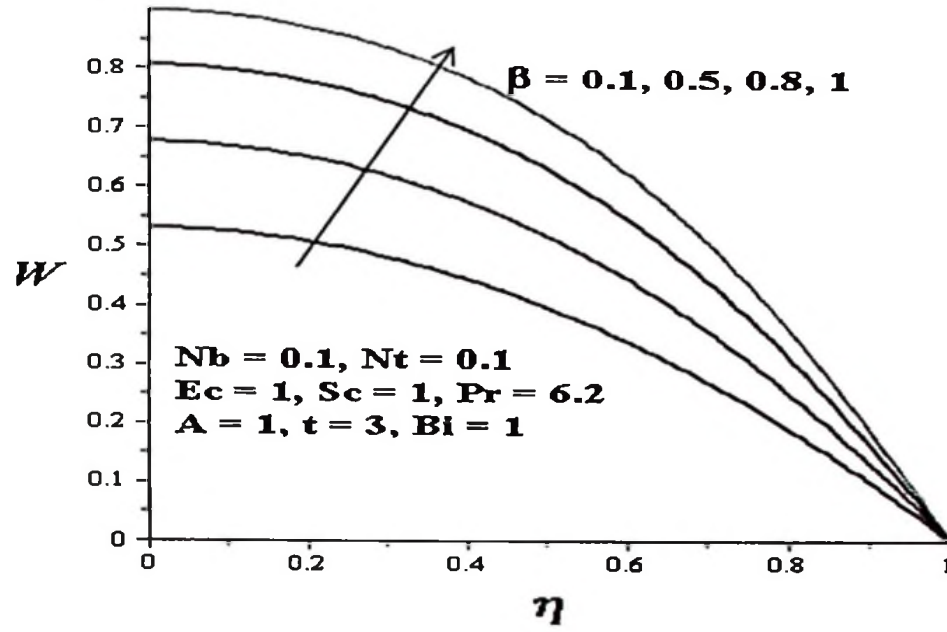


Figure 2.5: Velocity profiles with increasing β

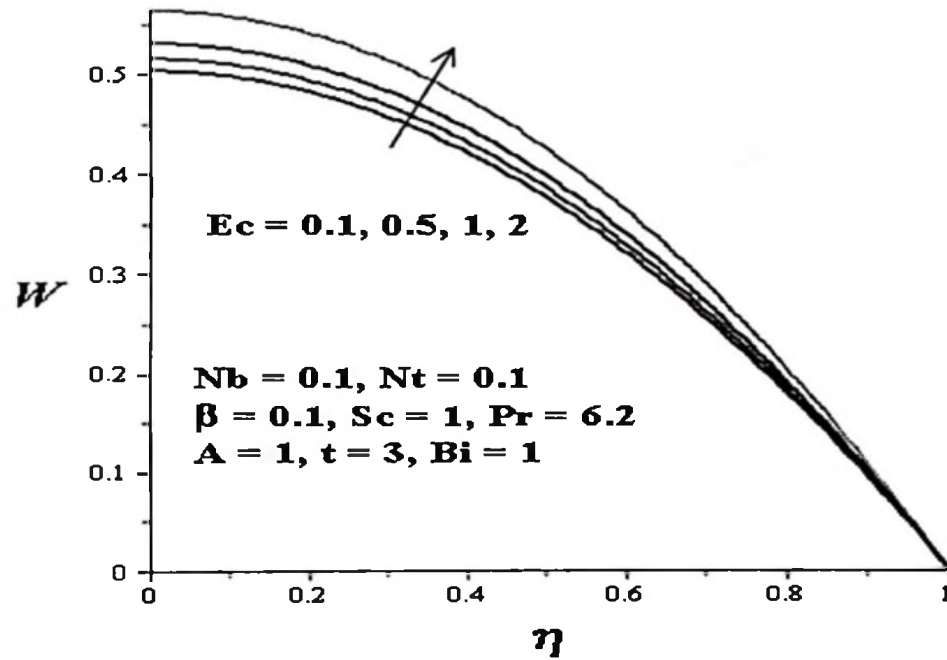


Figure 2.6: Velocity profiles with increasing Ec

2.5.2 Effects of parameter variation of temperature profiles

Figures (2.7-2.11) illustrate the effects of unsteadiness and parameter variation on the temperature profiles. In Figures 2.7-2.8, we observed the nanofluid temperature increases across the channel with time and space. However, the temperature tends to be lower within the channel centreline region. Figure 2.9 shows that the fluid temperature decreases across the channel with increasing convective cooling due to increasing heat loss to the ambient surrounding from the walls. As β increases the nanofluid viscosity decreases, consequently, the kinetic energy of nanoparticles increase and a rise in nanofluid temperature is observed as shown in Figure 2.10. Similar trend is noticed with increasing Ec in Figure 2.11, the nanofluid temperature increases due to an increase in the viscous heating effect.

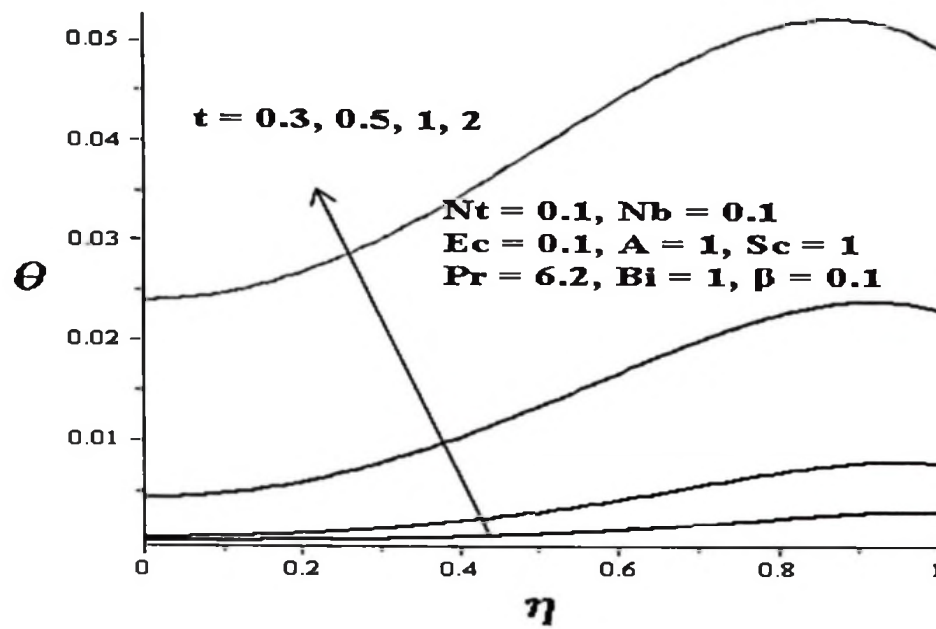


Figure 2.7: Temperature profiles with increasing time

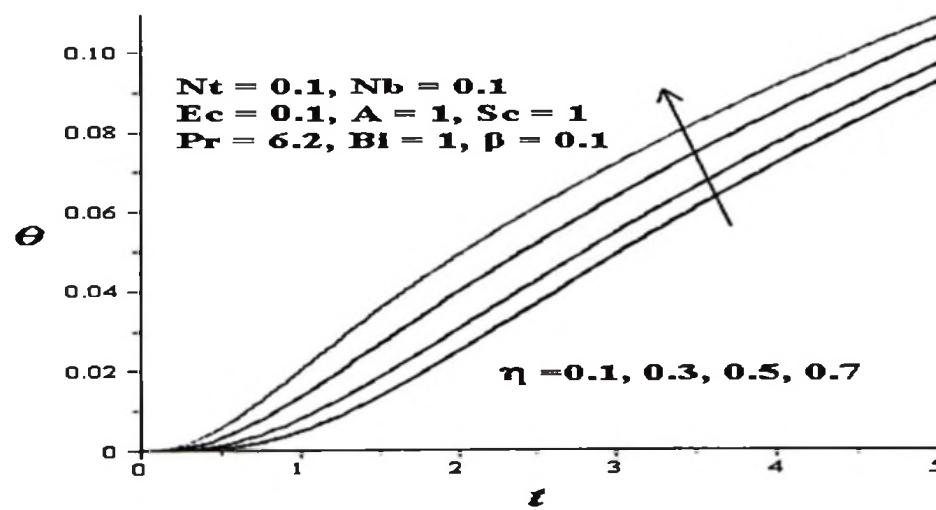


Figure 2.8: Temperature profiles with increasing time

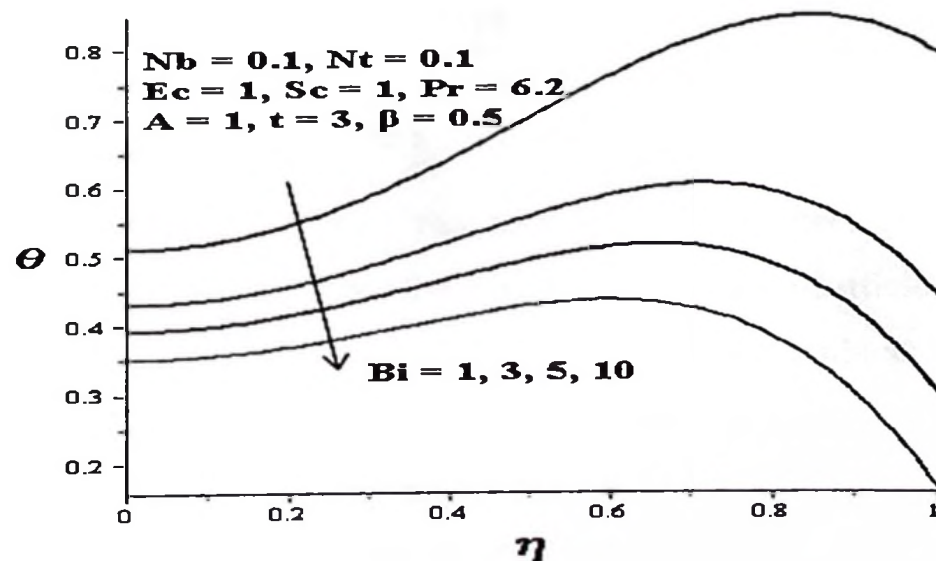


Figure 2.9: Temperature profiles with increasing Bi

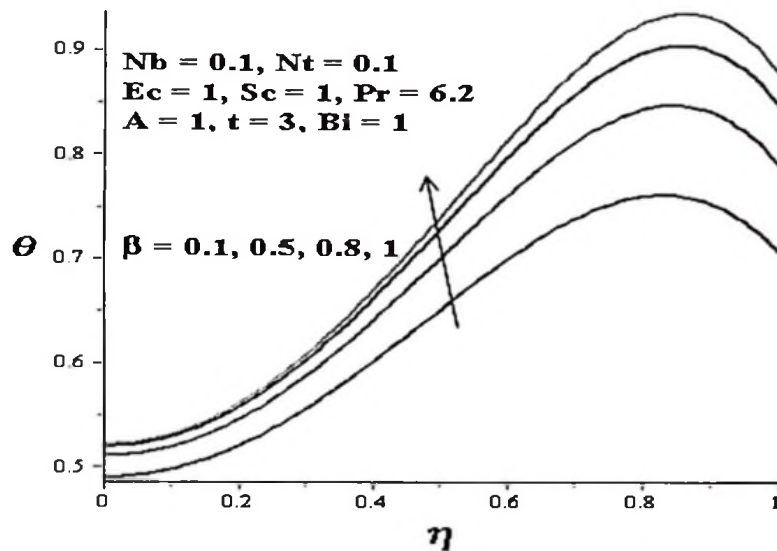


Figure 2.10: Temperature profiles with increasing β

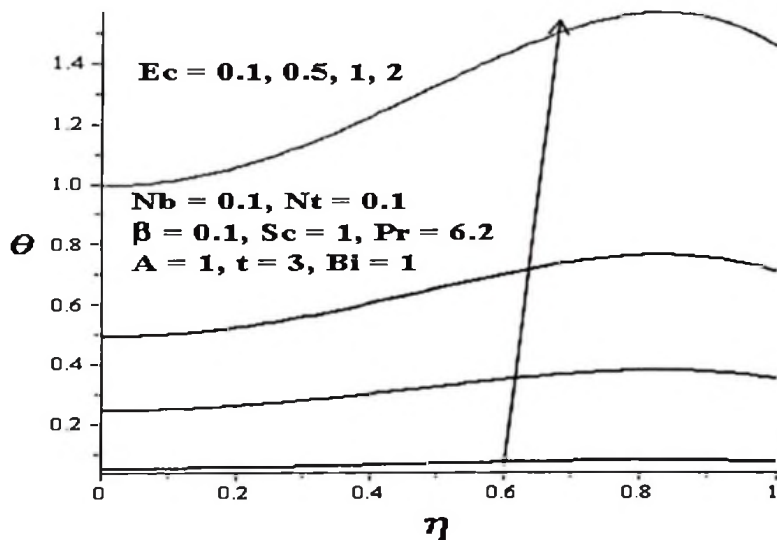


Figure 2.11: Temperature profiles with increasing Ec

2.5.3 Effects of parameter variation on nanoparticles concentration

Figures (2.12-2.18) depict the effects of various physical parameters on the nanoparticles concentration profile. It is observed that the concentration of nanoparticles increases along the channel centreline region $0 \leq \eta \leq 0.5$ and decreases near the walls as time increases as shown in Figures 2.12 -2.13. Figure 2.14 shows a decrease in nanoparticles concentration within the centreline region and increase in concentration near the walls as the Bi increases. This may be attributed to the fact that kinetic energy of the nanoparticles increases towards the wall with a rise in convective heat loss to the ambient. In Figures 2.15-2.16, a rise in nanoparticles concentration towards the channel centreline region is observed with an



increase in β and Ec . Interestingly, as the β and Ec increases, the nanofluid viscosity decreases while the temperature and velocity increase towards the channel centreline, consequently, the nanoparticles concentration along the centreline region increases and the concentration near the walls decreases. Similar trend was revealed in Figure 2.17 with increasing thermophoresis effect Nt due to temperature gradient, leading to an increase in nanoparticles concentration towards the channel centreline region. Moreover, increasing motion of particles (Brownian motion Nb) in a fluid as shown in Figure 2.18 may cause a decrease in the nanoparticles concentration within centreline region and an increase of nanoparticle concentration near the walls.

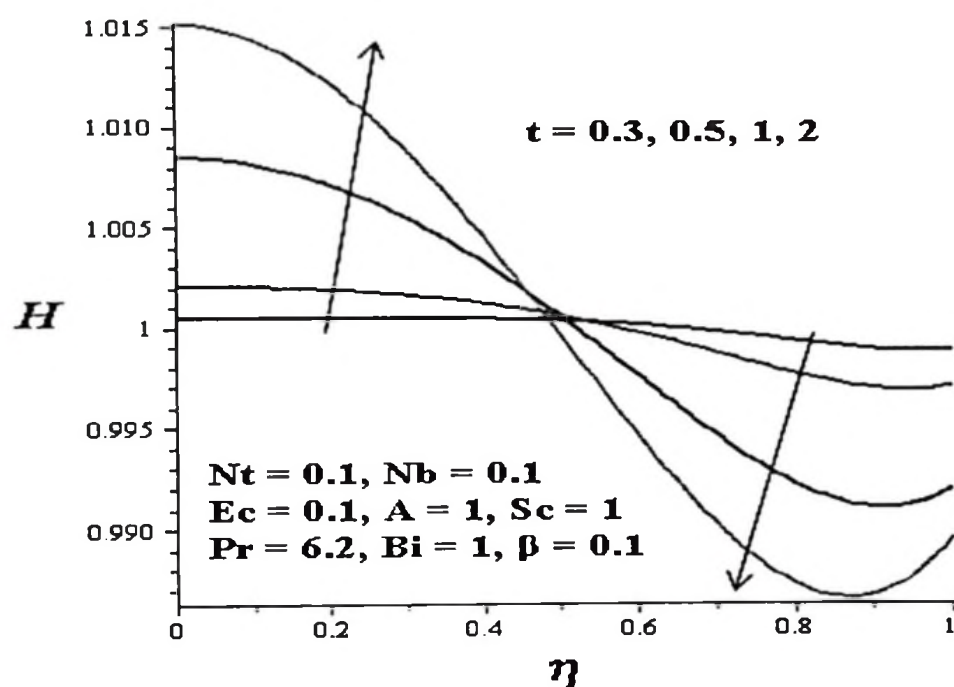


Figure 2.12: Nanoparticles distribution with increasing time

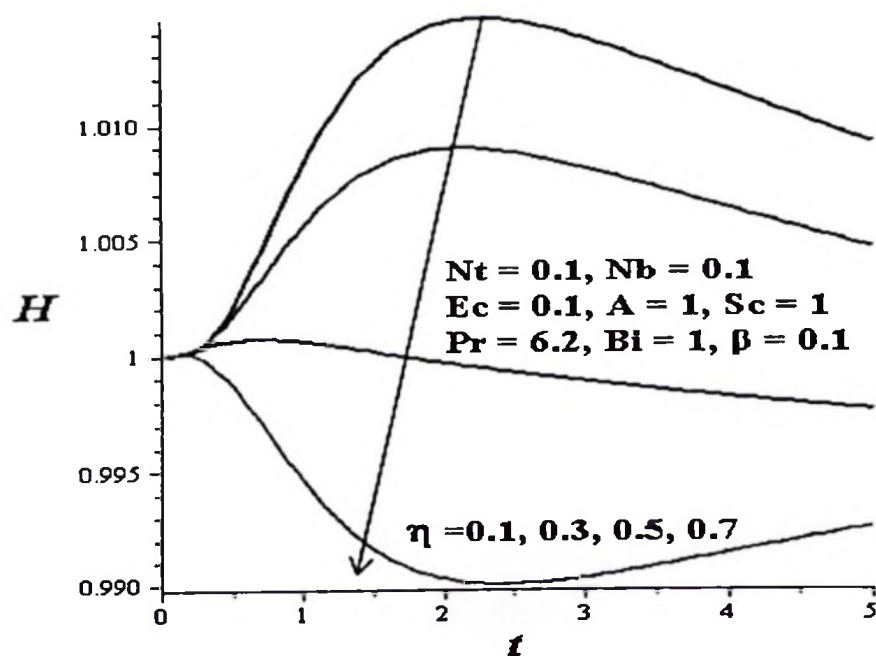


Figure 2.13: Nanoparticles distribution with increasing time

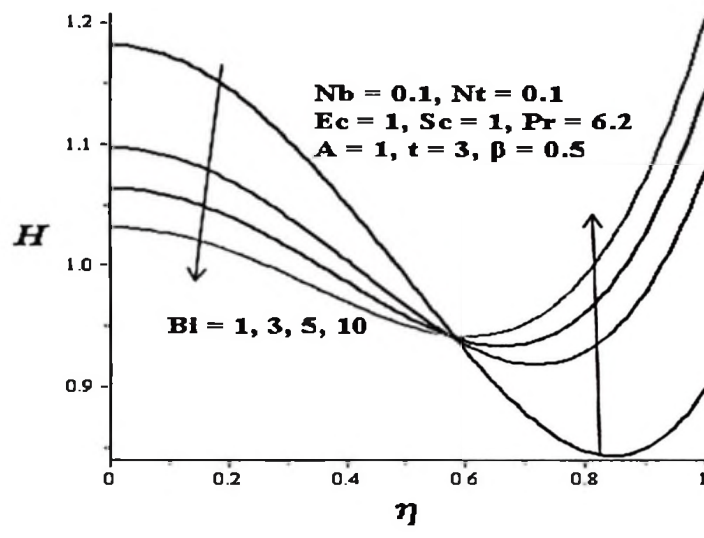


Figure 2.14: Nanoparticles distribution with increasing Bi

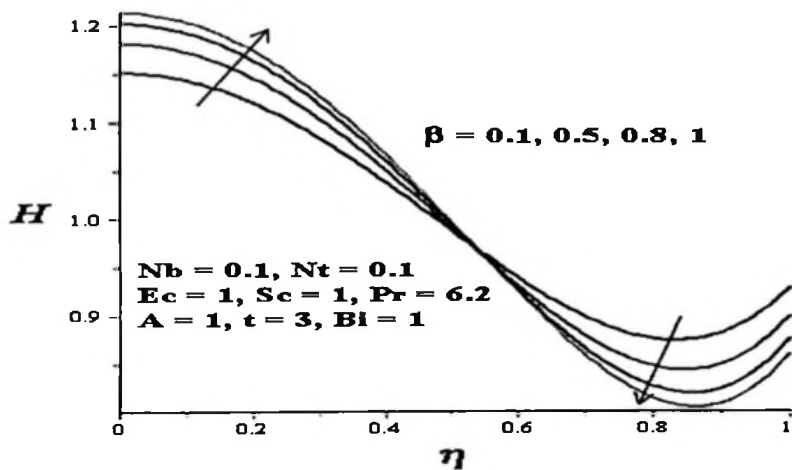


Figure 2.15: Nanoparticles distribution with increasing β

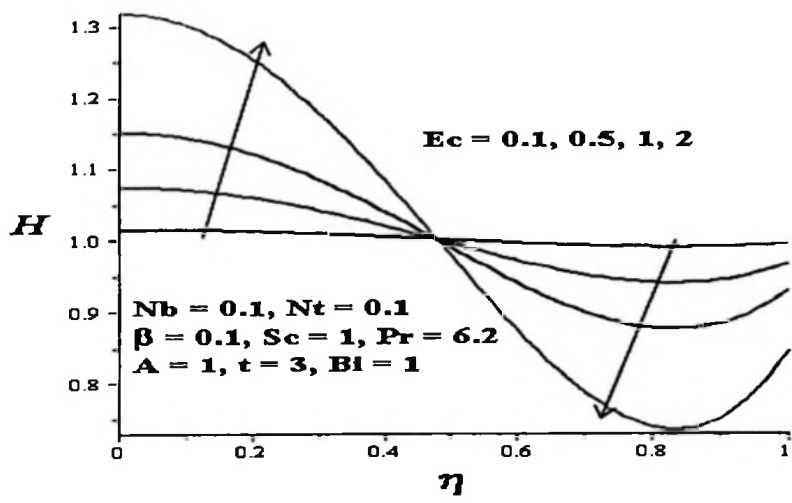


Figure 2.16: Nanoparticles distribution with increasing Ec

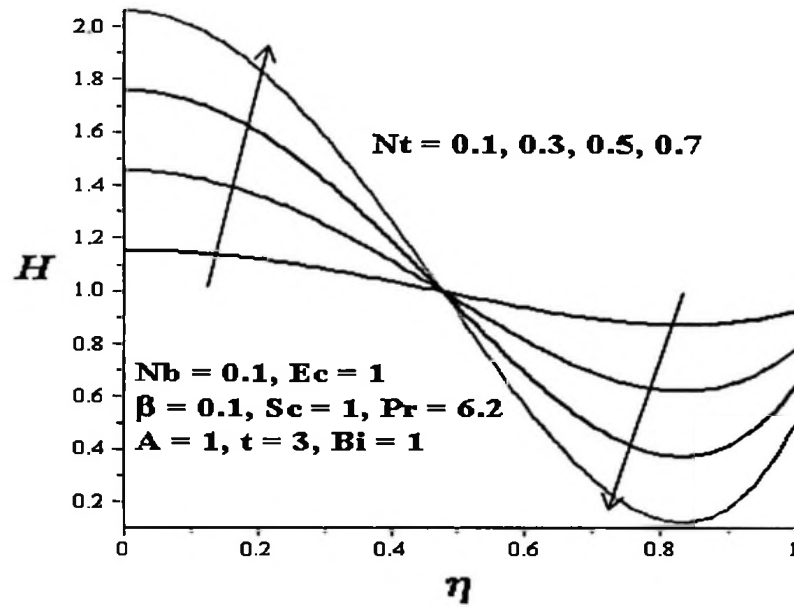


Figure 2.17: Nanoparticles distribution with increasing Nt

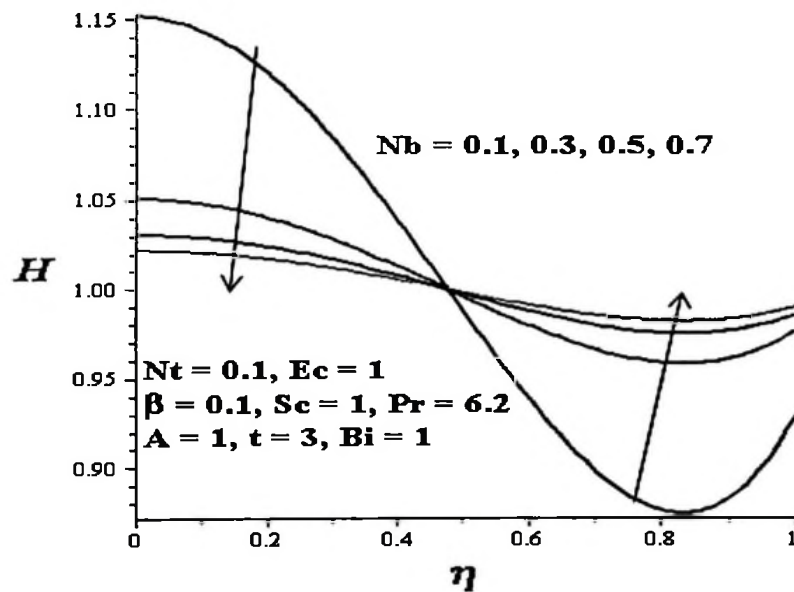


Figure 2.18: Nanoparticles distribution with increasing Nb

2.5.4 Effects of parameter variation on skin friction and Nusselt number

Table 2.1 below shows the effect of parameter variation on skin friction. The results showed that the skin friction at the channel walls increases with time and increasing parameter values of Bi , β , Nb and A . This may be attributed to a rise in velocity gradient at the walls due to combined effects of convective cooling, viscosity variation, Brownian motion and pressure gradient. Meanwhile, a decrease in skin friction is observed with increasing parameter values of Ec and Nt . In Figure 2.19, the results illustrate a rise in heat flux at the walls with time and increasing parameter values of Ec , Bi and β . It is evidence that a decrease in the fluid

viscosity coupled with the combined increase in viscous heating and convective cooling increase the temperature gradient at the channel walls, consequently, the Nusselt number increases.

Table 2.1: Computation showing the skin friction $Pr = 6.2$, $Sc = 1$.

T	Bi	β	Ec	Nt	Nb	A	C_f
1.0	1.0	0.1	0.1	0.1	0.1	1.0	1.087385958
3.0	1.0	0.1	0.1	0.1	0.1	1.0	1.097675134
5.0	1.0	0.1	0.1	0.1	0.1	1.0	1.109142224
3.0	3.0	0.1	0.1	0.1	0.1	1.0	1.113883200
3.0	5.0	0.1	0.1	0.1	0.1	1.0	1.120076893
3.0	1.0	0.5	0.1	0.1	0.1	1.0	1.656399435
3.0	1.0	1.0	0.1	0.1	0.1	1.0	2.854667188
3.0	1.0	0.1	0.5	0.1	0.1	1.0	1.070051922
3.0	1.0	0.1	1.0	0.1	0.1	1.0	1.032125297
3.0	1.0	0.1	0.1	0.3	0.1	1.0	1.083224047
3.0	1.0	0.1	0.1	0.5	0.1	1.0	1.068774187
3.0	1.0	0.1	0.1	0.1	0.3	1.0	1.102492475
3.0	1.0	0.1	0.1	0.1	0.5	1.0	1.103455943
3.0	1.0	0.1	0.1	0.1	0.1	2.0	1.192432794
3.0	1.0	0.1	0.1	0.1	0.1	3.0	1.282885825

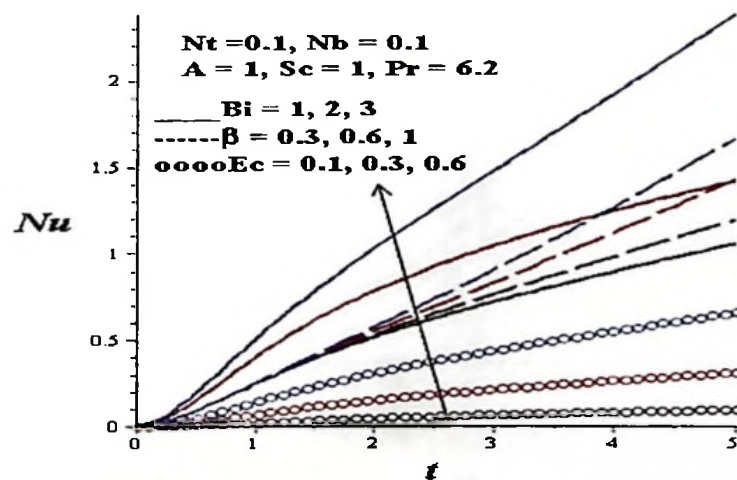


Figure 2.19: Nusselt number profiles

2.5.5 Effects of parameter variation on entropy generation rate

Figures 2.20-2.26 illustrate the effect of parameter variation on entropy generation rate across the channel. From Figures 2.20-2.21, the results revealed that the entropy generation rate increase with time and is minimum along the channel centreline and maximum at the walls. This may be attributed to the fact the entropy production depends on velocity, temperature and nanoparticles concentration gradients which vanish along the channel centreline, leading to the minimum entropy generation within this region. Moreover, increase in Biot number decreases the entropy generation within the channel but increases the entropy generation at the walls as shown in Figure 2.22. In Figures 2.23-2.24, we observed a general increase in entropy production across the channel with increasing viscous heating and a decrease in the nanofluid viscosity. Similar trend is observed in Figure 2.25 with increasing entropy production as the pressure gradient increases. This is because, mixtures of nanoparticles in the fluid with different responses to the pressure gradient increases velocity gradient, consequently, entropy generation rate increases. Figure 2.26 shows that an increase in thermophoresis effect due to temperature gradient increases the entropy generation rate within the channel and at the walls.

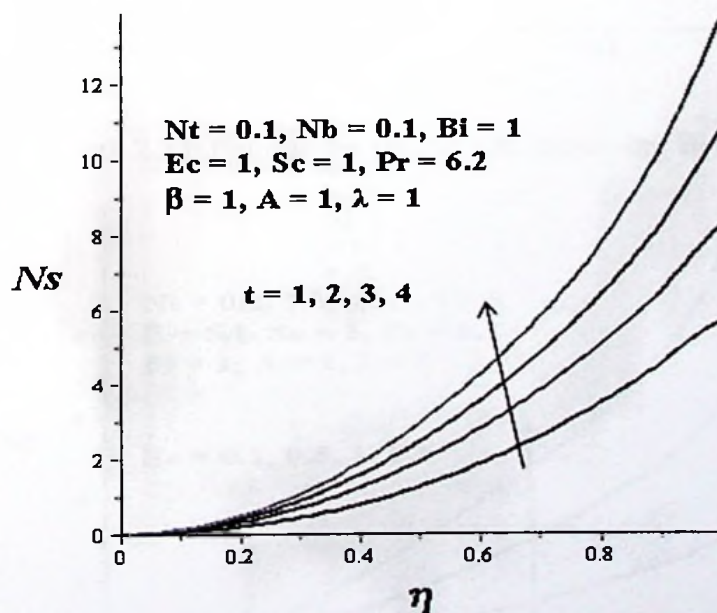


Figure 2.20: Entropy generation with increasing time

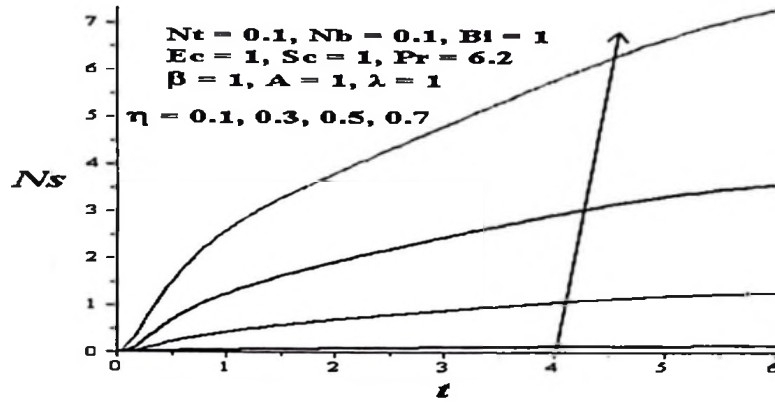


Figure 2.21: Entropy generation with increasing time

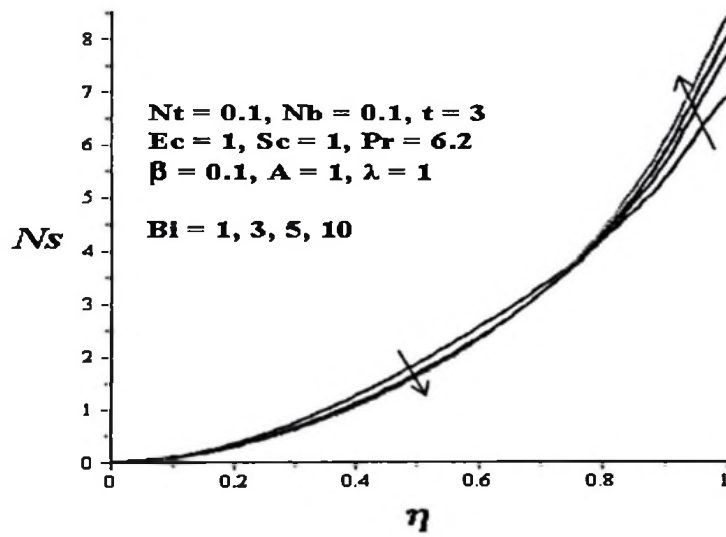


Figure 2.22: Entropy generation with increasing Bi

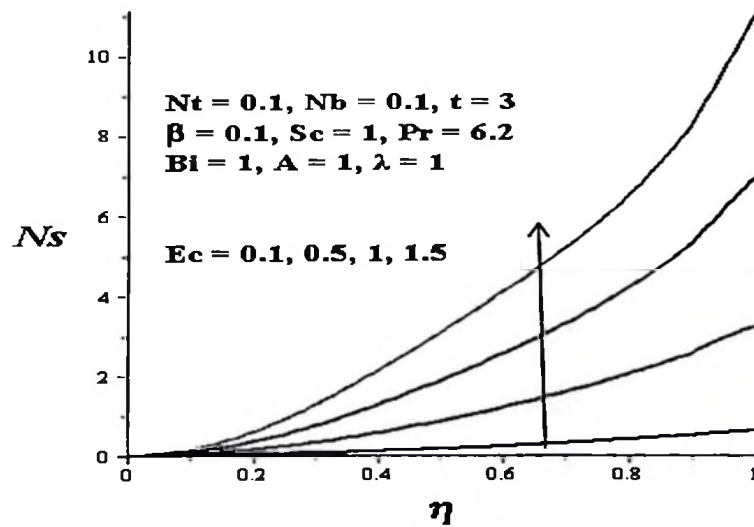


Figure 2.23: Entropy generation with increasing Ec

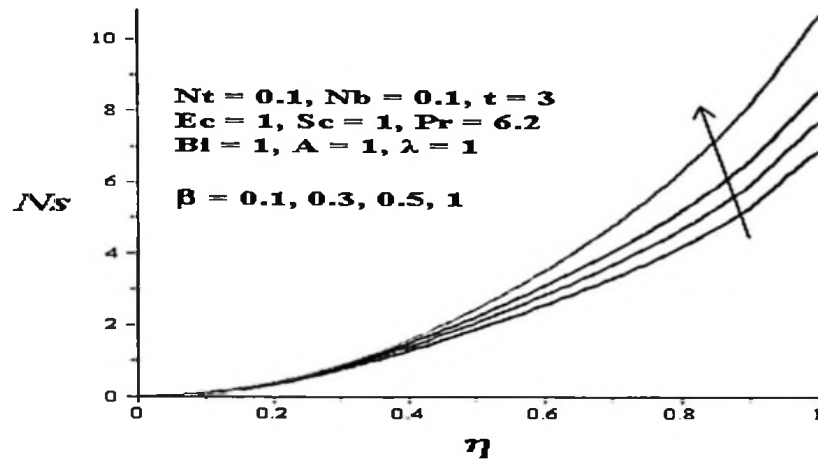


Figure 2.24: Entropy generation with increasing β

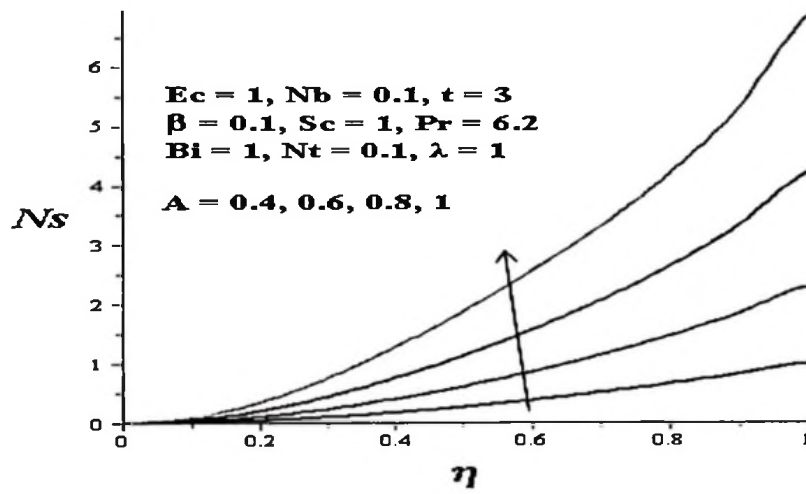


Figure 2.25: Entropy generation with increasing A

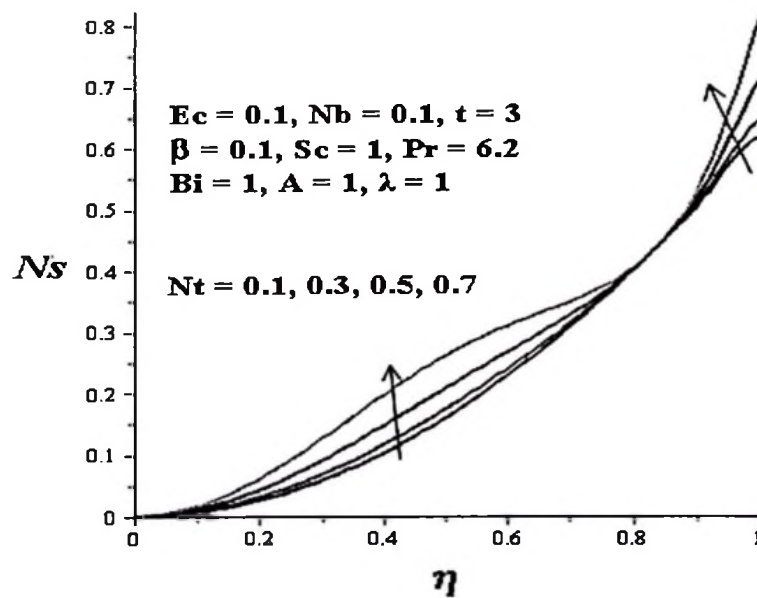


Figure 2.26: Entropy generation with increasing Nt

2.5.6 Effects of parameter variation on Bejan number

The variation in the Bejan number with time and the transverse distance is shown in Figures 2.27–2.35 for different parameters. In Figures 2.27–2.28, the results showed that Bejan number increases with time within the channel and at the walls. Moreover, maximum value of Bejan number is noticed along the channel centreline region as compared to the walls. Clearly, increasing Bejan number indicates a rise in the dominant effects of heat transfer and nanoparticles mass transfer irreversibility along the centreline region and at the walls. The results illustrate that a region very close to the walls exists where the Bejan number is zero and the irreversibility is dominated by the fluid friction. Figure 2.29 shows that the Bejan number decreases along the centreline region and increases near the walls with a rise in convective cooling, consequently, the dominant effect of fluid friction irreversibility increases along the centreline region while the heat and mass transfer irreversibilities effect dominates along the walls. In Figures 2.30–2.34, we observed that the Bejan number increases along the centreline region and at the walls with an increase in the parameter values of β , Ec , λ , Nt and A . This implies that a decrease in nanofluid viscosity coupled with combined increase in the viscous heating, thermophoresis and pressure gradient may enhance the dominant effect of heat and mass transfer irreversibilities along the centreline region and at the walls.

As the Brownian motion parameter Nb increases, the dominant effects of fluid friction irreversibility are enhanced both along the channel centreline region and at the walls as illustrated in Figure 2.35.

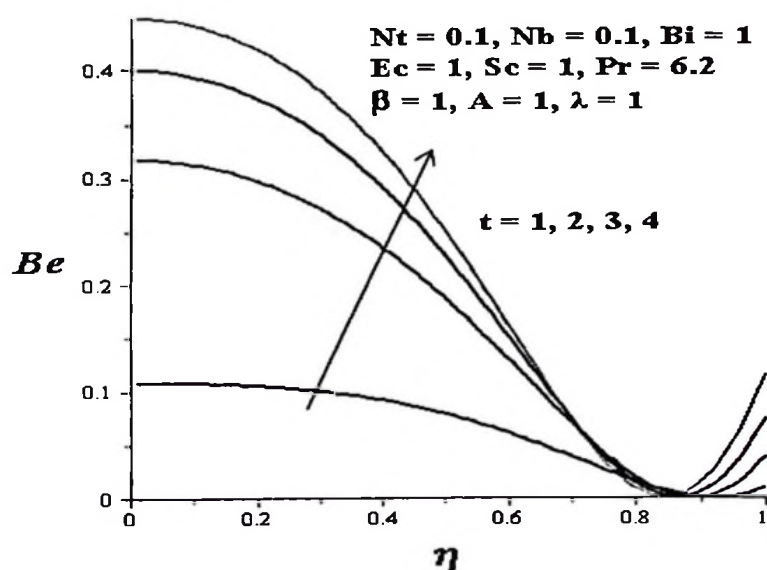


Figure 2.27: Bejan number with increasing time

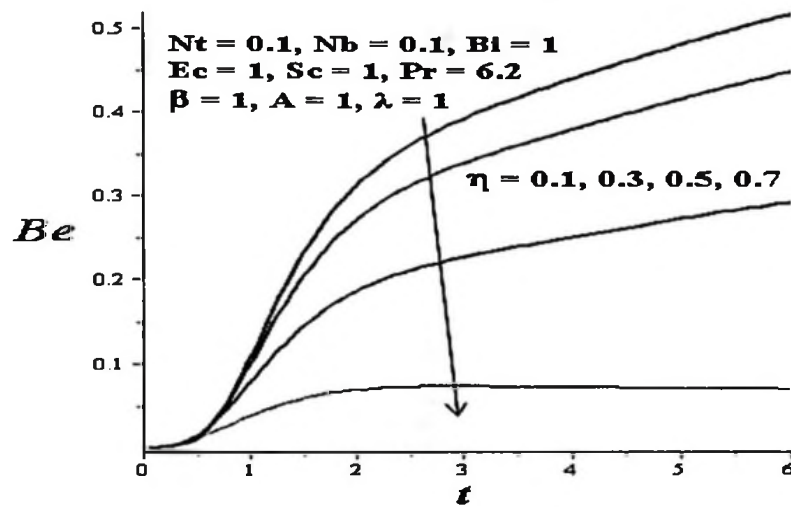


Figure 2.28: Bejan number with increasing time

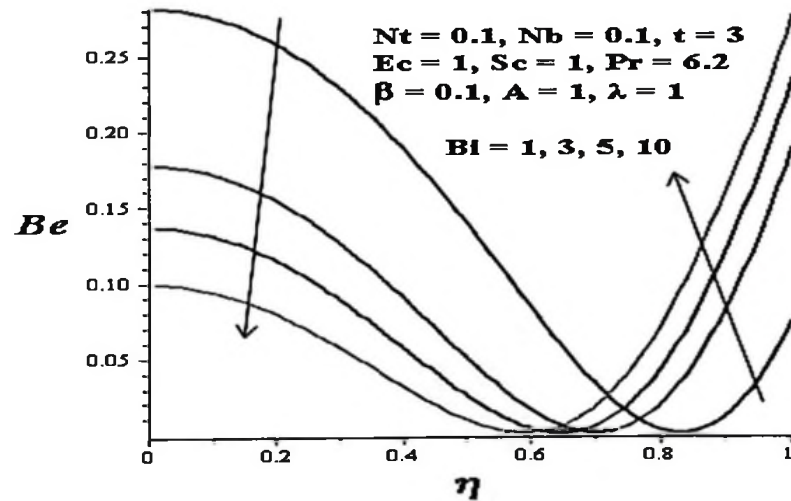


Figure 2.29: Bejan number with increasing Bi

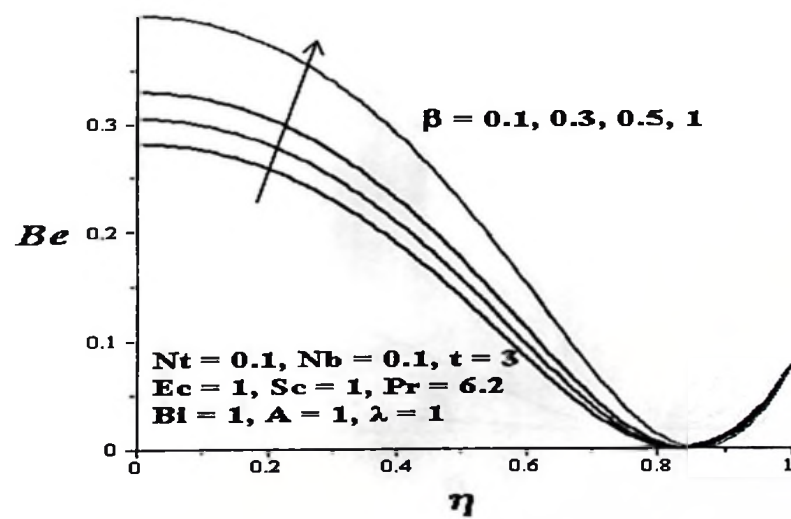


Figure 2.30: Bejan number with increasing β

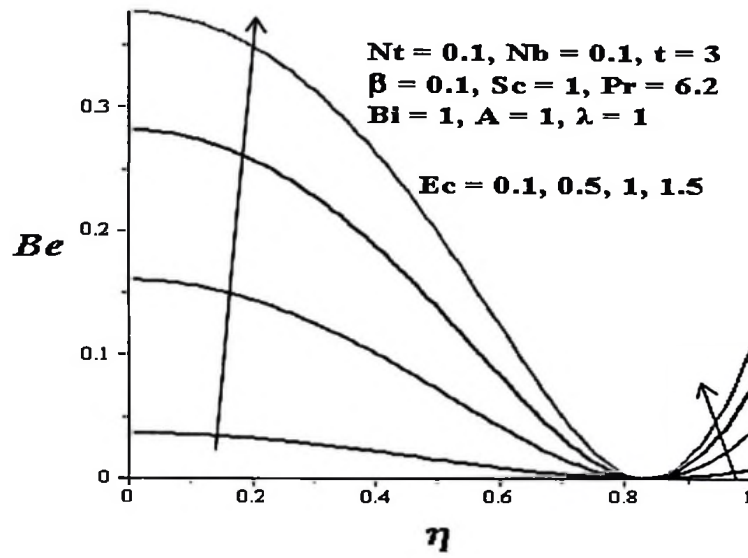


Figure 2.31: Bejan number with increasing Ec

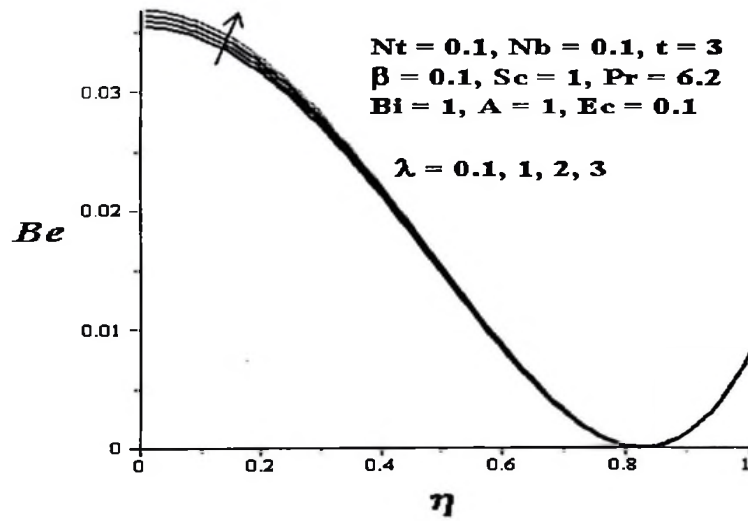


Figure 2.32: Bejan number with increasing λ

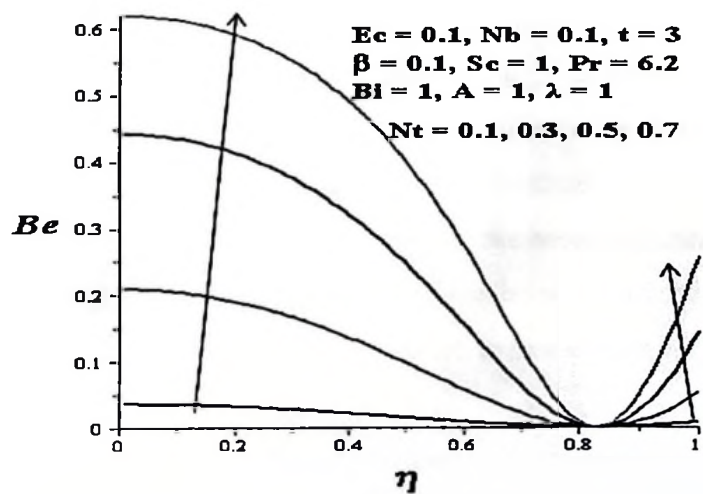


Figure 2.33: Bejan number with increasing Nt

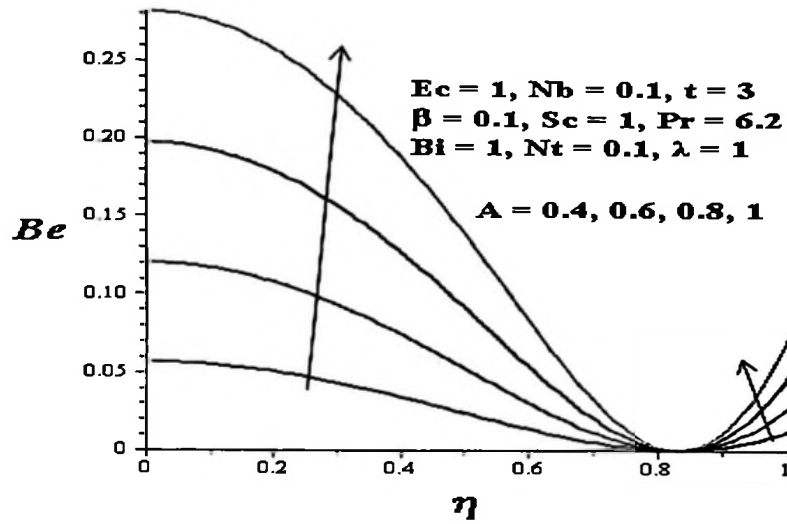


Figure 2.34: Bejan number with increasing A

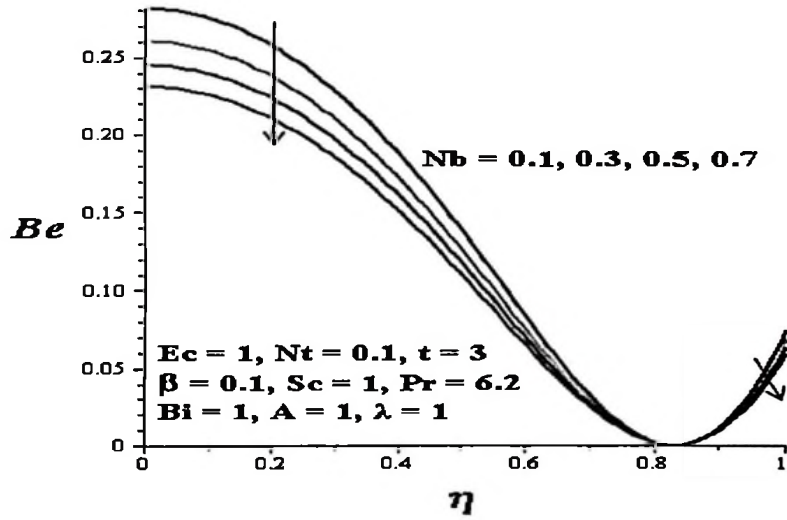


Figure 2.35: Bejan number with increasing Nb

2.6 Conclusions

The flow structure, heat transfer and entropy generation in unsteady channel flow of a variable viscosity water based nanofluids with convective heat exchange with the ambient at the walls are numerically investigated. Using a semi discretization finite difference method together with Runge-Kutta Fehlberg integration scheme, the model nonlinear initial boundary value problem is tackled. Some of the results obtained can be summarized as follows:

- The nanofluid velocity and temperature profiles increase with an increase in t , β , Ec but decreases with an increase in Bi .
- The nanoparticles concentration increases along the centreline region and decrease near the walls with an increase in t , β , Ec , Nt . However, an increase in Bi and Nb

causes a decrease in nanoparticles concentration along the centreline region and concentration increase near the walls.

- The skin friction increases with t , β , Ec , Nt and A but decreases with Ec and Nt . The Nusselt number increases with t , Ec , Bi and β .
- Entropy generation rate generally increases with t , Ec , β , A , Nt . Increase in Bi increase entropy generation at the walls but decreases entropy generation within the channel.
- Bejan number within the centreline region and at the walls increases with t , Ec , β , A , Nt and λ , consequently, the dominant effects of heat transfer and nanoparticles mass transfer irreversibilities increase.

Finally, from the above, we conclude that with careful combination of parameter values, the entropy production within the channel flow of variable viscosity water base nanofluid in the presence of convective cooling can be minimised.

CHAPTER THREE

Second Law Analysis of Buoyancy Driven Unsteady Channel Flow of Nanofluids with Convective Cooling²

Abstract

We investigate the combined effects of buoyancy force and convective cooling on entropy generation in unsteady channel flow of water based nanofluids containing Copper (Cu) and Alumina (Al_2O_3) as nanoparticles. Both first and second laws of thermodynamics are utilised to analyse the model problem. Using a semi discretization finite difference method together with Runge-Kutta Fehlberg integration scheme, the governing partial differential equations are solved numerically. Graphical results on the effects of parameter variation on velocity, temperature, skin friction, Nusselt number, entropy generation rate, irreversibility ratio and Bejan number are presented and discussed.

Keywords: Channel flow; Nanofluids; Buoyancy force; Heat transfer; Entropy generation; water; Copper; Alumina

3.1 Introduction

The knowledge of buoyancy driven flow and heat transfer in a vertical channel has many significant engineering and industrial applications; for example, geothermal engineering, solar-collectors, petroleum reservoirs, thermal insulation of buildings, nuclear waste repositories, electrical and microelectronic equipment containers. Ostrach (1972) and Khalifa (2001) presented a review of heat transfer due to natural convection. Yang *et al* (2012) studied forced convection in a channel with transverse fins. The problem of unsteady natural convection flow between two vertical parallel plates with one plate isothermally heated and the other thermally insulated was numerically studied by Jha and Ajibade (2010). Lee *et al* (2012) developed a computational model to investigate the cooling effect on the microchip of synthetic jet interacting with a cross-flow in a micro-channel. Meanwhile, engineering

²This chapter is based on the paper:

Mkwizu, M. H., Makinde, O. D., and Nkansah-Gyekye, Y. (2015). Second law analysis of buoyancy driven unsteady channel flow of nanofluids with convective cooling. *Applied and Computational Mathematics*, Vol. 4, No. 3, pp. 100-115, ISSN: 2328-5605 (Print); ISSN: 2328-5613.

applications of conventional heat transfer fluids such as water, ethylene glycol, and engine oil are limited due to their low thermal properties. A potential solution to improve these thermal properties is to add nanoparticles into the conventional fluids, hence forming so-called nanofluids (Choi, 1995). Recently, much attention has been paid to this new type of composite material, due to its enhanced properties and behaviour associated with heat transfer. Therefore when applied to heat transfer system, nanofluids are expected to enhance heat transfer compared with conventional liquids. Anoop *et al* (2009) conducted an experimental investigation for a convective heat transfer characteristics, in the developing region of a tube flow, with alumina-water nanofluid. They found that the enhancement of heat transfer coefficient of alumina nanofluids depended on particle sizes and the convective heat transfer coefficient of nanofluids was enhanced with increasing nanoparticle concentration. Khanafer *et al* (2003) presented a theoretical analysis for buoyancy-driven heat transfer enhancement in a two-dimensional enclosure utilizing nanofluids. Abu-Nada (2008) reported the application of nanofluids for heat transfer enhancement of separated flow encountered in a backward facing step. Mutuku-Njane and Makinde (2014) conducted a numerical study on the effects of magnetic field on nanofluid flow and heat transfer over a permeable vertical plate with convective cooling. Grosan and Pop (2012) presented a numerical solution for the problems of fully developed mixed convection in a vertical channel filled with nanofluids.

Moreover, all thermo-nanofluidic processes involve irreversibilities and therefore incur an efficiency loss. In practice, the extent of these irreversibilities can be measured by the entropy generation rate. The pioneer work on entropy generation in flow systems was conducted by Bejan Bejan (1982) and Bejan (1996). He showed that the engineering design of a flow and thermal systems could be improved through minimizing the entropy generation. A lot of literature is available relating to the study of entropy generation effects in pure fluids with different geometrical configurations and situations Makinde and Aziz (2010). There are only a few studies that consider the second thermodynamic laws in the presence of nanofluids. The entropy generation and natural convection in a square cavity with a vertical heat source which is filled with copper–water nanofluid was studied by Shahi *et al* (2011). They found that the entropy generation decreases with the solid volume fraction. Mahmoudi *et al* (2012) conducted a numerical study on the entropy generation due to natural convection cooling of a nanofluid in a partially open cavity. Their results showed that the presence of nanoparticles is less effective in enhancement of the Nusselt number and in the reduction of the entropy

generation. Makinde *et al* (2013) numerically studied the entropy production and irreversibility due to flow and heat transfer of nanofluids over a moving flat surface. It was found that the entropy generation can be minimized by appropriate combination of parameter values together with nanoparticles volume fraction.

Mkwizu and Makinde (2015) did a research on entropy generation in a variable viscosity channel flow of nanofluids with convective cooling. Results revealed that, general increase in entropy production across the channel with increasing viscous heating, pressure gradient and a decrease in nanofluid viscosity.

The main originality of the present work is the second law analysis due to unsteady natural convection in a vertical channel filled by Cu-water and Al_2O_3 -water nanofluids in the presence of convective cooling at the channel walls. To the best of authors' knowledge, no such a study which considers this problem has been reported in the literature yet. The numerical analysis has been performed for a wide range of Grashof number, solid volume fraction parameter, Biot number and Eckert number. The results are presented in the form of velocity and temperature profiles, skin friction and Nusselt number, entropy generation and Bejan number. Pertinent results are discussed with the help of graphs and tables.

3.1 Mathematical Model

Consider unsteady laminar flow of viscous incompressible nanofluids containing Copper (Cu) and Alumina (Al_2O_3) as nanoparticles through a vertical channel. It is assumed that the channel walls exchange heat with the ambient surrounding following the Newton's law of cooling. Take a Cartesian coordinate system (x, y) where x lies along the centre of the channel, y is the distance measured in the normal direction as depicted in Figure 3.1 below;

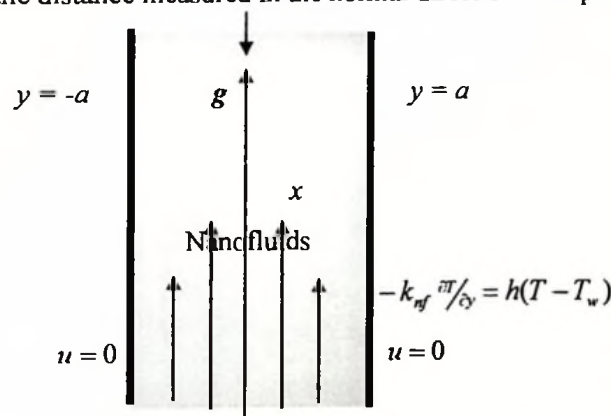


Figure 3.1: Schematic diagram of the problem under consideration

In accordance with the Boussinesq approximation, all the fluid properties are assumed to be constant except the density variation with temperature in the buoyancy force term. The Navier-Stokes nanofluids momentum and energy balance equation in one dimension under the Boussinesq approximation for the transient channel flow can be written as

$$\frac{\partial u}{\partial \bar{t}} = -\frac{1}{\rho_{nf}} \frac{\partial P}{\partial x} + \frac{\mu_{nf}}{\rho_{nf}} \frac{\partial^2 u}{\partial y^2} + \frac{g\beta_{nf}}{\rho_{nf}} (T - T_w), \quad (3.1)$$

$$\frac{\partial T}{\partial \bar{t}} = \alpha_{nf} \frac{\partial^2 T}{\partial y^2} + \frac{\alpha_{nf} \mu_{nf}}{k_{nf}} \left(\frac{\partial u}{\partial y} \right)^2, \quad (3.2)$$

where u is the nanofluid velocity in the x -direction, T is the temperature of the nanofluid, P is the nanofluid pressure, \bar{t} is the time, a is the channel half width, T_w is the ambient temperature, μ_{nf} is the dynamic viscosity of the nanofluid, k_{nf} is the nanofluid thermal conductivity, ρ_{nf} is the density of the nanofluid, β_{nf} is volumetric expansion coefficient of the nanofluids and α_{nf} is the thermal diffusivity of the nanofluid which are given by Khanafer *et al* (2003)

$$\begin{aligned} \mu_{nf} &= \frac{\mu_f}{(1-\phi)^{2.5}}, \quad \rho_{nf} = (1-\phi)\rho_f + \phi\rho_s, \\ \alpha_{nf} &= \frac{k_{nf}}{(\rho c_p)_{nf}}, \quad \tau = \frac{(\rho c_p)_s}{(\rho c_p)_f}, \quad \frac{k_{nf}}{k_f} = \frac{(k_s + 2k_f) - 2\phi(k_f - k_s)}{(k_s + 2k_f) + \phi(k_f - k_s)}, \\ (\rho c_p)_{nf} &= (1-\phi)(\rho c_p)_f + \phi(\rho c_p)_s, \quad \beta_{nf} = (1-\phi)\rho_f\beta_f + \phi\rho_s\beta_s \end{aligned} \quad (3.3)$$

The nanoparticles volume fraction is represented by ϕ ($\phi = 0$ correspond to a regular fluid), ρ_f and ρ_s are the densities of the base fluid and the nanoparticle respectively, β_f and β_s are the thermal expansion coefficients of the base fluid and the nanoparticle respectively, k_f and k_s are the thermal conductivities of the base fluid and the nanoparticles respectively, $(\rho c_p)_f$ and $(\rho c_p)_s$ are the heat capacitance of the base fluid and the nanoparticle respectively. It worth mentioning that the use of the above expression for k_{nf} , is restricted to spherical nanoparticles given by Maxwell (1904) and does not account for other shapes of nanoparticles. Also, Brinkman (1952) approximation has been employed to approximate the effective viscosity of the nanofluid μ_{nf} as viscosity of a base fluid μ_f containing dilute suspension of fine spherical particles. The initial and boundary conditions are given as follows:

$$u(y,0) = 0, \quad T(y,0) = T_w, \quad (3.4)$$

$$\frac{\partial u}{\partial y}(0,\bar{t}) = \frac{\partial T}{\partial y}(0,\bar{t}) = 0, \quad (\text{axial-symmetric conditions}) \quad (3.5)$$

$$u(a,\bar{t}) = 0, \quad -k_{nf} \frac{\partial T}{\partial y}(a,\bar{t}) = h(T(a,\bar{t}) - T_w), \quad (3.6)$$

where T_w is the ambient temperature. Table 1 below presents thermo physical properties of water, copper and alumina at the reference temperature.

Table 3.1: Thermophysical properties of the fluid phase (water) and nanoparticles

Physical properties	Fluid phase (water)	Cu	Al ₂ O ₃
c_p (J/kg K)	4179	385	765
ρ (kg/m ³)	997.1	8933	3970
k (W/m K)	0.613	401	40
β (K ⁻¹)	21×10^{-5}	1.67×10^{-5}	0.85×10^{-5}

We introduce the dimensionless variables and parameters as follows:

$$\left. \begin{aligned} \theta &= \frac{T - T_w}{T_w}, \quad W = \frac{ua}{v_f}, \quad t = \frac{\bar{t} v_f}{a^2}, \quad v_f = \frac{\mu_f}{\rho_f}, \quad Bi = \frac{ha}{k_f}, \quad \bar{P} = \frac{\rho_f a^2 P}{\mu_f^2}, \\ A &= -\frac{\partial \bar{P}}{\partial X}, \quad X = \frac{x}{a}, \quad Gr = \frac{\beta_f g T_w a^3}{v_f^2}, \quad \eta = \frac{y}{a}, \quad Pr = \frac{\mu_f c_{pf}}{k_f}, \quad Ec = \frac{v_f^2}{c_{pf} T_w a^2}, \\ \tau &= \frac{(\rho c_p)_s}{(\rho c_p)_f}, \quad m = \frac{(k_s + 2k_f) + \phi(k_f - k_s)}{(k_s + 2k_f) - 2\phi(k_f - k_s)}, \quad n = \frac{(1 - \phi + \phi \beta_s \rho_s / \beta_f \rho_f)}{(1 - \phi + \phi \rho_s / \rho_f)} \end{aligned} \right\}. \quad (3.7)$$

The dimensionless governing equations together with the appropriate initial and boundary conditions can be written as:

$$\frac{\partial W}{\partial t} = \frac{A}{(1 - \phi + \phi \rho_s / \rho_f)} + \frac{1}{(1 - \phi + \phi \rho_s / \rho_f)(1 - \phi)^{2.5}} \frac{\partial^2 W}{\partial \eta^2} + n Gr \theta, \quad (3.8)$$

$$Pr \frac{\partial \theta}{\partial t} = \frac{1}{m(1 - \phi + \phi \tau)} \frac{\partial^2 \theta}{\partial \eta^2} + \frac{Pr Ec}{(1 - \phi)^{2.5}(1 - \phi + \phi \tau)} \left(\frac{\partial W}{\partial \eta} \right)^2, \quad (3.9)$$

with

$$W(\eta,0) = 0, \quad \theta(\eta,0) = 0 \quad (3.10)$$

$$\frac{\partial W}{\partial \eta}(0,t) = \frac{\partial \theta}{\partial \eta}(0,t) = 0 \quad (3.11)$$

$$W(1,t) = 0, \quad \frac{\partial \theta}{\partial \eta}(1,t) = -mBi\theta(1,t), \quad (3.12)$$

where Bi is the Biot number, Gr is the Grashof number, Pr is the Prandtl number, Ec is the Eckert number and A is the pressure gradient parameter. The quantities of practical interest in this study are the skin friction coefficient C_f and the local Nusselt number Nu are defined as

$$C_f = \frac{a^2 \tau_w}{\rho_f \nu_f^2}, \quad Nu = \frac{a q_w}{k_f T_w}, \quad (3.13)$$

where τ_w is the wall shear stress and q_w is the heat flux at the channel walls given by

$$\tau_w = -\mu_{nf} \left. \frac{\partial u}{\partial y} \right|_{y=a}, \quad q_w = -k_{nf} \left. \frac{\partial T}{\partial y} \right|_{y=a} \quad (3.14)$$

Substituting equations (3.14) into (3.13), we obtain

$$\left. \begin{aligned} C_f &= -\frac{1}{(1-\phi)^{2.5}} \frac{\partial W}{\partial \eta} \\ Nu &= -\frac{1}{m} \frac{\partial \theta}{\partial \eta} \end{aligned} \right\} \text{at } \eta = 1. \quad (3.15)$$

3.3 Entropy Analysis

The second law of thermodynamics is an important tool to scrutinize the irreversibility effects due to flow and heat transfer. Thermodynamic irreversibility is closely related to entropy production. Convection process involving channel flow of nanofluids is inherently irreversible due to the exchange of energy and momentum, within the nanofluid and at solid boundaries. Following Woods (1975), the local volumetric rate of entropy generation is given by

$$S'' = \frac{k_{nf}}{T_w^2} \left(\frac{\partial T}{\partial y} \right)^2 + \frac{\mu_{nf}}{T_w} \left(\frac{\partial u}{\partial y} \right)^2. \quad (3.16)$$

The first term in equation (3.16) is the irreversibility due to heat transfer while the second term is the entropy generation due to fluid friction. Using equation (3.7), we express the entropy generation number in dimensionless form as,

$$N_s = \frac{a^2 S'''}{k_f} = \frac{1}{m} \left(\frac{\partial \theta}{\partial \eta} \right)^2 + \frac{Br}{(1-\phi)^{2.5}} \left(\frac{\partial W}{\partial \eta} \right)^2, \quad (3.17)$$

where $Br = Ec Pr$ is the Brinkmann number. Let

$$N_1 = \frac{1}{m} \left(\frac{\partial \theta}{\partial \eta} \right)^2, \quad N_2 = \frac{Br}{(1-\phi)^{2.5}} \left(\frac{\partial W}{\partial \eta} \right)^2, \quad (3.18)$$

The irreversibility distribution ratio is define as $\Phi = N_2/N_1$. Heat transfer irreversibility dominates for $0 \leq \Phi < 1$ and fluid friction irreversibility dominates when $\Phi > 1$. The contribution of both irreversibilities to entropy generation are equal when $\Phi = 1$. We define the Bejan numbers (Be) mathematically as

$$Be = \frac{N_1}{N_s} = \frac{1}{1 + \Phi}. \quad (3.19)$$

Equation (3.19) shows that the Bejan number ranges from 0 to 1. The zero value of the Bejan number corresponds to the limit where the irreversibility is dominated by the effect of fluid friction while $Be = 1$ is the limit where the irreversibility due to heat transfer dominates the flow system. The contribution of both heat transfer and fluid friction to irreversibility are the same when $Be = 0.5$.

3.4 Numerical Procedure

The nonlinear IBVP in equations (3.8)-(3.12) are solved numerically using a semi-discretization finite difference method known as method of lines Na (1979). We partition the spatial interval $0 \leq \eta \leq 1$ into N equal parts and define grid size $\Delta\eta = 1/N$ and grid points $\eta_i = (i-1)\Delta\eta$, $1 \leq i \leq N+1$. The discretization is based on a linear Cartesian mesh and uniform grid on which finite-differences are taken. The first and second spatial derivatives in equations (3.8)-(3.9) are approximated with second-order central finite differences.

Let $W_i(t)$ and $\theta_i(t)$ be approximation of $W(\eta_i, t)$ and $\theta(\eta_i, t)$, then the semi-discrete system for the problem becomes

$$\frac{dW_i}{dt} = \frac{A}{(1-\phi + \phi\rho_s/\rho_f)} + \frac{(W_{i+1} - 2W_i + W_{i-1}))}{(1-\phi + \phi\rho_s/\rho_f)(1-\phi)^{2.5}(\Delta\eta)^2} + nGr\theta_i, \quad (3.20)$$

$$Pr \frac{d\theta_i}{dt} = \frac{(\theta_{i+1} - 2\theta_i + \theta_{i-1}))}{m(1-\phi + \phi\tau)(\Delta\eta)^2} + \frac{Ec Pr}{(1-\phi + \phi\tau)(1-\phi)^{2.5}} \left(\frac{W_{i+1} - W_{i-1}}{2\Delta\eta} \right)^2, \quad (3.21)$$

with initial conditions

$$W_i(0) = \theta_i(0) = 0, \quad , \quad 1 \leq i \leq N+1 . \quad (3.22)$$

The equations corresponding to the first and last grid points are modified to incorporate the boundary conditions as follows

$$W_2 = W_1, \quad \theta_2 = \theta_1, \quad w_{N+1} = 0, \quad \theta_{N+1} = \theta_N(1 - mBi\Delta\eta), \quad (3.23)$$

Equations (3.20)-(3.23) is a system of first order ODEs with known initial conditions and can be easily solved iteratively using Runge-Kutta Fehlberg integration technique Na (1979) implemented on computer using MATLAB. From the process of numerical computation, the skin-friction coefficient and the Nusselt number in equation (3.15) are obtained and their numerical values are presented.

3.5 Results and Discussions

Pure water and water-based Newtonian nanofluids containing copper (*Cu*) and alumina (Al_2O_3) as nanoparticles are considered. The Prandtl number of the base fluid (water) is kept constant at 6.2 and the effect of solid volume fraction is investigated in the range of $0 \leq \phi \leq 0.3$. Numerical solution for the representative velocity field, temperature field, skin friction, Nusselt number, Entropy generation rate and Bejan number have been carried out by assigning some arbitrary chosen specific values to various thermophysical parameters controlling the flow system (see Figures 2-29). The detailed discussion and graphical representation of the results of above equations are reported in this section.

3.5.1 Effects of parameter variation on velocity profiles

Figures 3.2-3.3 depict the transient effects on the nanofluids velocity profiles. Generally, the velocity increases with time for a given set of parameter values until a steady state profile is achieved as shown in Figure 3.2. For instance the steady state velocity profile is attained at $\tau = 3.5$. Interestingly, the Al_2O_3 -water nanofluid tends to flow faster than Cu-water nanofluids as shown in Figure 3.3. This may be attributed to the high density of Cu nanoparticle as compare to Al_2O_3 nanoparticle. Moreover, the velocity profile is parabolic in nature with maximum value along the channel centreline and the minimum value at the walls. Figures 3.4-3.7 illustrates the effects of parameter variation on the velocity profiles with Cu-water as the working nanofluid. An increase in nanoparticles volume fraction causes a decrease in the velocity profile as shown in Figure 3.4. This is expected since both density and the dynamic

viscosity of the nanofluid increase with increasing nanoparticles volume fraction leading to decrease in the velocity. In Figures 3.5-3.7, a rise in the nanofluid velocity is observed with an increase in Grashof number, Eckert number and the pressure gradient parameter. As Gr increases, the thermal buoyancy effect increases due to temperature gradient, leading to an increase in velocity profile. Similar effect of increasing velocity results from increasing viscous dissipation within the flow system as Ec increases.

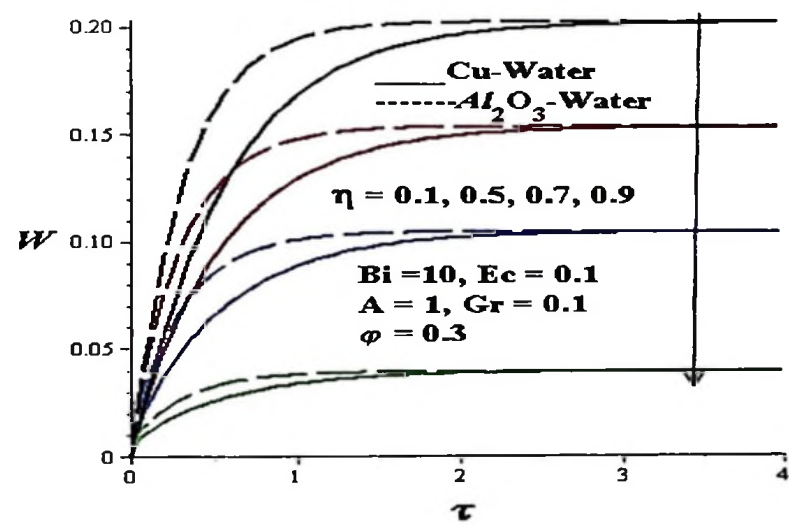


Figure 3.2: Nanofluids velocity profiles with increasing time

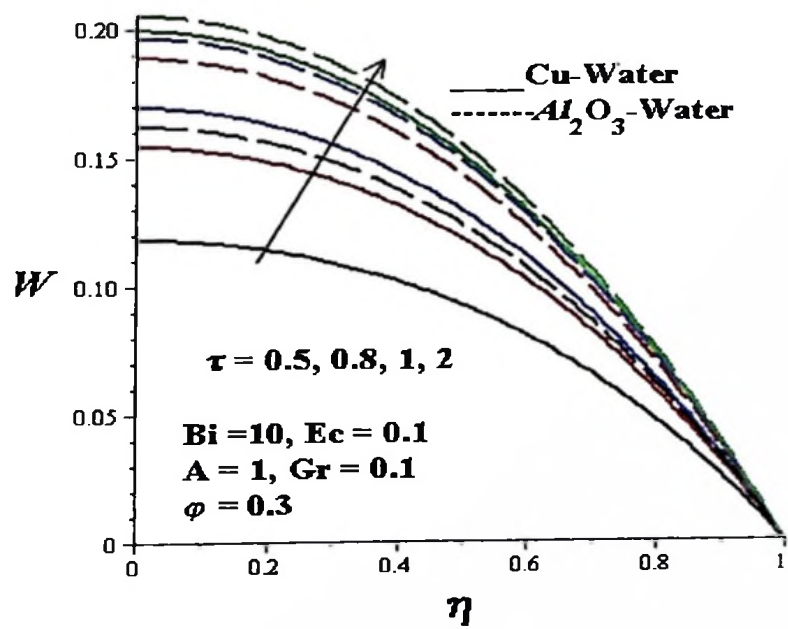


Figure 3.3: Nanofluids velocity profiles across the channel with increasing time

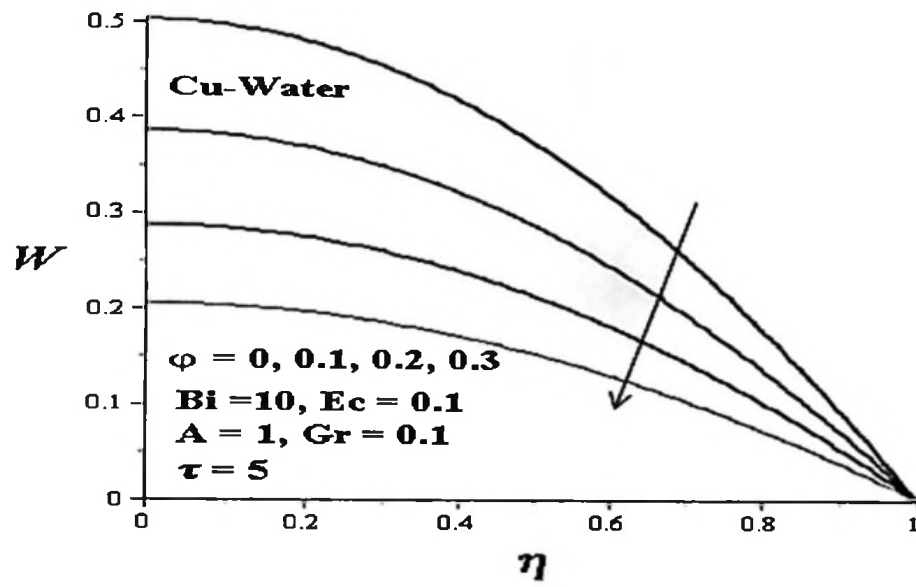


Figure 3.4: Nanofluid velocity profiles with increasing ϕ

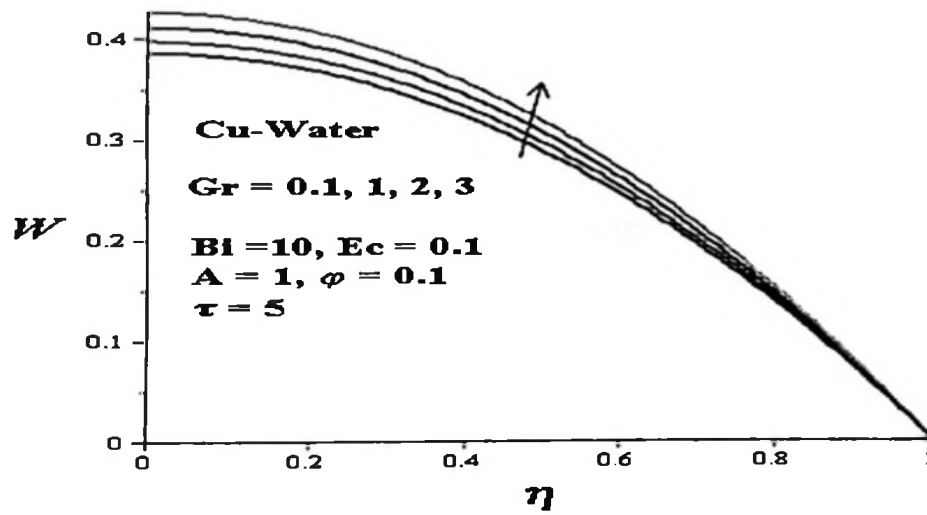


Figure 3.5: Nanofluid velocity profiles with increasing Gr

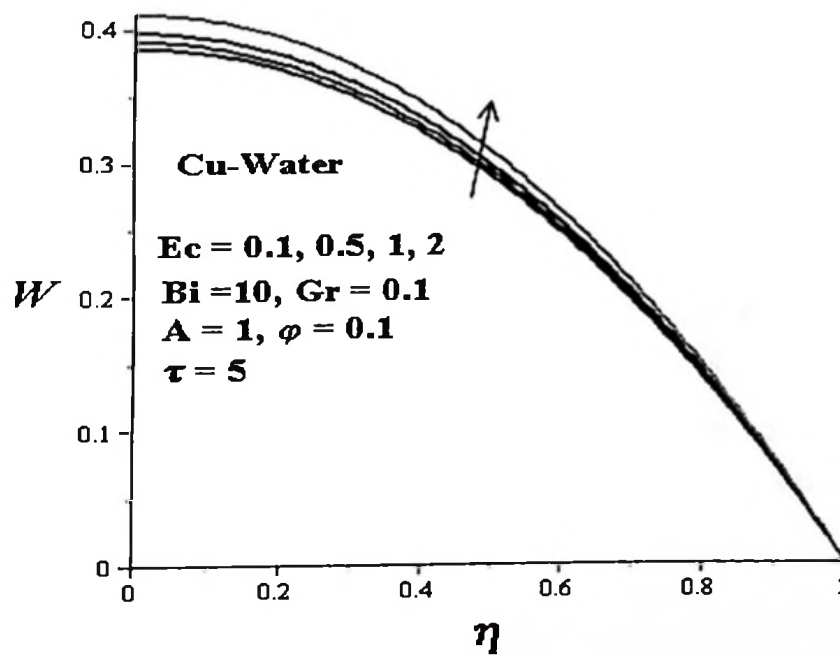


Figure 3.6: Nanofluid velocity profiles with increasing Ec

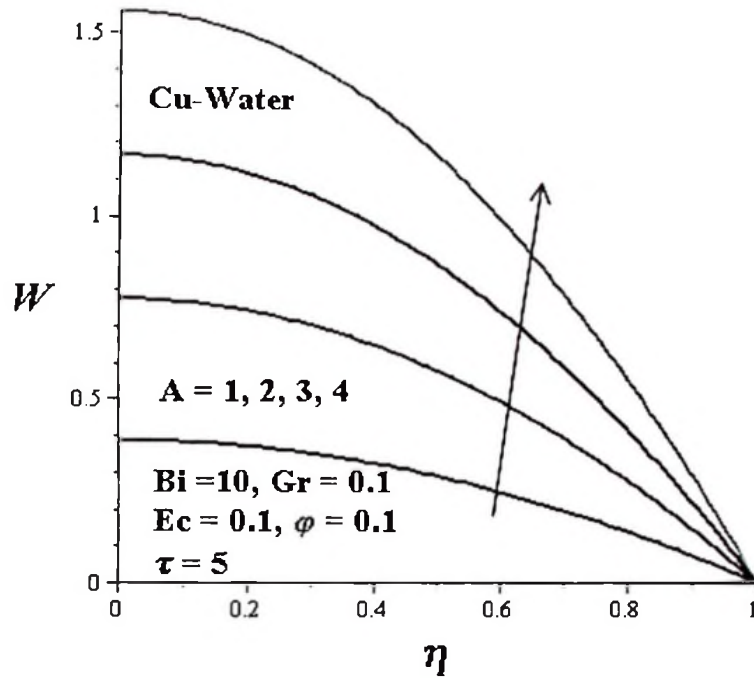


Figure 3.7: Nanofluid velocity profiles with increasing A

3.5.2 Effects of parameter variation on temperature profiles

In Figures 3.8-3.9, the transient effects on the nanofluids temperature profiles are displayed. The temperature increases with time for a given set of parameter values until a corresponding steady state profile is achieved as shown in Figure 3.2. The steady state temperature profile is attained at $\tau = 8$. It is noteworthy that the steady state velocity profile is attained earlier than that of temperature profile as shown in Figure 3.8. Interestingly, the temperature of Al_2O_3 -water nanofluid rises higher than that of Cu-water nanofluids as shown in Figure 3.9. Moreover, the temperature profile attains its maximum value within channel and the minimum value at the walls due to convective heat loss to the ambient. Figures 3.10-3.14 illustrates the effects of parameter variation on the temperature profiles with Cu-water as the working nanofluid. As the nanoparticles volume fraction increases, a decrease in the temperature profile is observed as shown in Figure 3.10. Similarly trend of a decrease in temperature is noticed with a rise in Biot number due to a convective cooling at the walls as shown in Figure 3.11. In Figures 3.12-3.14, a rise in the nanofluid temperature is observed with an increase in Grashof number, Eckert number and the pressure gradient parameter. This increase in temperature can be attributed to the combined effects of buoyancy force and viscous dissipation.

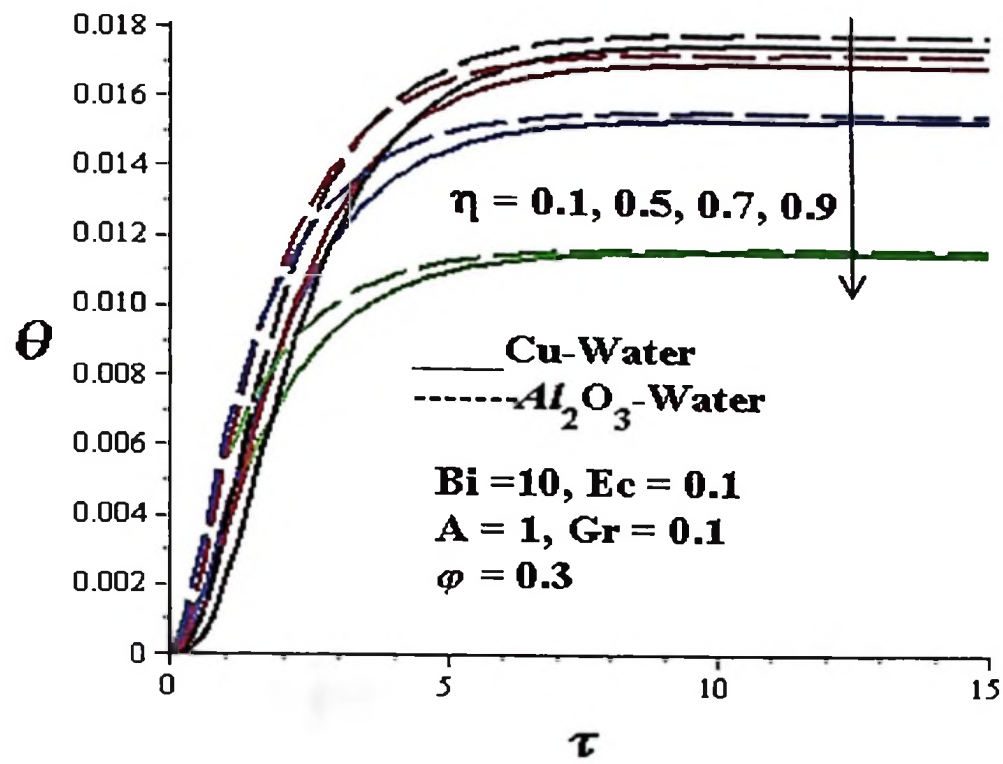


Figure 3.8: Nanofluids temperature profiles with increasing time

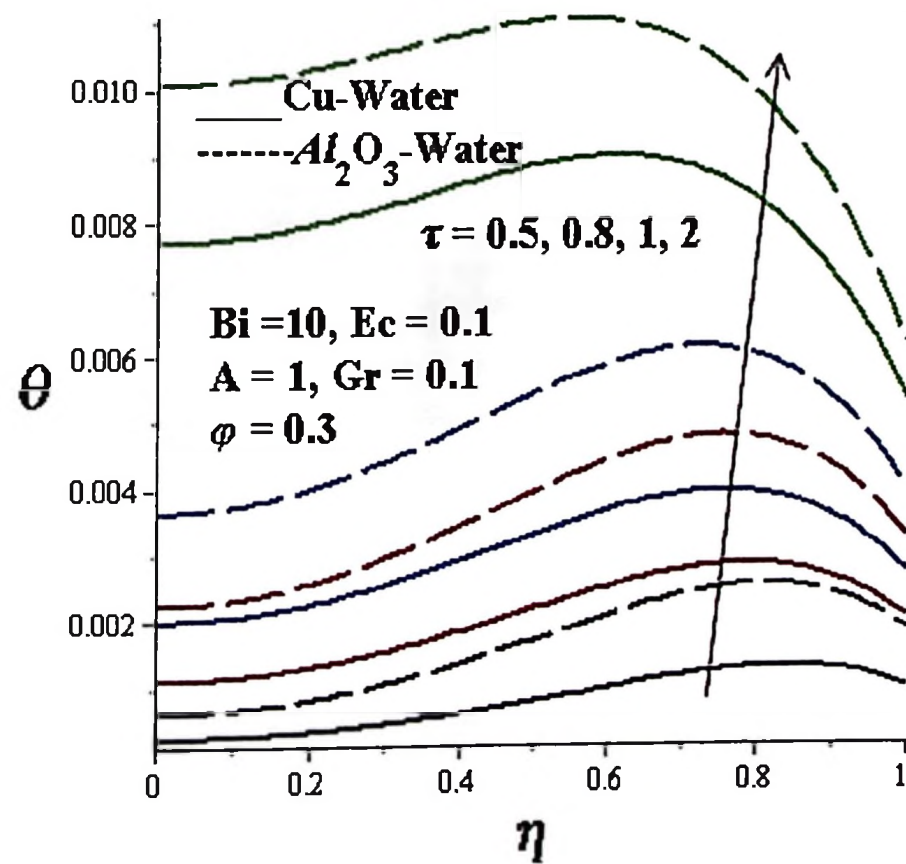


Figure 3.9: Nanofluids temperature profiles across the channel with increasing time

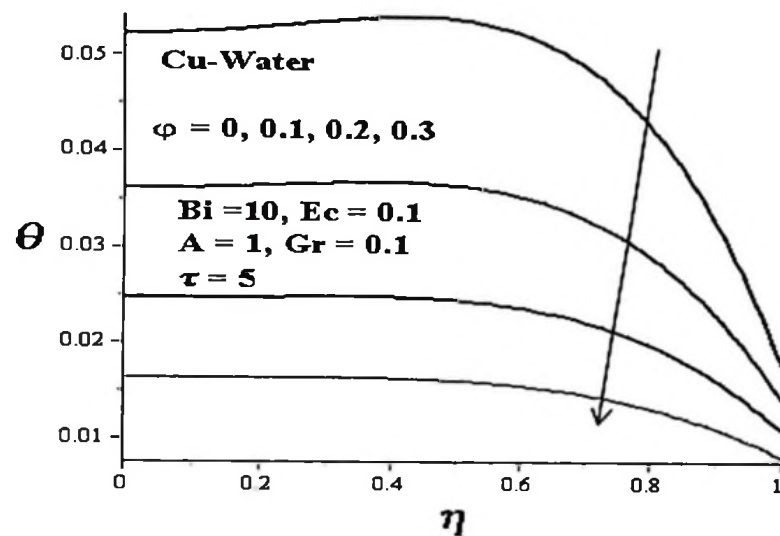


Figure 3.10: Nanofluid temperature profiles with increasing ϕ

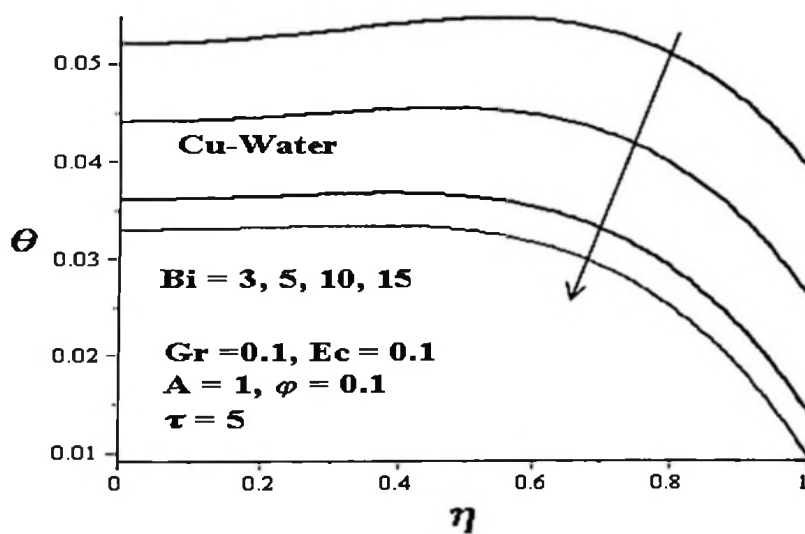


Figure 3.11: Nanofluid temperature profiles with increasing Bi

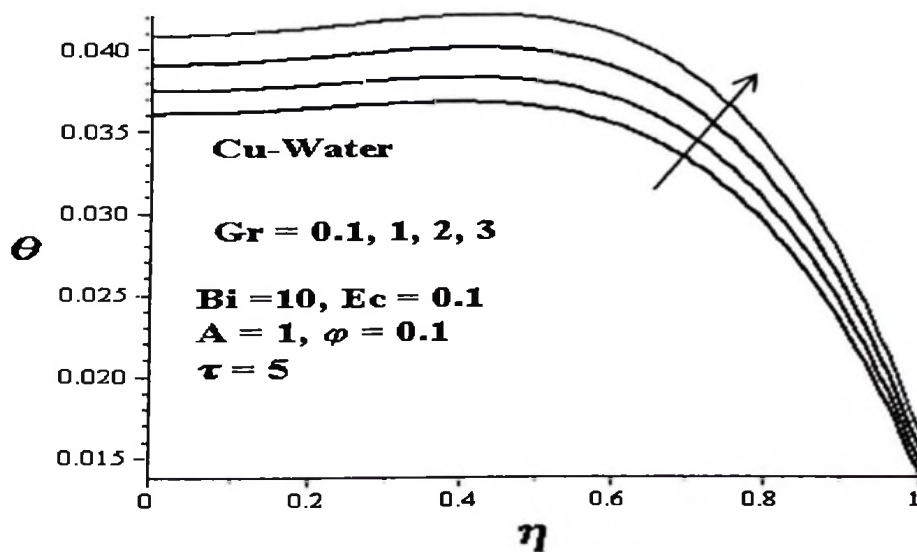


Figure 3.12: Nanofluid temperature profiles with increasing Gr

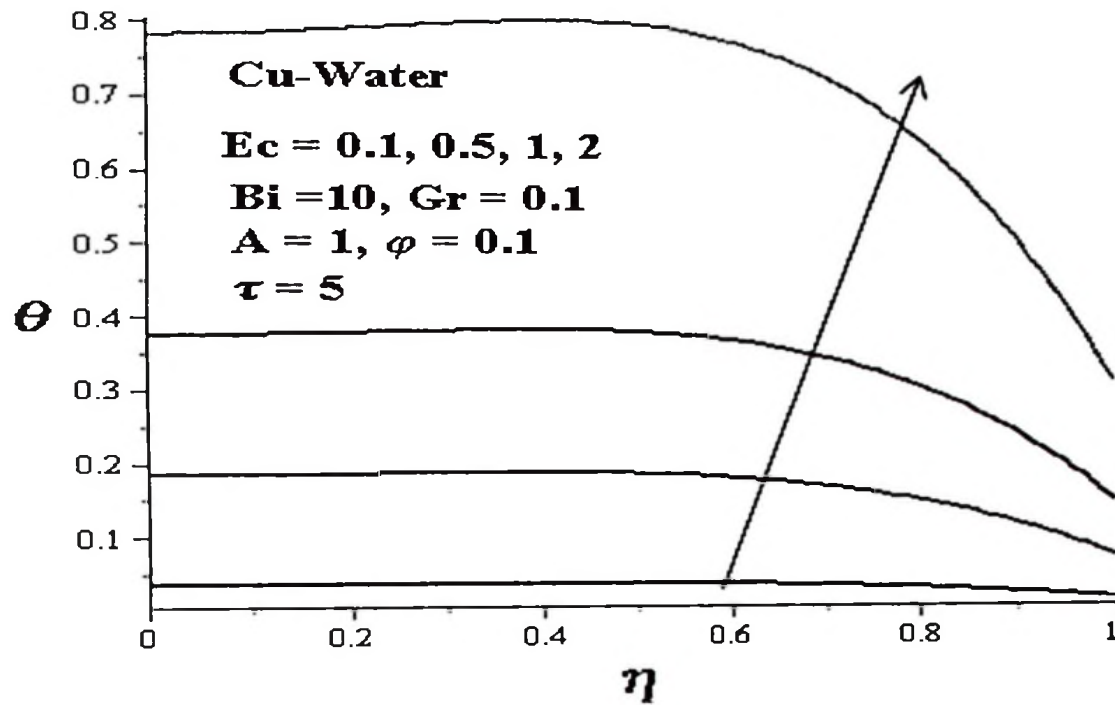


Figure 3.13: Nanofluid temperature profiles with increasing Ec

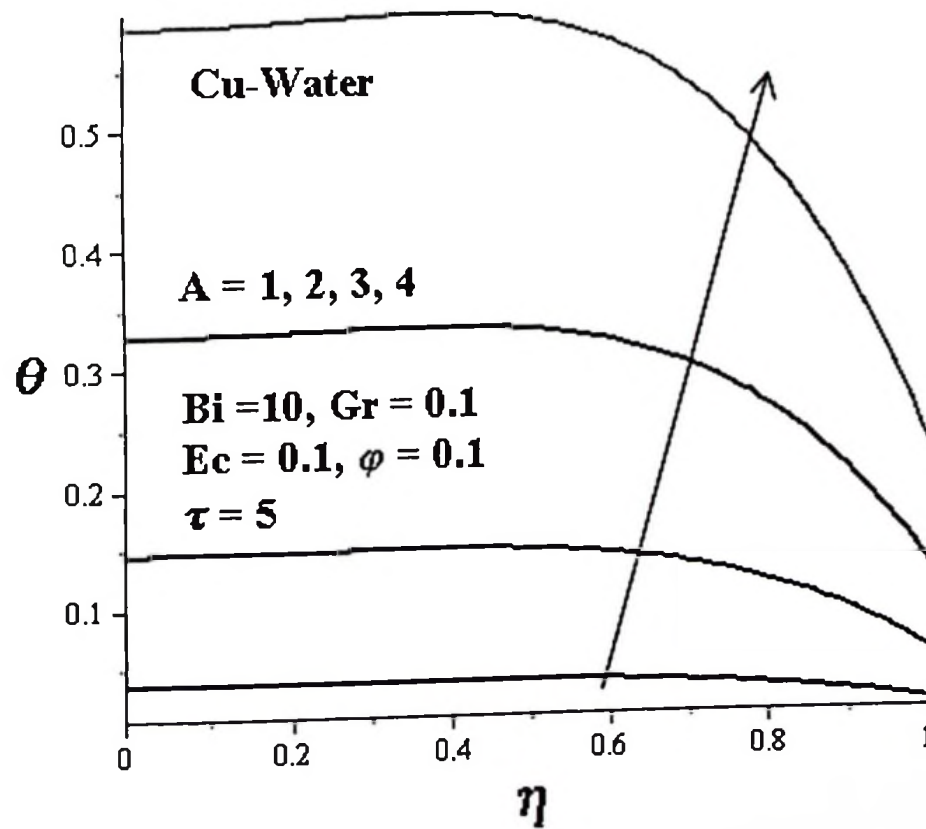


Figure 3.14: Nanofluid temperature profiles with increasing A

3.5.3 Skin friction and Nusselt number

Figures 3.15-3.18 illustrate the effects of parameter variation on skin friction and Nusselt number. In Figure 3.15, it is observed that the skin friction decreases with an increase in number. In Figure 3.15, it is observed that the skin friction decreases with an increase in nanoparticles volume fraction. This is due to a decrease in the velocity gradient at the channel walls. Moreover, the skin friction produced by Cu-water nanofluid is higher than the one

produced by Al_2O_3 -water nanofluid. Interestingly, the skin friction increases with an increase in buoyancy force and viscous dissipation (i.e. Gr , Ec) but decrease with increase in convective heat loss at the walls to the ambient (i.e. Bi) as illustrated in Figure 3.16. Figure 3.17 shows that the heat flux at the channel walls decreases with an increase in nanoparticles volume fraction due to a fall in the temperature gradient. The Nusselt number produced by Cu-water nanofluid is higher than that of Al_2O_3 -water nanofluid. Hence, Cu-water may serve as a better heat transfer nanofluid and compare to Al_2O_3 -water. Meanwhile, the Nusselt number increases with an increase in buoyancy force and viscous dissipation but decrease with increase in Biot number as illustrated in Figure 3.18. This may be attributed to an increase or a decrease in the temperature gradient at the walls with a rise in parameter values.

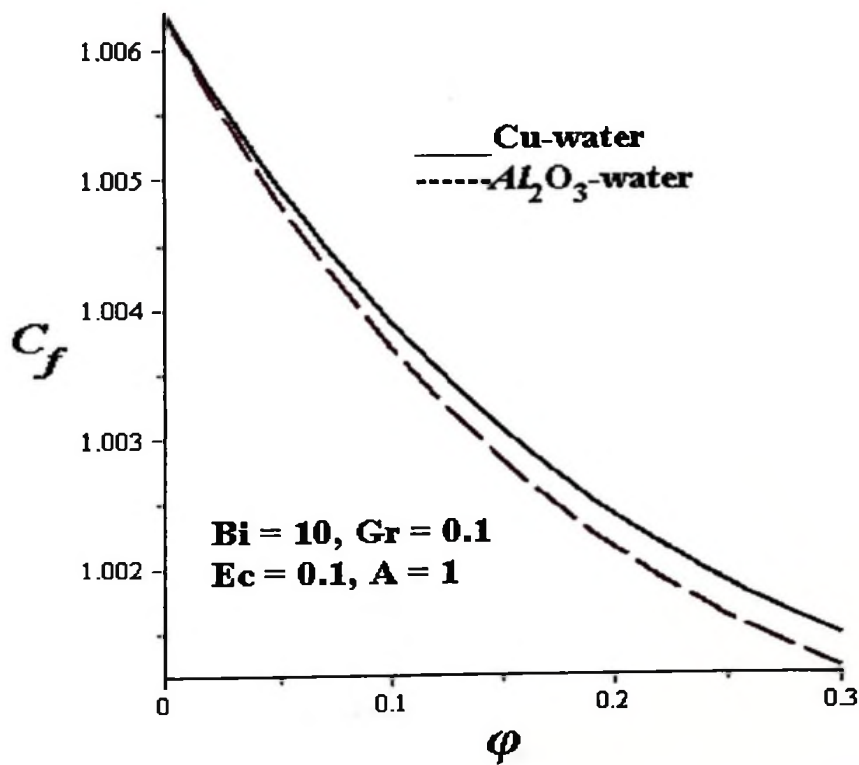


Figure 3.15: Skin friction with increasing ϕ

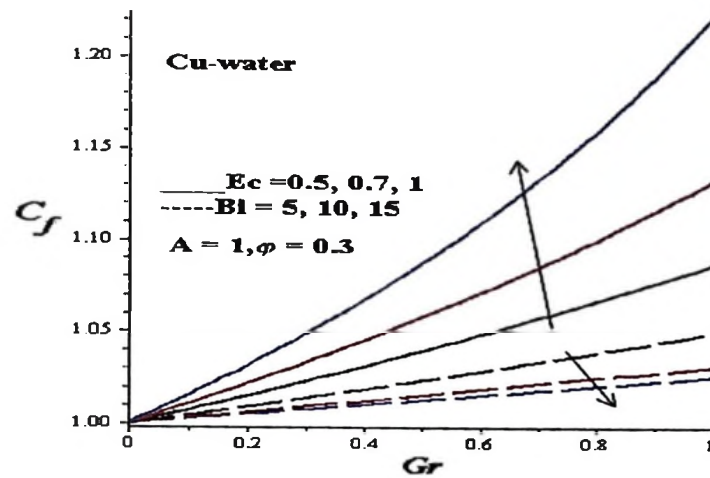


Figure 3.16: Skin friction with increasing Gr , Ec , Bi

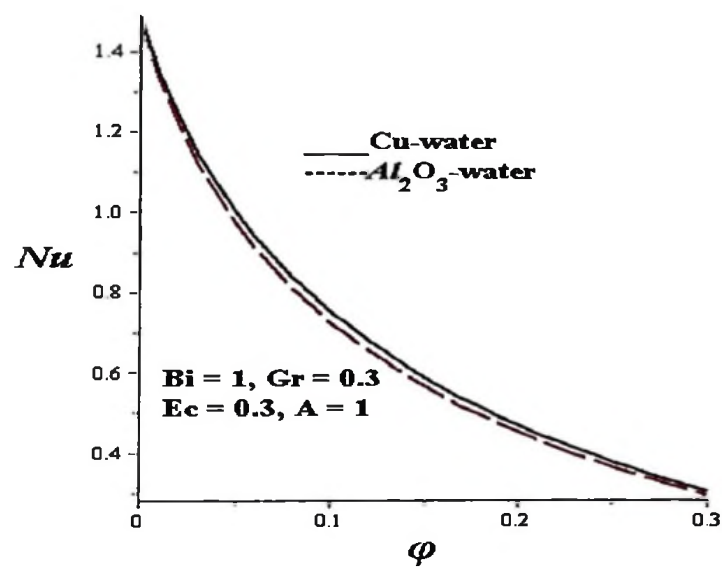


Figure 3.17: Nusselt number with increasing ϕ

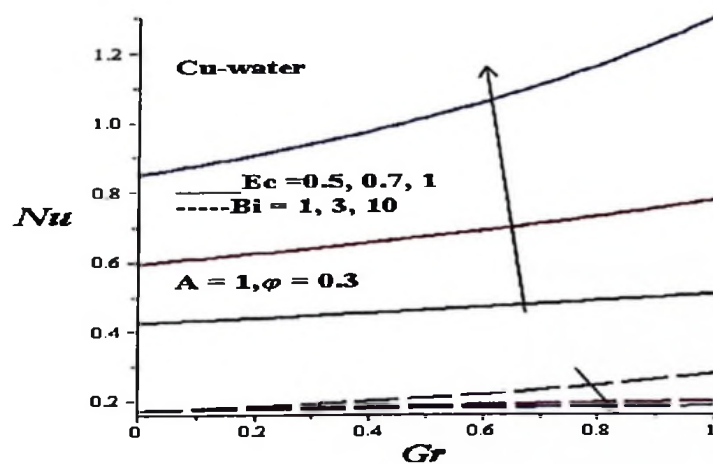


Figure 3.18: Nusselt number with increasing Gr , Ec , Bi

3.5.4 Effects of parameter variation on entropy generation rate

Figure 3.19 depicts the transient effect on the entropy generation rate across the channel. The entropy production increases with time for a given set of parameter values. Interestingly, the entropy generated by Al_2O_3 -water nanofluid is higher than that of Cu-water nanofluids as shown in Figure 3.19. Generally, minimum entropy is produced along the channel centreline region due to the zero velocity and temperature gradients, however, the entropy production increases towards the channel walls. A fall in entropy generation rate is observed with an increase in nanoparticles volume fraction and Biot number as shown in Figures 3.20-3.21. This is due to the fact that both velocity and temperature gradients within the channel decrease as ϕ and Bi increases. Figures 3.22-3.24 show that the entropy generation rate increases with increasing parameter values of Gr , Ec and A . Both velocity and temperature gradients increase as the buoyancy force, viscous dissipation and pressure gradient increase, leading to a rise in entropy production.

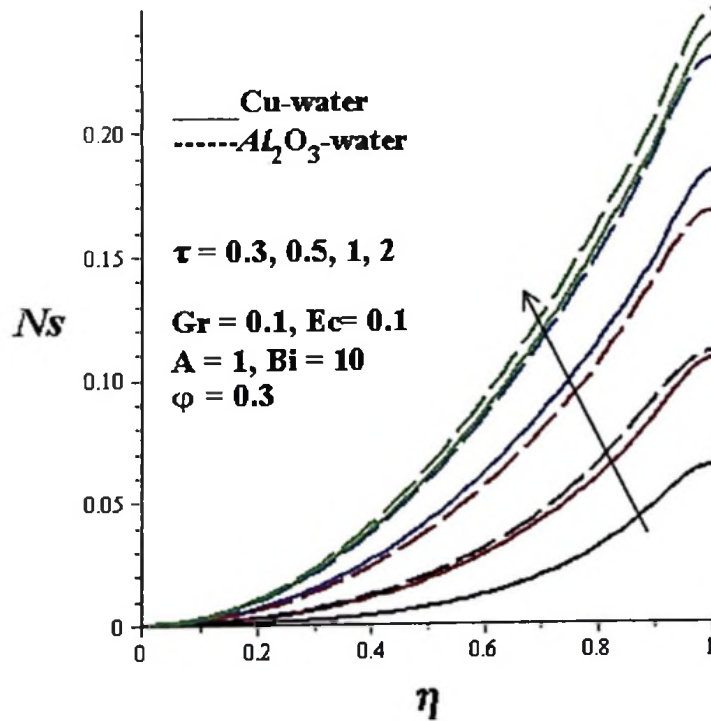


Figure 3.19: Entropy generation rate with increasing time

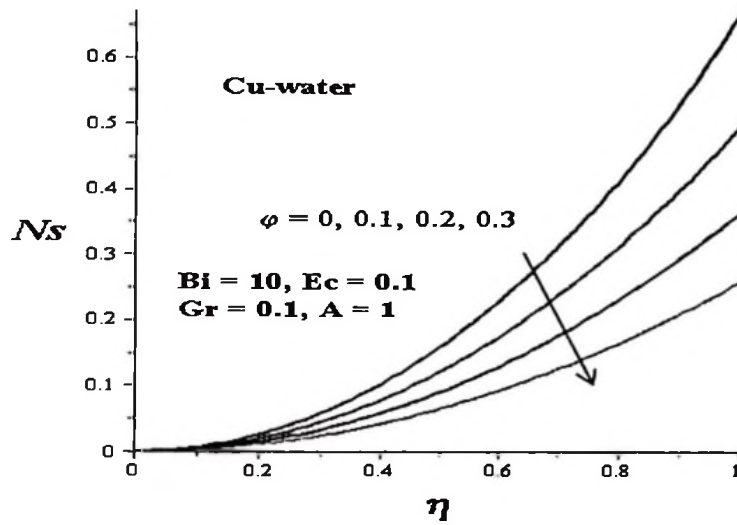


Figure 3.20: Entropy generation rate with increasing ϕ

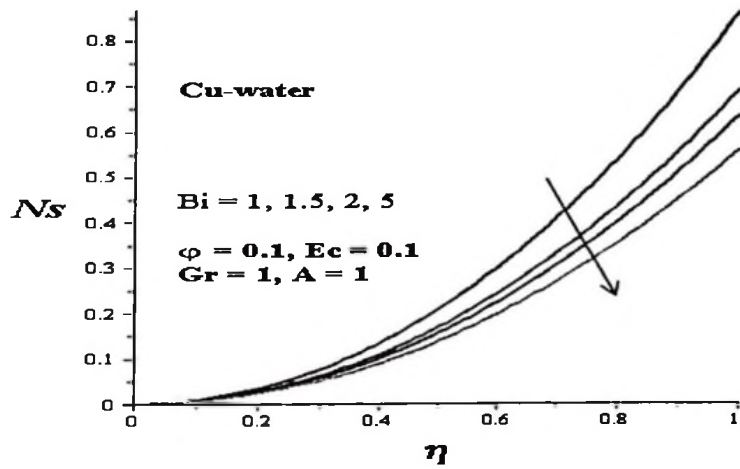


Figure 3.21: Entropy generation rate with increasing Bi

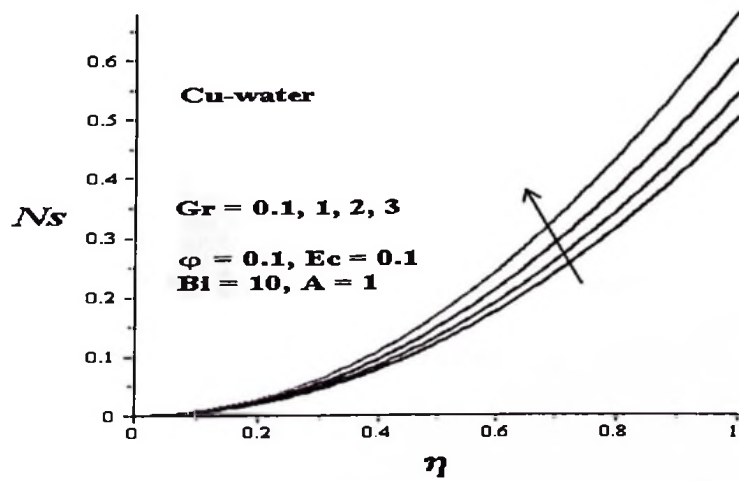


Figure 3.22: Entropy generation rate with increasing Gr

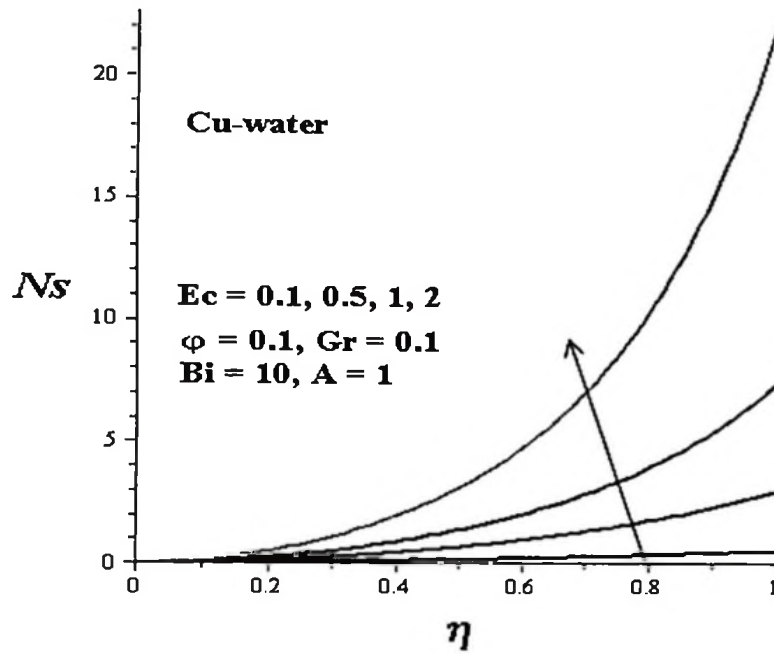


Figure 3.23: Entropy generation rate with increasing Ec

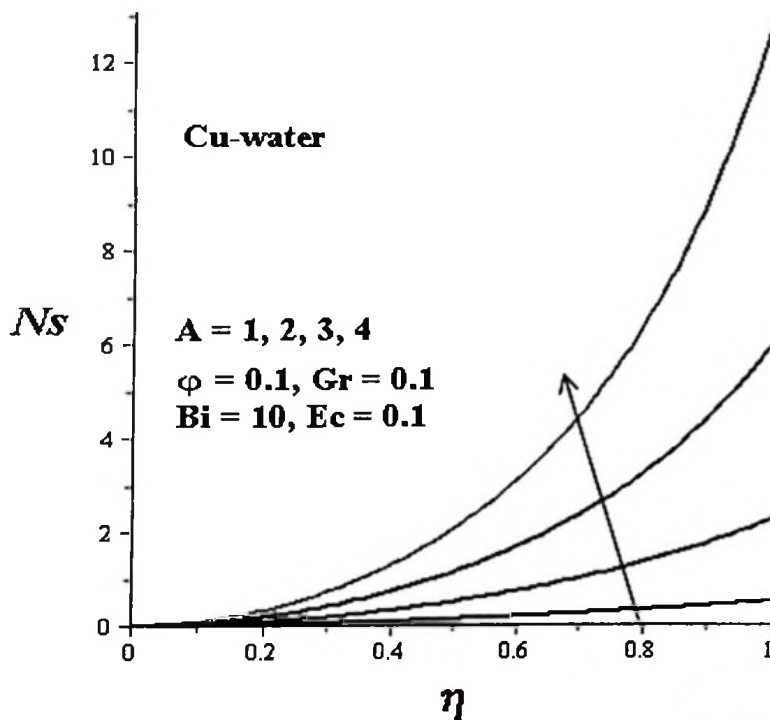


Figure 3.24: Entropy generation rate with increasing A

3.5.5 Effects of parameter variation on Bejan number

Figure 3.25 illustrates the transient effect on the Bejan number across the channel. The Bejan number increases with time near the channel walls but decreases near the channel centreline. This can be attributed to a rise in the dominant effect of fluid friction irreversibility within the channel centreline region and the heat transfer irreversibility at the channel walls. It is

interesting to note that the Bejan number produced by Al_2O_3 -water nanofluid near the walls is higher than that of Cu-water nanofluids. Figures 3.26-3.27 show a decrease in Bejan number near the walls with an increase in nanoparticles volume fraction and Biot number. This implies an increase in dominant effects of fluid friction irreversibility as ϕ and Bi increase. Moreover, as Gr, Ec and A increases, the Bejan number near the walls increases leading to a rise in the dominant effects of heat transfer irreversibility as shown in Figures 3.28-3.30.

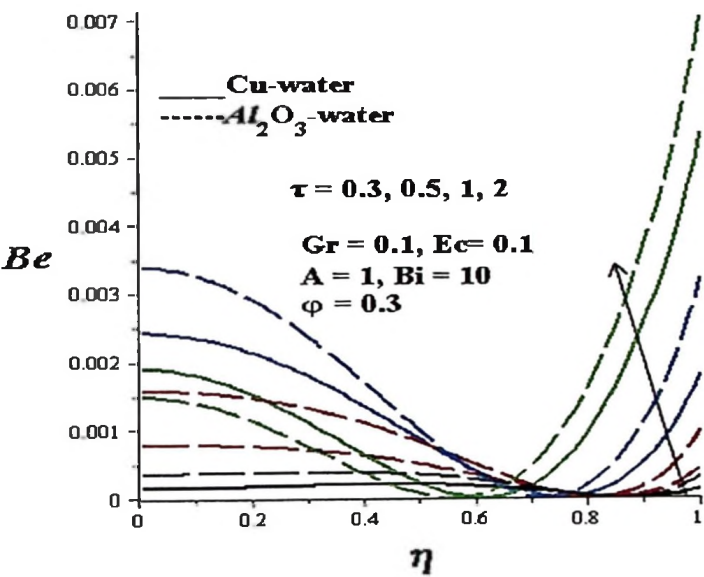


Figure 3.25: Bejan number with increasing time

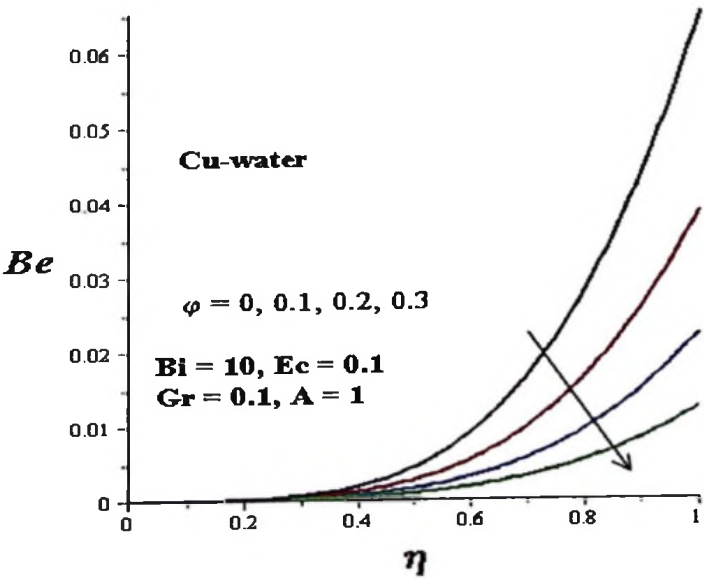


Figure 3.26: Bejan number with increasing ϕ

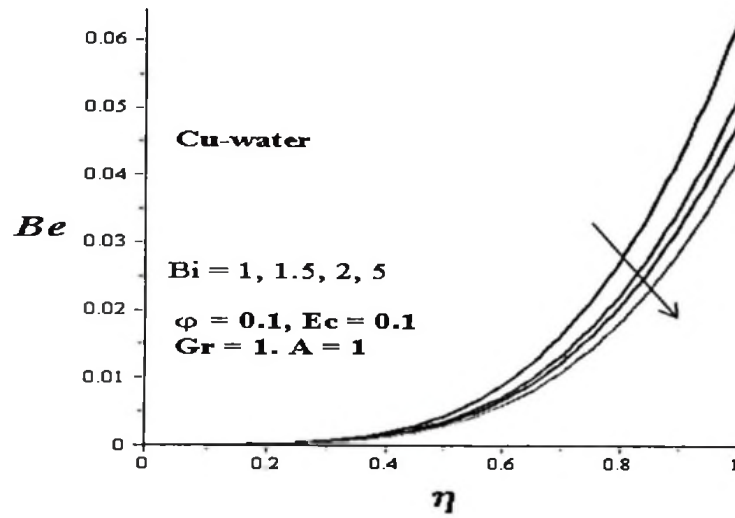


Figure 3.27: Bejan number with increasing Bi

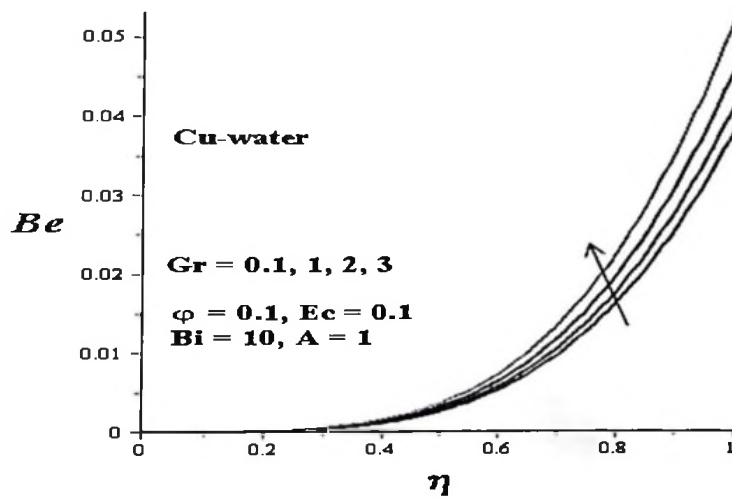


Figure 3.28: Bejan number with increasing Gr

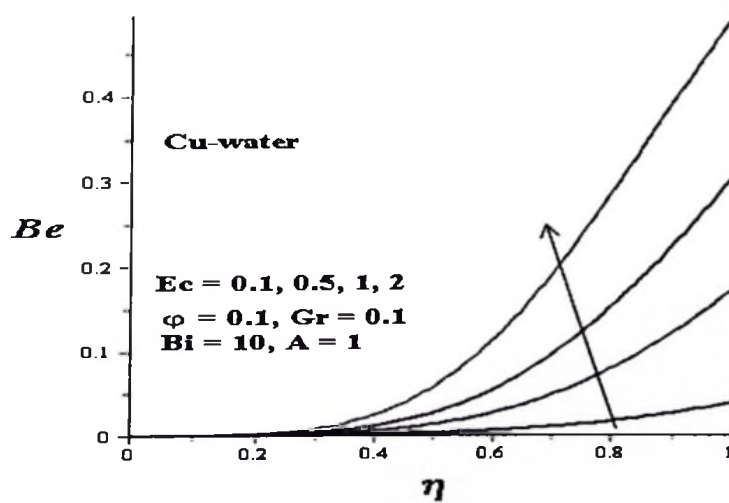


Figure 3.29: Bejan number with increasing Ec

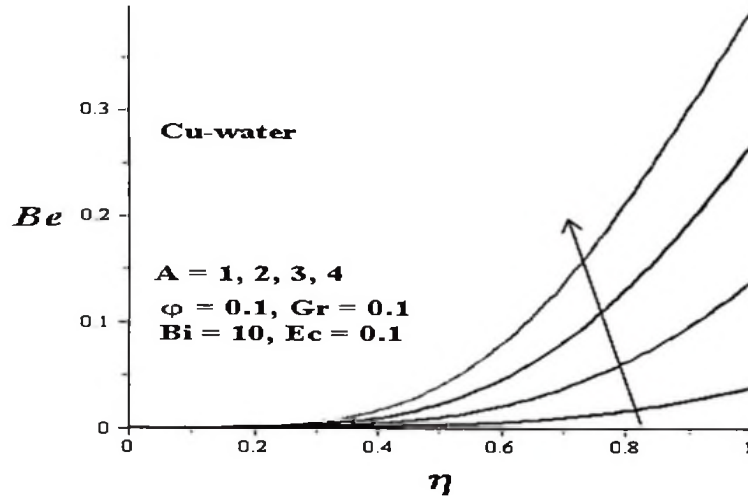


Figure 3.30: Bejan number with increasing A

3.6 Conclusions

The combined effect of buoyancy force and convective cooling on the unsteady flow, heat transfer and entropy generation rate in a water based nanofluids containing Copper (Cu) and Alumina (Al_2O_3) as nanoparticles was investigated. The nonlinear governing partial differential equations are solved numerically using a semi discretization finite difference method together with Runge-Kutta Fehlberg integration scheme. Our results are summarised as follows:

- The Al_2O_3 -water nanofluid tends to flow faster than Cu-water nanofluid and the velocity profile increases with Ec , Gr , A but decreases with ϕ .
- The temperature of Al_2O_3 -water nanofluid rises higher than Cu-water nanofluid and the temperature profile increases with Ec , Gr , A but decreases with ϕ and Bi .
- The Cu-water nanofluid produces higher skin friction than Al_2O_3 -water nanofluid and the skin friction increases with Ec , Gr but decreases with ϕ and Bi .
- The Cu-water nanofluid produces higher Nusselt number than Al_2O_3 -water nanofluid and the Nusselt number increases with Ec , Gr but decreases with ϕ and Bi .
- The Al_2O_3 -water nanofluid produces higher entropy than Cu-water nanofluid and the skin generation increases with Ec , Gr , A but decreases with ϕ and Bi .
- Fluid friction irreversibility dominants the channel centreline region while the effects of heat transfer irreversibility near the walls increases with Gr , Ec , A but decreases with ϕ and Bi .

CHAPTER FOUR

Numerical Investigation into Entropy Generation in a Transient Generalized Couette Flow of Nanofluids with Convective Cooling³

Abstract

This chapter investigates the effects of convective cooling on entropy generation in a transient generalized Couette flow of water based nanofluids containing Copper (Cu) and Alumina (Al_2O_3) as nanoparticles. Both First and Second Laws of thermodynamics are utilised to analyse the problem. The model partial differential equations for momentum and energy balance are tackled numerically using a semi discretization finite difference method together with Runge-Kutta Fehlberg integration scheme. Graphical results on the effects of parameter variation on velocity, temperature, skin friction, Nusselt number, entropy generation rate, irreversibility ratio and Bejan number are presented and discussed.

Keywords: Channel flows; Nanofluids; Couette flow; Entropy generation; Bejan number

4.1 Introduction

In this chapter the researcher looks on theoretical study of nanofluids heat transfer characteristics and entropy generation between two parallel plates, one of which is moving relative to the other under the combined action of axial pressure gradient and imposed uniform velocity on the upper plate known as generalised Couette flow. The study has application not only in a present mathematical fascinating problems but also find various applications in engineering and industrial processes such as tribological devices, cooling of heat exchanging devices, solar water heating, cooling of electronics, cooling of transformer oil, improving diesel generator efficiency, improving heat transfer efficiency of chillers, domestic refrigerator-freezers, cooling in machining and in nuclear reactor. Nanofluid is the addition of nanoscale particles into the base fluid like water, engine oil, ethylene glycol, etc.

³This chapter is based on the paper:

Mkwizu, M. H., Makinde, O. D., and Nkansah-Gyekye, Y. (2015). Numerical Investigation into Entropy Generation in a Transient Generalized Couette Flow of Nanofluids with Convective Cooling. *Sadhana - Academy Proceedings in Engineering Science*, Vol. 40, Part 7, pp. 2073–2093.

The research done by Choi showed that nanofluids possess enhanced thermophysical properties. Nanofluid may be considered as a single phase flow in low solid concentration because of very small sized solid particles. Several experimental and theoretical studies have been made on the flow of nanofluids in different geometries Choi *et al* (2001). The nanofluid in the enclosure was assumed to be in single phase. The results revealed that for any given Grashof number, the average Nusselt number increased with the solid volume concentration parameter.

The buoyancy effects on stagnation point flow and heat transfer of a nanofluid past a convectively heated stretching/shrinking sheet with or without magnetic field were considered by Makinde *et al* (2013) and Makinde (2013). Oztop and Abu-Nada (2008) considered natural convection in partially heated enclosures having different aspect ratio and filled with nanofluid. The results showed that the heat transfer was more pronounced at low aspect ratio and high volume fraction of nanoparticles. Wang and Mujumdar (2007) presented a comprehensive review of heat transfer characteristics of nanofluids. Detailed reports on convective transport in nanofluids can be found in Buongiorno (2006), Mutuku-Njane and Makinde (2014), Tiwari and Das (2007).

Makinde and Eegunjobi (2013) did the study on thermodynamic analysis of variable viscosity magnetohydrodynamics (MHD) unsteady generalized Couette flow with permeable walls. The results illustrate that local entropy generation rate increases with group parameter but decreases with viscosity exponent. Increase in magnetic field parameter decreases entropy production at the moving upper plate while increase in Reynolds number decreases entropy generation at the lower fixed plate. Thermodynamic analysis of variable viscosity MHD unsteady generalized Couette flow with permeable walls was done by Theuri and Makinde (2014). The obtained result was that, the decrease in fluid viscosity increases the Bejan number while an increase group parameter $Br\Omega^{-1}$ (where Ω is temperature difference parameter and Br Brinkman number) decreases the Bejan number. Increase in Reynolds number increases Bejan number at the lower fixed plate and decreases Bejan number at the upper moving plate. The situation is reversed with increasing magnetic field.

Knowledge of entropy production started from Clausius and Kelvin's studies on the irreversible aspects of the second law of thermodynamics. Since then the theories based on these foundations have rapidly developed Bejan (1982) and Bejan (1996). The main cause of entropy generation was found to be heat and mass transfer together with viscous dissipation

in nanofluids and has remained untreated by classical thermodynamics. This motivates many researchers to conduct analyses of fundamental and applied engineering problems based on second law analysis with respect to nanofluid. Optimal designs of thermodynamic systems have been extensively suggested by the thermodynamic second law based on the concept of efficient energy use and the minimal entropy generation principle Woods (1975). Entropy generation minimization techniques may improve the efficiency and overall performance of all kinds of flow and thermal systems.

The primary objective in designing a thermal system is the analysis of energy utilization and entropy generation. It has been the main concern in many fields such as heat exchangers, turbo machinery, electronic cooling, porous media and combustion. Several studies have thoroughly dealt with conventional fluid flow irreversibility due to viscous effect and heat transfer by conduction Narusawa (1998). Numerous investigations to calculate entropy production and irreversibility due to flow and heat transfer of nanofluids over a moving flat surface was considered by Makinde *et al.* (2013). Their observation was that, the entropy generation in the flow system can be minimized by appropriate combination of parameter values together with nanoparticles volume fraction.

In this chapter, we focus on the analysis of the effects of convective cooling and entropy generation rate in unsteady Couette flow channel of water base nanofluid. We have made use of a single component homogenous model in describing the nanofluids. The justification of this model is based on the fact that the particles sizes are of nano-meter (1–100 nm) and these particles are mechanically and chemically suspended into the base fluid. Consequently, the entire flow behaviour is similar to homogenous fluid with different thermophysical properties due to the presence of nano-sized particles. In addition, the single component homogenous model enables one to compare the flow/thermal behaviour of Cu-water nanofluid to that of Al_2O_3 -water nanofluid. We are fully aware of the Buongiorno (2006) models approach which incorporates the effects of thermophoresis and Brownian motion of nanoparticles. This model approach has been utilised in some of our earlier studies. Secondly, we have assumed no-slip condition at both the fixed lower plate and the moving upper plate, however, the movement of the fluid near the upper plate is due to the impose uniform velocity of the upper plate and the axial pressure gradient Makinde and Eegunjobi (2013) and Makinde and Theuri (2014).

The mathematical model for the problem is formulated in the section 4.2. Entropy analysis is done in section 4.3. Both mathematical model and entropy analysis are numerically solved. Relevant results are displayed graphically and discussed in section 4.5. The final section concludes the chapter.

4.2 Mathematical Model

Consider unsteady Couette flow of viscous incompressible nanofluids containing Copper (Cu) and Alumina (Al_2O_3) as nanoparticles. It is assumed that the upper wall moves with uniform velocity U at time $t > 0$ and exchange heat with the ambient surrounding following the Newton's law of cooling. Take a Cartesian coordinate system (x, y) where x lies along the flow direction, y is the distance measured in the normal direction as depicted in Figure 4.1 below;

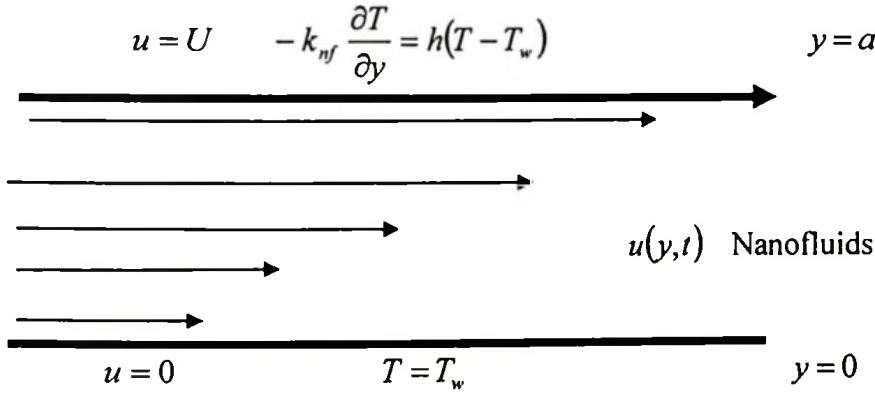


Figure 4.1: Schematic diagram of the problem under consideration

The Navier-Stokes nanofluids momentum and energy balance equation in one dimension for the transient flow can be written as

$$\frac{\partial u}{\partial x} = 0 \quad (4.1)$$

$$\frac{\partial u}{\partial \bar{t}} = -\frac{1}{\rho_{nf}} \frac{\partial P}{\partial x} + \frac{\mu_{nf}}{\rho_{nf}} \frac{\partial^2 u}{\partial y^2} \quad (4.2)$$

$$\frac{\partial T}{\partial \bar{t}} = \alpha_{nf} \frac{\partial^2 T}{\partial y^2} + \frac{\alpha_{nf} \mu_{nf}}{k_{nf}} \left(\frac{\partial u}{\partial y} \right)^2 \quad (4.3)$$

where u is the nanofluid velocity in the x -direction, T is the temperature of the nanofluid, P is the nanofluid pressure, \bar{t} is the time, a is the channel width, T_w is the ambient temperature, μ_{nf} is the dynamic viscosity of the nanofluid, k_{nf} is the nanofluid thermal conductivity, ρ_{nf} is the density of the nanofluid and α_{nf} is the thermal diffusivity of the nanofluid which are

given by Tiwari and Das (2007). The dynamic viscosity of nanofluid is assumed to be temperature independent as follows:

$$\begin{aligned}\mu_{nf} &= \frac{\mu_f}{(1-\phi)^{2.5}}, \quad \rho_{nf} = (1-\phi)\rho_f + \phi\rho_s, \\ \alpha_{nf} &= \frac{k_{nf}}{(\rho c_p)_{nf}}, \quad \tau = \frac{(\rho c_p)_s}{(\rho c_p)_f}, \quad \frac{k_{nf}}{k_f} = \frac{(k_s + 2k_f) - 2\phi(k_f - k_s)}{(k_s + 2k_f) + \phi(k_f - k_s)}, \\ (\rho c_p)_{nf} &= (1-\phi)(\rho c_p)_f + \phi(\rho c_p)_s\end{aligned}\tag{4.4}$$

The nanoparticles volume fraction is represented by ϕ ($\phi=0$ correspond to a regular fluid), ρ_f and ρ_s are the densities of the base fluid and the nanoparticle respectively, k_f and k_s are the thermal conductivities of the base fluid and the nanoparticles respectively, $(\rho c_p)_f$ and $(\rho c_p)_s$ are the heat capacitance of the base fluid and the nanoparticle respectively. It worth mentioning that the use of the above expression for k_{nf} , is restricted to spherical nanoparticles given by Maxwell (1904) and does not account for other shapes of nanoparticles. Also, Brinkman (1952) approximation has been employed to approximate the effective viscosity of the nanofluid μ_{nf} as viscosity of a base fluid μ_f containing dilute suspension of fine spherical particles. The initial and boundary conditions are given as follows:

$$u(y,0) = 0, \quad T(y,0) = T_w, \tag{4.5}$$

$$u(0,\bar{t}) = 0, \quad T(0,\bar{t}) = T_w, \tag{4.6}$$

$$u(a,\bar{t}) = U, \quad -k_{nf} \frac{\partial T}{\partial y}(a,\bar{t}) = h(T(a,\bar{t}) - T_w), \tag{4.7}$$

where T_w is the ambient temperature which also corresponds to the lower wall temperature. Table 4.1 below presents thermo physical properties of water, copper and alumina at the reference temperature.

Table 4.1: Thermophysical properties of the fluid phase (water) and nanoparticles

Physical properties	Fluid phase (water)	Cu	Al ₂ O ₃
c_p (J/kg K)	4179	385	765
ρ (kg/m ³)	997.1	8933	3970
k (W/m K)	0.613	401	40

We introduce the dimensionless variables and parameters as follows:

$$\left. \begin{aligned} \theta &= \frac{T - T_w}{T_w}, \quad W = \frac{u}{U}, \quad t = \frac{\bar{t}U}{a}, \quad v_f = \frac{\mu_f}{\rho_f}, \quad \bar{P} = \frac{Pa}{\mu_f U}, \\ A &= -\frac{\partial \bar{P}}{\partial X}, \quad X = \frac{x}{a}, \quad \eta = \frac{y}{a}, \quad \text{Pr} = \frac{\mu_f c_{pf}}{k_f}, \quad \text{Ec} = \frac{U^2}{c_{pf} T_a}, \\ \tau &= \frac{(\rho c_p)_s}{(\rho c_p)_f}, \quad m = \frac{(k_s + 2k_f) + \phi(k_f - k_s)}{(k_s + 2k_f) - 2\phi(k_f - k_s)}, \quad \text{Re} = \frac{Ua}{v_f} \end{aligned} \right\} \quad (4.8)$$

The dimensionless governing equations together with the appropriate initial and boundary conditions can be written as:

$$\frac{\partial W}{\partial t} = \frac{A}{\text{Re} (1 - \phi + \phi \rho_s / \rho_f)} + \frac{1}{\text{Re} (1 - \phi + \phi \rho_s / \rho_f) (1 - \phi)^{2.5}} \frac{\partial^2 W}{\partial \eta^2} \quad (4.9)$$

$$\frac{\partial \theta}{\partial t} = \frac{1}{m \text{Pr} \text{Re} (1 - \phi + \phi \tau)} \frac{\partial^2 \theta}{\partial \eta^2} + \frac{\text{Ec}}{\text{Re} (1 - \phi + \phi \tau) (1 - \phi)^{2.5}} \left(\frac{\partial W}{\partial \eta} \right)^2 \quad (4.10)$$

with initial and boundary conditions

$$W(\eta, 0) = \theta(\eta, 0) = 0 \quad (4.11)$$

$$W(0, t) = \theta(0, t) = 0 \quad (4.12)$$

$$W(1, t) = 1, \quad \frac{\partial \theta}{\partial \eta}(1, t) = -m \text{Bi} \theta(1, t) \quad (4.13)$$

Physical quantities of practical interest in this problem are the skin friction coefficient C_f and the local Nusselt number Nu which are defined as

$$C_f = \frac{a \tau_w}{\mu_f U}, \quad Nu = \frac{a q_w}{k_f T_w}, \quad (4.14)$$

where τ_w is the wall shear stress and q_w is the heat flux at the channel walls given by

$$\tau_w = \mu_{nf} \left. \frac{\partial u}{\partial y} \right|_{y=a}, \quad q_w = -k_{nf} \left. \frac{\partial T}{\partial y} \right|_{y=a} \quad (4.15)$$

Substituting equations (4.15) in equations (4.14) and using dimensionless variables, we obtain

$$\left. \begin{aligned} C_f &= \frac{1}{(1 - \phi)^{2.5}} \frac{\partial W}{\partial \eta} \\ Nu &= -\frac{1}{m} \frac{\partial \theta}{\partial \eta} \end{aligned} \right\} \text{at } \eta = 1. \quad (4.16)$$

4.3 Entropy Analysis

The second law of thermodynamics is an important tool to scrutinize the irreversibility effects due to flow and heat transfer. Thermodynamic irreversibility is closely related to entropy production. Convection process involving channel flow of nanofluids is inherently irreversible due to the exchange of energy and momentum, within the nanofluid and at solid boundaries. Following Woods (1975), the local volumetric rate of entropy generation is given by

$$S'' = \frac{k_{nf}}{T_w^2} \left(\frac{\partial T}{\partial y} \right)^2 + \frac{\mu_{nf}}{T_w} \left(\frac{\partial u}{\partial y} \right)^2. \quad (4.17)$$

The first term in equation (4.17) is the entropy generation due to heat transfer while the second term is the entropy generation due to fluid friction. Using dimensionless variables from equation (4.8), we express the entropy generation number in dimensionless form as,

$$Ns = \frac{a^2 S''}{k_f} = \frac{1}{m} \left(\frac{\partial \theta}{\partial \eta} \right)^2 + \frac{Br}{(1-\phi)^{2.5}} \left(\frac{\partial W}{\partial \eta} \right)^2, \quad (4.18)$$

where $Br = Ec Pr$ is the Brinkmann number.

Let

$$N_1 = \frac{1}{m} \left(\frac{\partial \theta}{\partial \eta} \right)^2, \quad N_2 = \frac{Br}{(1-\phi)^{2.5}} \left(\frac{\partial W}{\partial \eta} \right)^2, \quad (4.19)$$

The irreversibility distribution ratio is define as $\Phi = N_2/N_1$. Heat transfer irreversibility dominates for $0 \leq \Phi < 1$ and fluid friction irreversibility dominates when $\Phi > 1$. The contribution of both irreversibilities to entropy generation are equal when $\Phi = 1$. We define the Bejan numbers (Be) mathematically as

$$Be = \frac{N_1}{Ns} = \frac{1}{1 + \Phi}. \quad (4.20)$$

Equation (4.20) shows that the Bejan number ranges from 0 to 1. The zero value of the Bejan number corresponds to the limit where the irreversibility is dominated by the effect of fluid friction while $Be = 1$ is the limit where the irreversibility due to heat transfer dominates the flow system. The contribution of both heat transfer and fluid friction to irreversibility are the same when $Be = 0.5$.

4.4 Numerical Procedure

Using a semi-discretization finite difference method (method of lines Woods (1975)), the nonlinear IBVP in equations (4.9)-(4.13) can be solved numerically. We partition the spatial interval $0 \leq \eta \leq 1$ into N equal parts and define grid size $\Delta\eta = 1/N$ and grid points $\eta_i = (i-1)\Delta\eta$, $1 \leq i \leq N+1$. The discretization is based on a linear Cartesian mesh and uniform grid on which finite-differences are taken. The first and second spatial derivatives in equations 4.9 and 4.10 are approximated with second-order central finite differences. Let $W_i(t)$ and $\theta_i(t)$ be approximation of $W(\eta_i, t)$ and $\theta(\eta_i, t)$, then the semi-discrete system for the problem becomes

$$\frac{dW_i}{dt} = \frac{A}{\text{Re} (1 - \phi + \phi \rho_s / \rho_f)} + \frac{(W_{i+1} - 2W_i + W_{i-1}))}{\text{Re} (1 - \phi + \phi \rho_s / \rho_f)(1 - \phi)^{2.5} (\Delta\eta)^2}, \quad (4.21)$$

$$\frac{d\theta_i}{dt} = \frac{(\theta_{i+1} - 2\theta_i + \theta_{i-1}))}{m \text{Pr} \text{Re} (1 - \phi + \phi \tau)(\Delta\eta)^2} + \frac{Ec}{\text{Re} (1 - \phi + \phi \tau)(1 - \phi)^{2.5}} \left(\frac{W_{i+1} - W_{i-1}}{2\Delta\eta} \right)^2, \quad (4.22)$$

with initial conditions

$$W_i(0) = \theta_i(0) = 0, \quad 1 \leq i \leq N+1, \quad (4.23)$$

and boundary conditions

$$W_1 = 0, \quad \theta_1 = 0, \quad W_{N+1} = 1, \quad \theta_{N+1} = \theta_N(1 - m \text{Bi} \Delta\eta). \quad (4.24)$$

Considering equations (4.21)-(4.24), we can see that, they are first order ODEs with known initial conditions. So they can be easily solved iteratively using the Runge-Kutta-Fehlberg integration technique implemented on a computer using Matlab. From the process of numerical computation, the skin-friction coefficient and the Nusselt number in equation (4.16) are also worked out and their numerical values are presented graphically.

4.5 Results and Discussions

In this chapter, the pure water has been considered as the base fluid, copper (Cu) and alumina (Al_2O_3) as nanoparticles. The Prandtl number of the base fluid (water) is kept constant at 6.2 and the effect of solid volume fraction is investigated in the range of $0 \leq \phi \leq 0.3$. Numerical solution for the representative velocity field, temperature field, skin friction, Nusselt number, Entropy generation rate and Bejan number have been carried out by assigning some arbitrary chosen specific values to various thermophysical parameters

controlling the flow system (see Figures 4.2 - 4.27). Moreover, it is important to note that $\phi=0$ correspond to base fluid scenario while $\phi > 0$ correspond to nanofluids scenario. The detailed discussion and graphical representation of the results of above equations are reported in this section.

4.3.1 Effects of parameter variation on velocity profiles

Graphical results are presented in Figures 4.2-4.6 to give a better understanding of the effect of different parameters on the velocity profiles. In general, the velocity increases with time for a given set of parameter values until a steady state profile is achieved as shown in Figure 4.2. It can be noted that the steady state velocity profile is attained at $t = 1.4$. Figure 4.3 shows an interesting observation that, alumina-water nanofluid tends to flow faster than copper-water nanofluids. This result may be due to the high density of copper nanoparticle as compared to alumina nanoparticle. Figures 4.4-4.6 show the effects of parameters variation on the velocity profiles using Cu-water nanofluid. It is observed from Figure 4.4 that, an increase in nanoparticles volume fraction causes a decrease in the velocity profile. This result may be attributed by both the density and the dynamic viscosity of the nanofluid which increases with an increasing nanoparticles volume fraction as a result the decrease in the velocity is observed. Figure 4.5 shows a rise in the nanofluid velocity with an increase in the pressure gradient parameter. It is true that, for standard Couette flow ($A = 0$) the velocity is small and constant compared to the generalized Couette flow scenario in which ($A > 0$). The opposite effect of decreasing velocity is observed when increasing Reynolds number; this happens because the viscous force increases within the flow system as indicated in Figure 4.6.

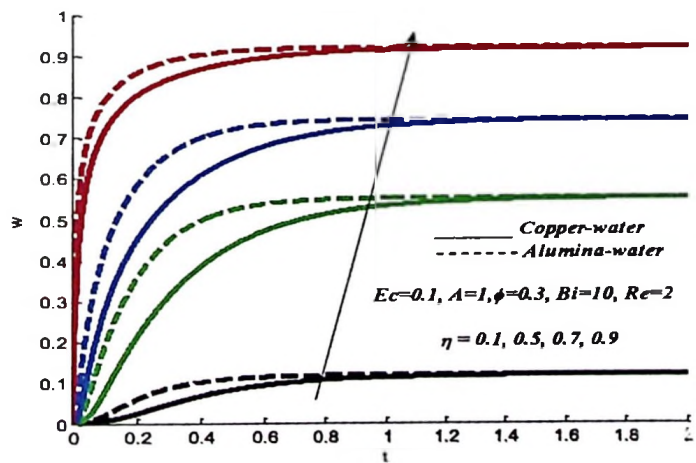


Figure 4.2: Nanofluids velocity profiles with increasing time

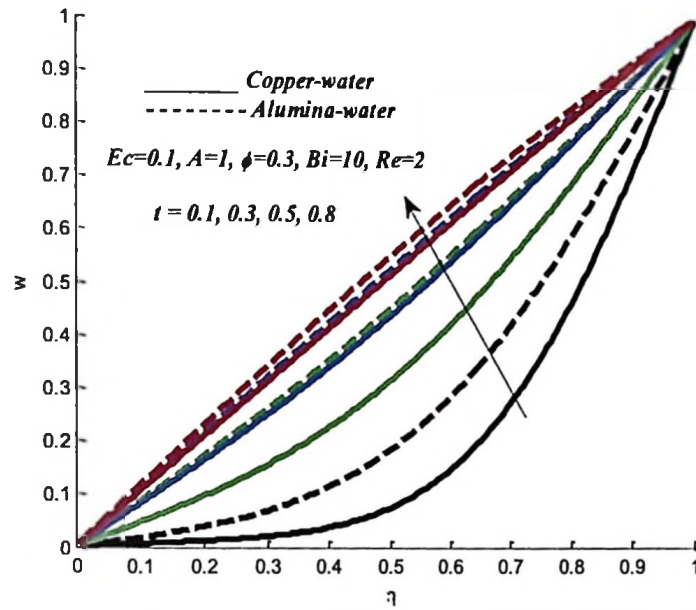


Figure 4.3: Nanofluids velocity profiles across the channel with increasing time

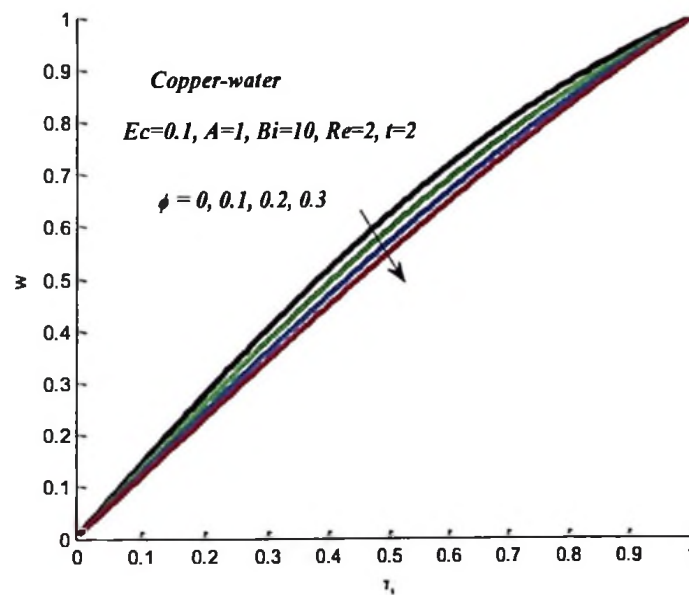


Figure 4.4: Nanofluid velocity profiles with increasing ϕ

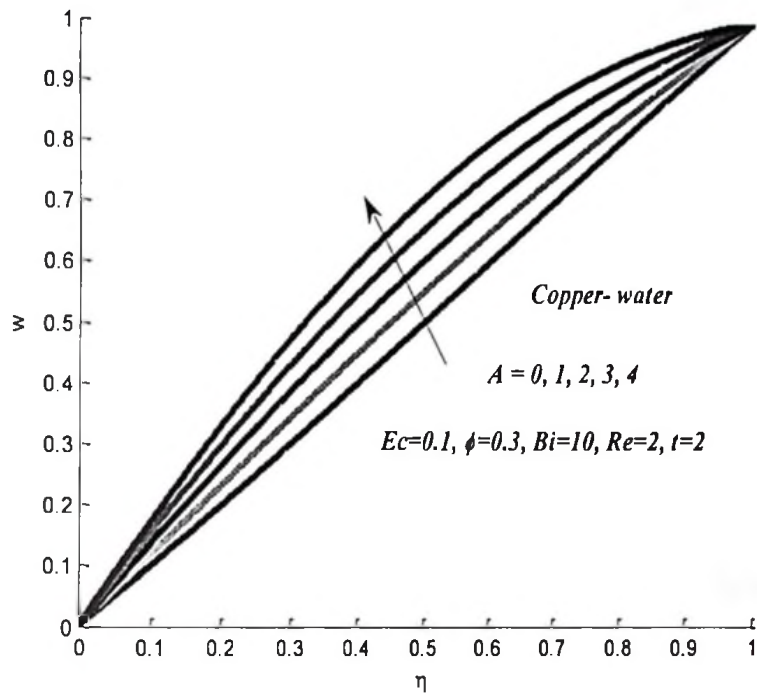


Figure 4.5: Nanofluid velocity profiles with increasing A

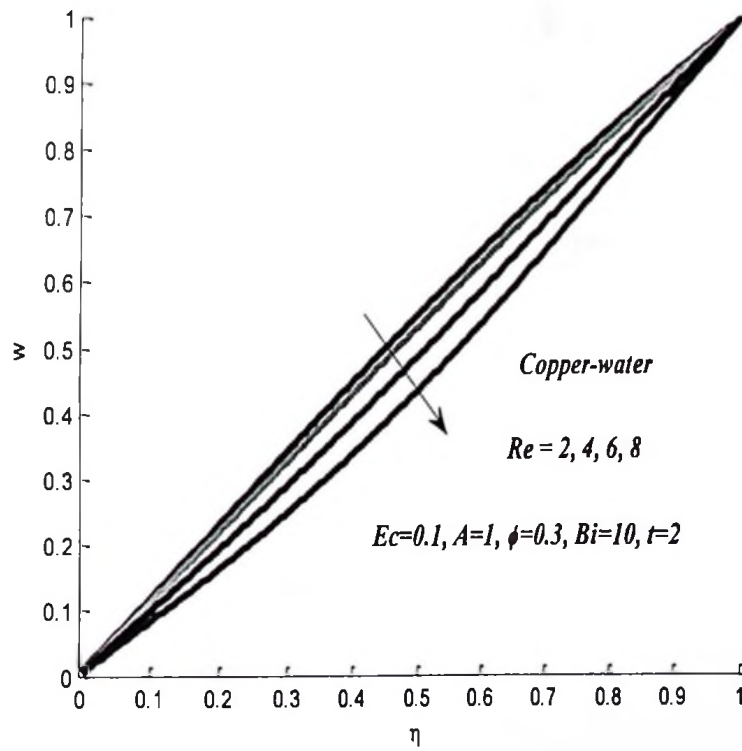


Figure 4.6: Nanofluid velocity profiles with increasing Re

4.5.2 Effects of parameter variation on temperature profiles

Figure 4.7 and 4.8 represent the transient effects on the nanofluids temperature profiles. The results revealed that the temperature decreases with time for a given set of parameter values until a corresponding steady state profile is achieved. The steady state temperature profile is attained at $t = 3$. The temperature of Al_2O_3 -water nanofluids, fall faster than that of Cu -water nanofluids. In addition as the flow continues, the temperature increases near the lower wall and reverse its behaviour as it approaches the upper wall, may be is because of the moving upper plate as shown in Figure 4.7. Comparing Figure 4.2 and Figure 4.7, the researcher observed that the steady state of velocity profile is attained earlier than that of temperature profile. It attains its maximum temperature within the channel and the minimum value at the walls as shown in Figure 4.8. The effect of parameter variation on the temperature profiles with Cu -water nanofluid is shown in Figures 4.9-4.12. The increase in temperature profile is observed as the nanoparticles volume fraction increases as shown in Figure 4.9. Moreover, Figures 4.4 and 4.9 illustrate the flow and thermal characteristics of base fluid (water) as compare to that of nanofluids. This observation is in perfect agreement with the results of Oztop and Abu-Nada (2008) and Makinde et al. (2013), and validates the present results. The opposite trend of a decrease in temperature is noticed with a rise in Biot number, this is due to a convective cooling at the walls as shown in Figure 4.10. The results in Figure 4.11 revealed that, temperature increases with an increase in Eckert number, this behaviour may be attributed to the viscous dissipation. In Figure 4.12 a rise in the nanofluid temperature and reverse situation as it approaches the upper wall is observed with an increase of the pressure gradient parameter. However, the nanofluid temperature for standard Couette flow ($A = 0$) is small at the lower wall compared to the generalizer Couette flow ($A > 0$) and vice versa at the upper wall. Figure 4.13, a rise in the nanofluid temperature and reverse situation as it approaches the upper wall is

observed with an increase in Reynolds number. This increase and decrease in temperature can be because of the upper moving wall.

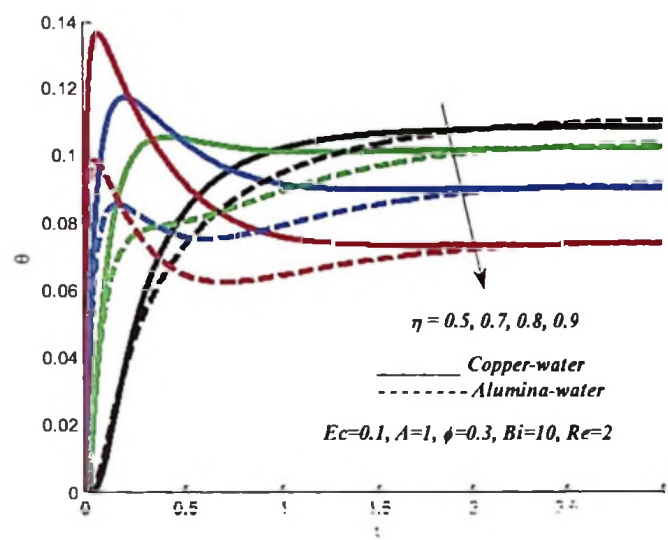


Figure 4.7: Nanofluids temperature profiles with increasing time

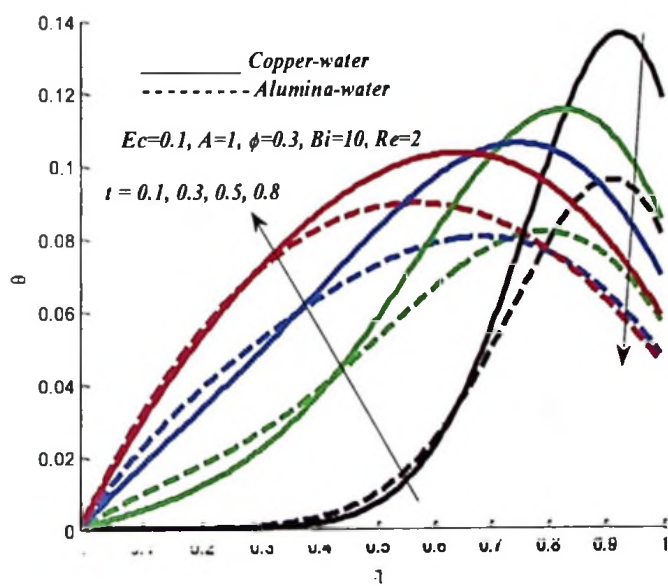


Figure 4.8: Nanofluids temperature profiles across the channel with increasing time

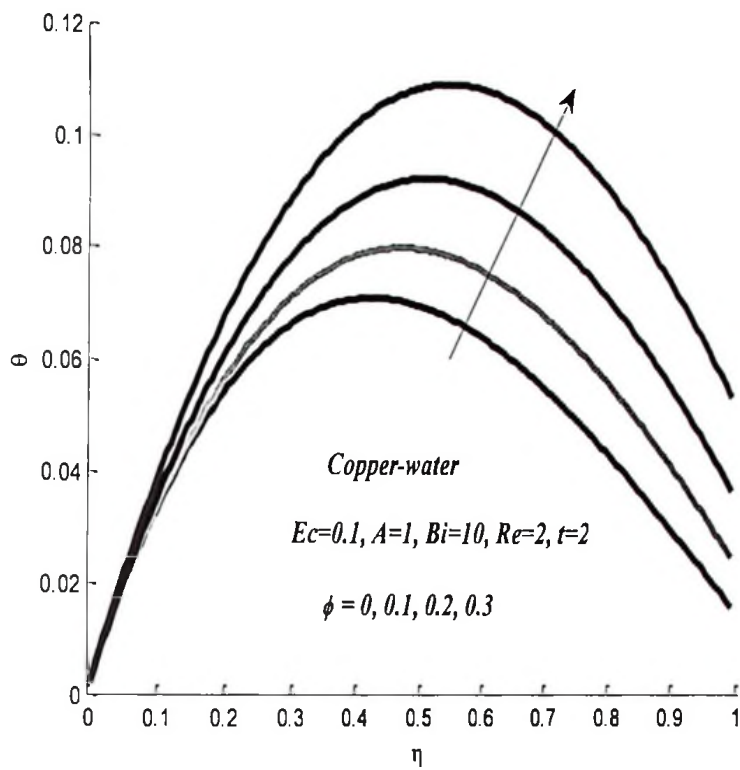


Figure 4.9: Nanofluid temperature profiles with increasing ϕ

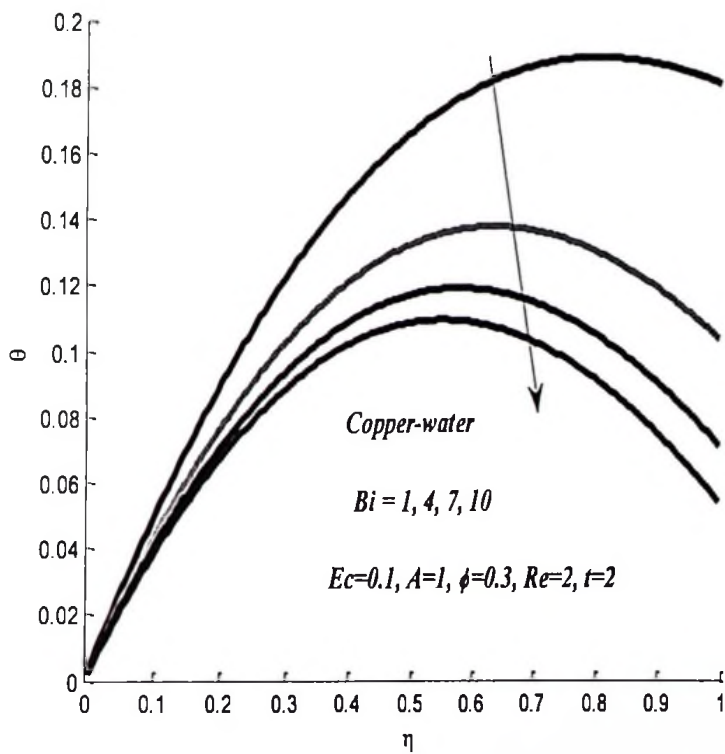


Figure 4.10: Nanofluid temperature profiles with increasing Bi

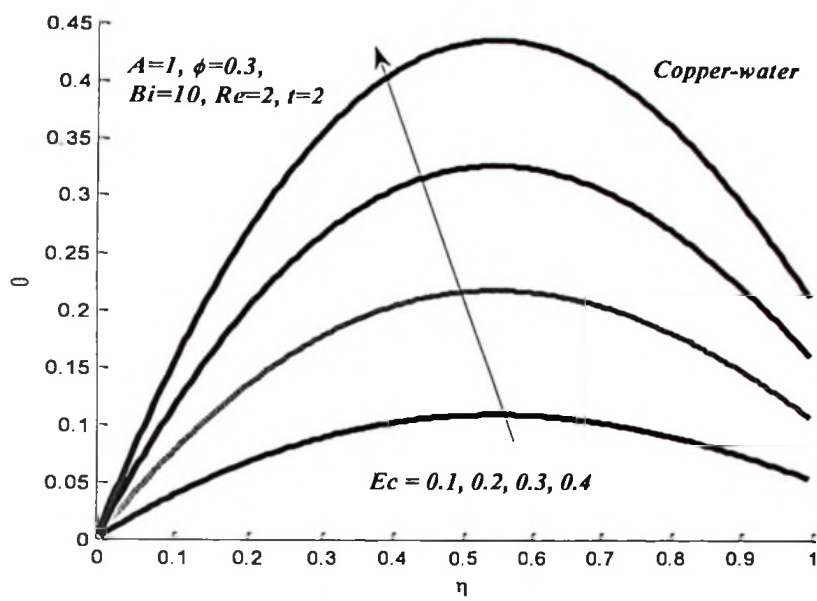


Figure 4.11: Nanofluid temperature profiles with increasing Ec

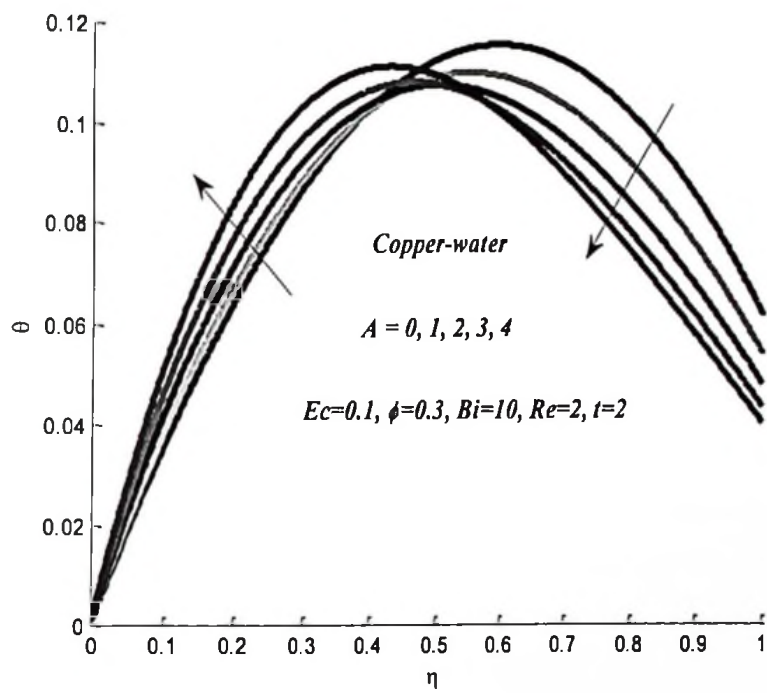


Figure 4.12: Nanofluid temperature profiles with increasing A

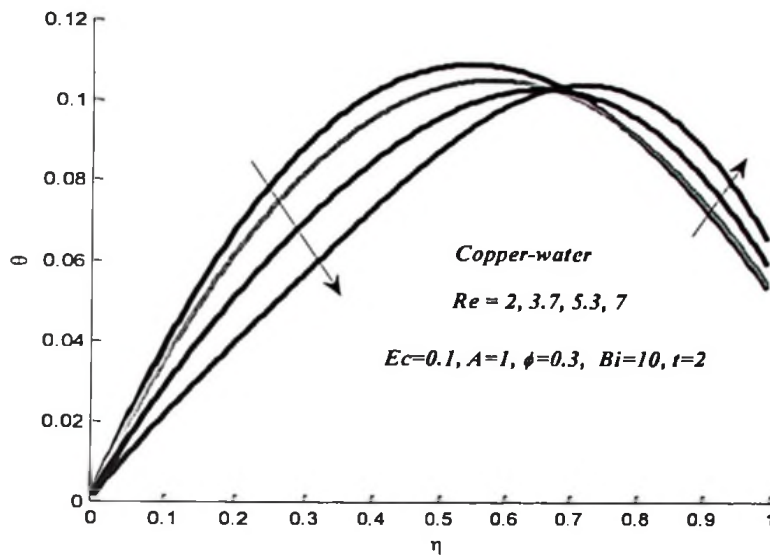


Figure 4.13: Nanofluid temperature profiles with increasing Re

4.5.3 Skin friction and Nusselt number

The effects of parameter variation on skin friction and Nusselt number is illustrated in Figures 4.14-4.17. It is observed in Figure 4.14 that, the skin friction increases with an increase in nanoparticles volume fraction. This is due to an increase in the velocity gradient at the channel walls, which may be caused by Couette flow. Furthermore, the skin friction produced by Cu-water nanofluid is higher than the one produced by Al_2O_3 -water nanofluid. Also, the skin friction increases with an increase in the Reynolds number but decreases with increase in pressure gradient A as illustrated in Figure 4.15. The Nusselt number Nu is based on the thermophysical properties of nanofluids. Note that the temperature gradient depends on the thermophysical properties of nanofluids as highlighted in table 4.1. Figure 4.16 shows that the heat flux at the channel walls increases with an increase in nanoparticles volume fraction due to a rise in the temperature gradient. Moreover, the Nusselt number produced by Cu-water nanofluid is higher than that of Al_2O_3 -water nanofluid. Furthermore, the Nusselt number increases with an increase in Reynolds number and the opposite situation of decreasing Nusselt number is observed when increasing pressure gradient as shown in Figure 4.17. The observed results may be attributed by movement of the upper plate (Couette flow) and viscous dissipation at the walls with a rise in parameter values. The Nu for the base fluid (water) can be obtained when the parameter that $\phi = 0$. Generally, the increase in Nu is not only due to the factor k_{nf} / k_f multiplying the temperature gradient as showing in equation

(4.16), but it depends on the entire thermophysical properties of nanoparticles with parameter $\phi > 0$ as shown in Figures 4.16 and 4.17.

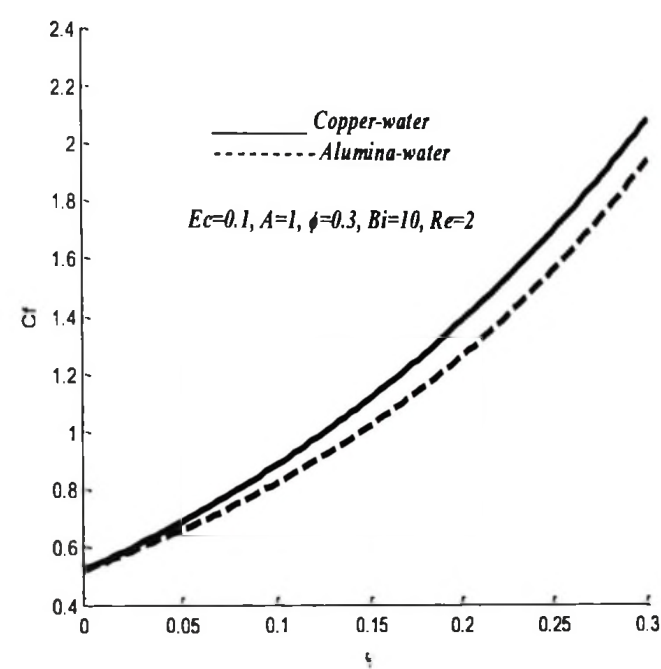


Figure 4.14: Skin friction with increasing ϕ

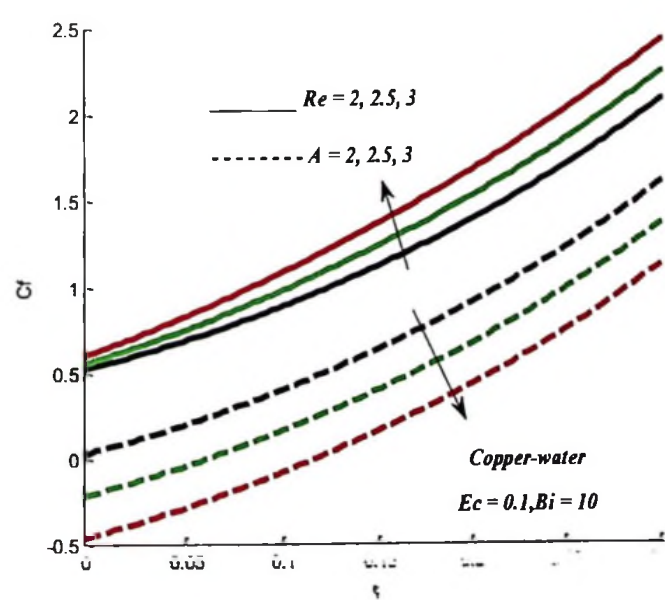


Figure 4.15: Skin friction with increasing ϕ , A and Re

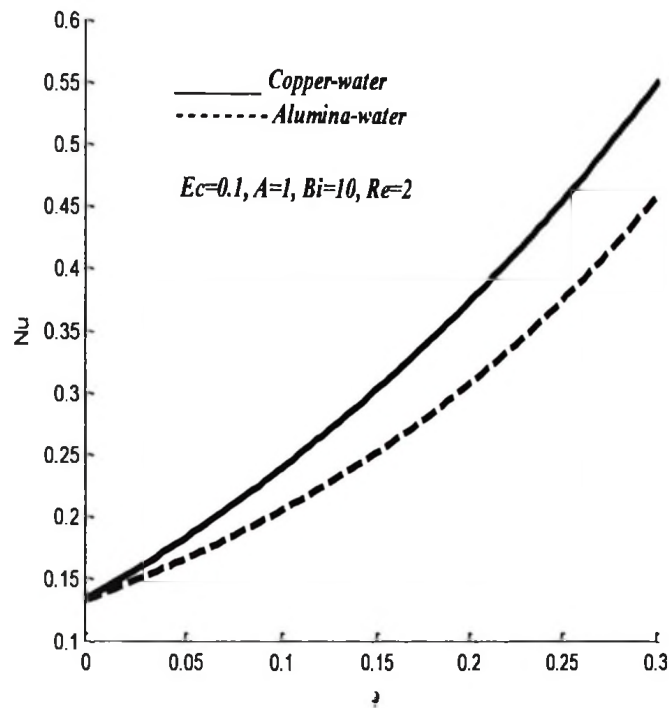


Figure 4.16: Nusselt number with increasing ϕ

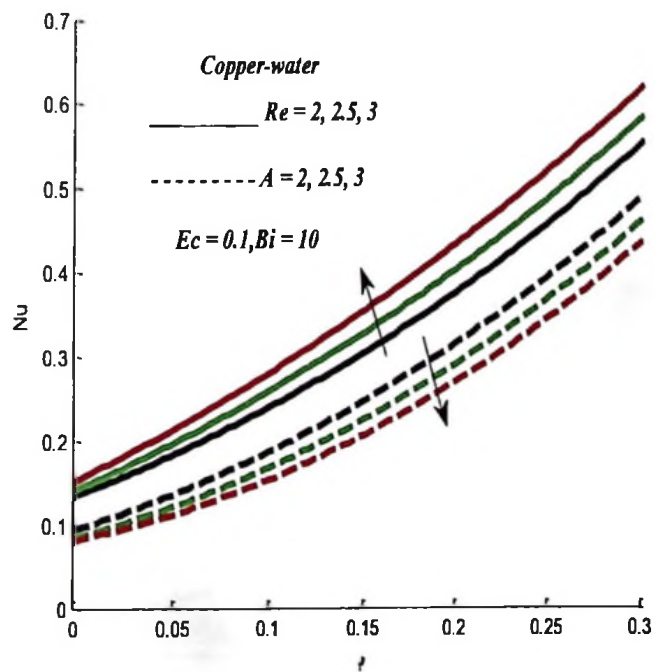


Figure 4.17: Nusselt number with increasing ϕ , A and Re

4.5.4 Effects of parameter variation on entropy generation rate

It is noted in Figure 4.18 that the entropy generation rate increases with time and its behaviour is reversed after half a distance for a given set of parameter values. Also, the entropy generated by Al_2O_3 -water nanofluid is higher than that of Cu-water nanofluid at the beginning but it is vice versa as it approaches the upper moving plate. This shows that, the combination of moving plate and materials with low conductivity lower entropy generation than combination of moving plate and materials with high conductivity and vice versa. So machine with the system of moving plate nanoparticle used to prepare the nanofluid should be of lower conductivity to make it more efficiency. Figure 4.19 shows that a rise in an entropy generation rate is observed with an increase in nanoparticles volume fraction. This is due to the fact that temperature gradients within the channel increase as ϕ increases. Figures 4.20 shows that, the entropy generation rate decreases and increases as it approaches the upper moving plate with an increase in Biot number Bi , while it increases with an increase in Eckert number Ec as shown in Figure 4.21. An entropy generation rate decreases with an increase in pressure gradient A as shown in Figure 4.22. Generally, this situation may be attributed to the increase in temperature gradient with an increase in Eckert number, as well as decrease in temperature gradient with an increase in Biot number and the movement of the upper wall.

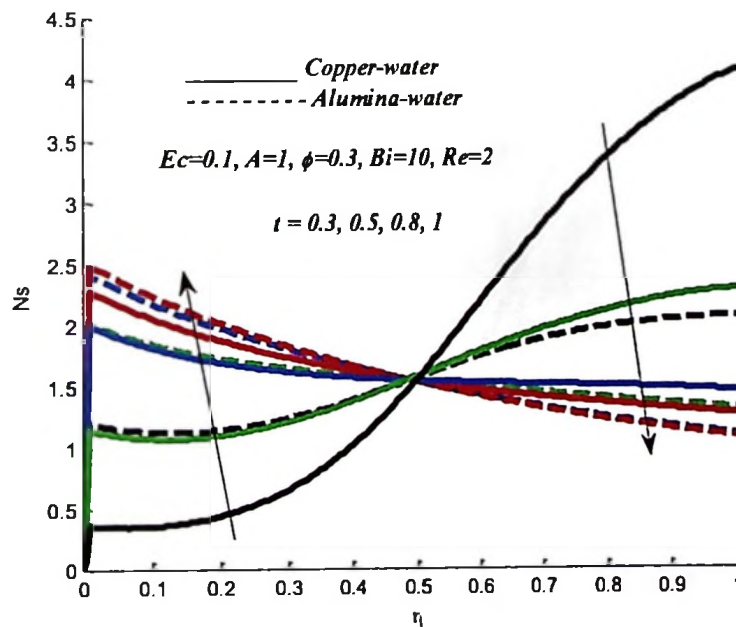


Figure 4.18: Entropy generation rate with increasing time

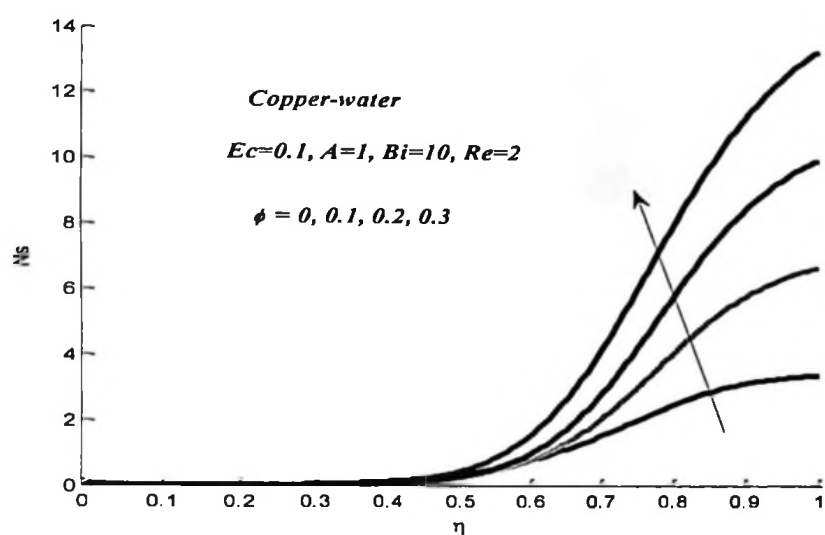


Figure 4.19: Entropy generation rate with increasing ϕ

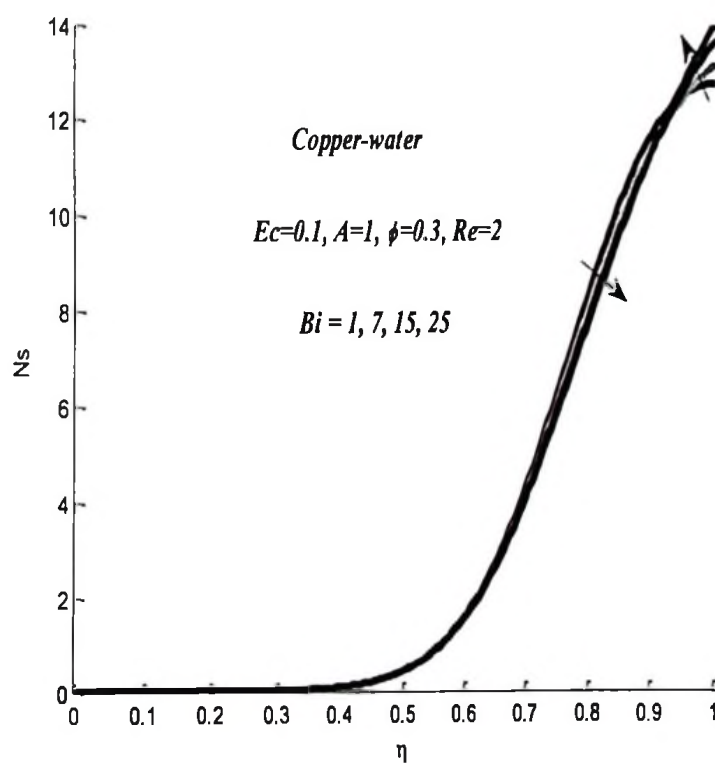


Figure 4.20: Entropy generation rate with increasing Bi

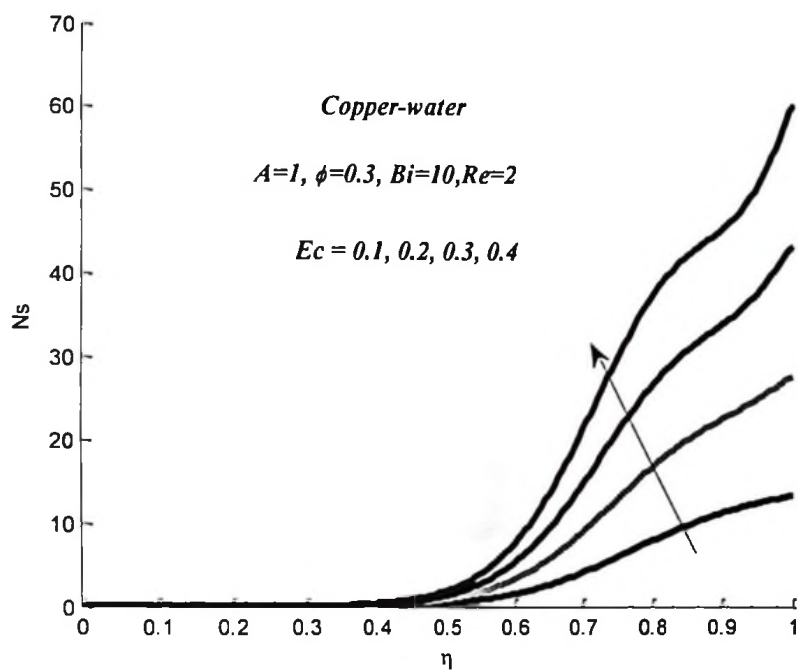


Figure 4.21: Entropy generation rate with increasing Ec

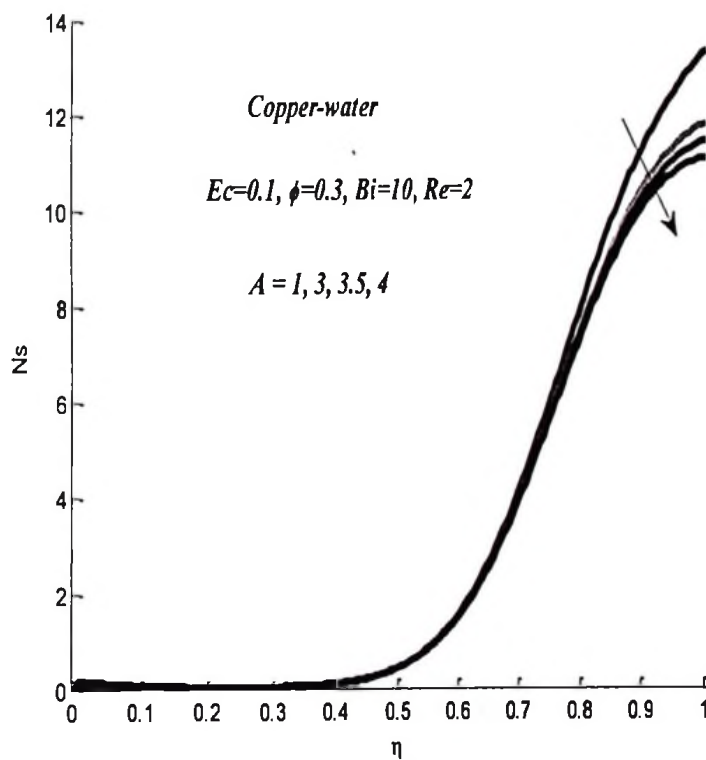


Figure 4.22: Entropy generation rate with increasing A

4.3.5 Effects of parameter variation on Bejan number

Figure 4.23 illustrates the transient effect on the Bejan number across the channel. The Bejan number increases with time near the channel walls but decreases at the channel centreline. This can be attributed to a rise in the dominant effect of fluid friction irreversibility within the channel centreline region, the heat transfer irreversibility at the channel walls and the Couette flow. The Bejan number produced by Cu-water nanofluid near the walls is higher than that of Al_2O_3 -water nanofluids. Figure 4.24 shows an increase in the Bejan number with an increase in nanoparticles volume fraction. It is also noted that the Bejan number became stable as it approached the moving wall (upper wall). This implies an increase in dominant effects of fluid friction irreversibility as ϕ increases. Furthermore, as Bi increases, the Bejan number decreases near the lower wall and at the centre of the channel, but increases as it approaches the upper wall as shown in Figure 4.25. An increase in Ec causes the increase in Bejan at the lower wall, at the centre of the channel and as it approaches the upper wall of the channel as shown in Figure 4.26. Figure 4.27 shows a decrease in Bejan number at the lower wall and increase at the centre of the channel and at the upper wall with an increase in pressure gradient A . This may be attributed by the movement of the upper wall (Couette flow) leading to a rise in the dominant effects of heat transfer irreversibility.

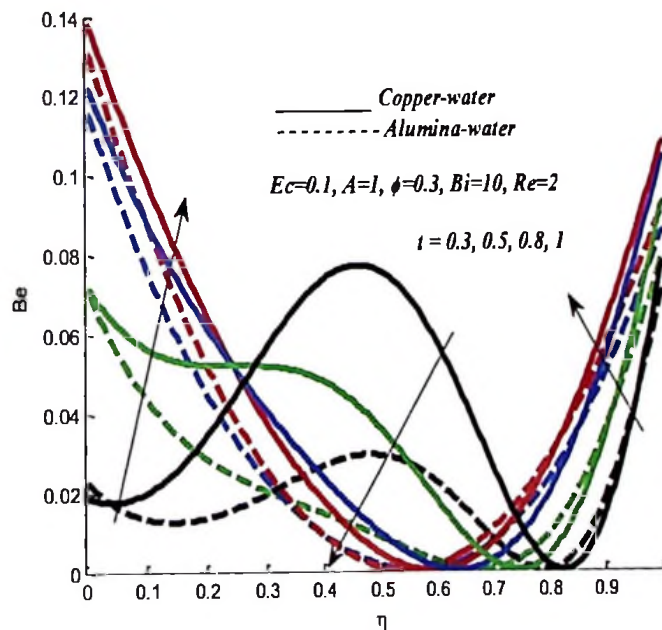


Figure 4.23: Bejan number with increasing time

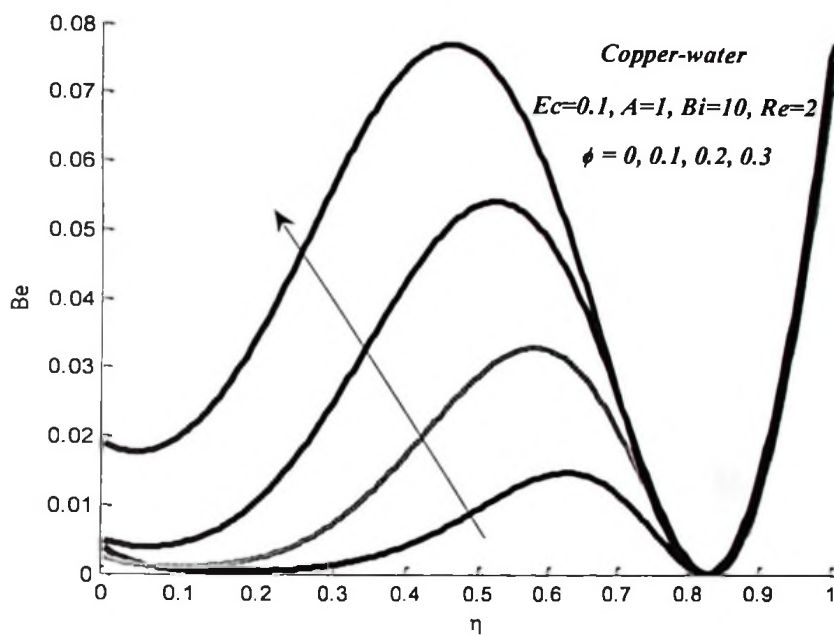


Figure 4.24: Bejan number with increasing ϕ

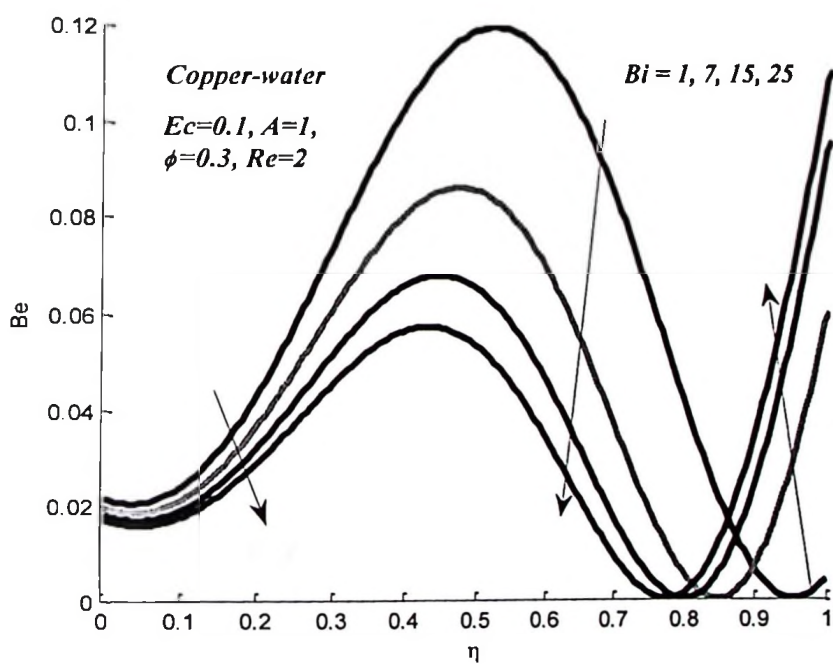


Figure 4.25: Bejan number with increasing Bi

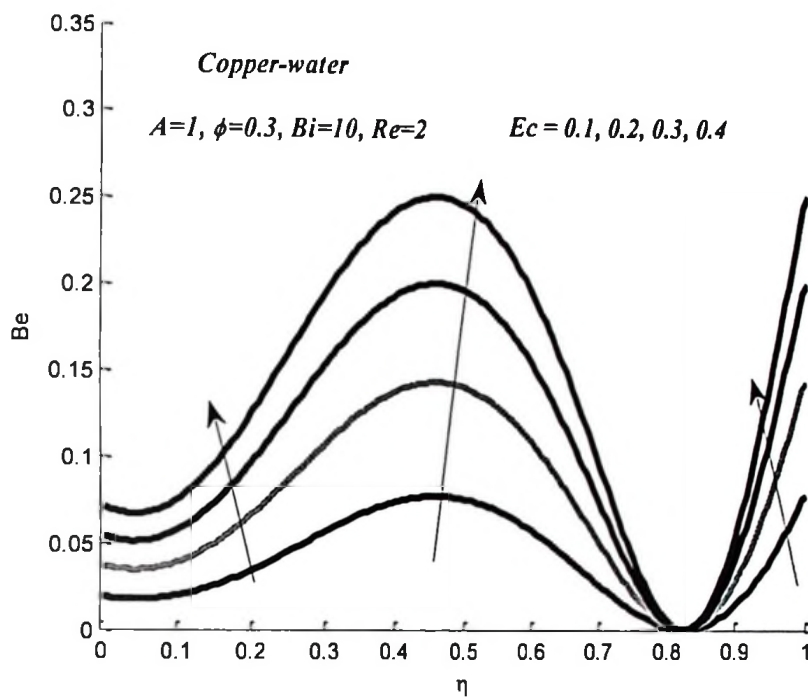


Figure 4.26: Bejan number with increasing Ec

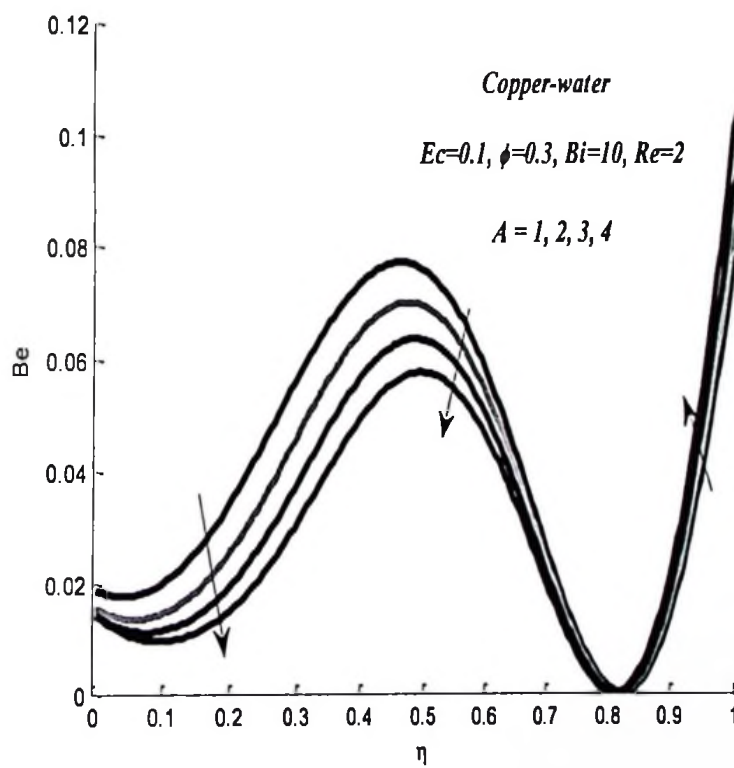


Figure 4.27: Bejan number with increasing A

4.6 Conclusions

The flow structure, heat transfer and entropy generation in unsteady generalized Couette flow of a water-based nanofluid with convective cooling are numerically investigated. The nonlinear governing partial differential equations are solved numerically using a semi discretization finite difference method together with the Runge-Kutta-Fehlberg integration scheme. The observed results in this paper can be summarized as follows:

- The Al_2O_3 -water nanofluid tends to flow faster than Cu-water nanofluid and the velocity profile increases with A but decreases with ϕ and Re .
- The temperature of Cu-water nanofluid rises higher than Al_2O_3 -water nanofluid and the temperature profile increases with ϕ and Ec but decreases with Bi . Moreover temperature profile increases near the lower wall and decreases as it approaches the upper wall with an increase in A , the opposite situation is observed with an increase in Re .
- Cu-water nanofluid produces higher skin friction than Al_2O_3 -water nanofluid and the skin friction increases with Re and ϕ but decreases with A .
- Cu-water nanofluid produces higher Nusselt number than Al_2O_3 -water nanofluid and the Nusselt number increases with Re and ϕ but decreases with A .
- The Al_2O_3 -water nanofluid produces higher entropy generation rate than Cu-water nanofluid near the lower wall, but as it approaches the upper wall, Cu-water nanofluid produces higher entropy generation rate than Al_2O_3 -water nanofluid. The entropy generation increases with ϕ and Ec , it decreases with A . With an increase in Bi the entropy generation rate decreases and reverse its behaviour near the upper wall.
- The Bejan number produced by Cu-water nanofluid is greater than Al_2O_3 -water nanofluid. The Bejan number increases with time at the walls but decreases at the centre of the channel. It increases with an increase in ϕ . But as Bi increases, Bejan number decreases near the lower wall and at the centre of the channel, and increases as it approaches the upper wall. An increase in Ec causes the increase in the Bejan number. It is low at the lower wall, high at the centre of the channel and at the upper wall as A increases.

CHAPTER FIVE

Effects of Navier slip and wall permeability on entropy generation in unsteady generalized Couette flow of nanofluids with convective cooling⁴

Abstract

Present work investigates the effects of generalized Couette flow with convective cooling, Navier slip and permeable walls on entropy generation in an unsteady of water based nanofluids containing Copper (Cu) and Alumina (Al_2O_3) as nanoparticles. Both first and second laws of thermodynamics are applied to analyse the problem. The nonlinear governing equations of momentum and energy are solved numerically using a semi discretization finite difference method together with Runge-Kutta Fehlberg integration scheme. Graphical results on the effects of different parameter variations on velocity, temperature, skin friction, Nusselt number, entropy generation rate, and Bejan number are presented and discussed.

Keywords: Channel flows; Nanofluids; Couette flow; Entropy generation; permeable walls; Navier slip

5.1 Introduction

Thermodynamic irreversibility in the flow system provides information on the energy and power losses in the system. Minimization of entropy generation in the flow system enables for the parametric optimization of the system operation. With the growing demand for efficient cooling systems, more effective coolants are required to keep the temperature of heat generating engines and engineering devices such as electronic components below safe limits. In recent time, the use of nanofluids has provided an innovative technique to enhance heat transfer.

The interest here is the study of the effect of heat transfer, permeable wall and Navier slip on entropy generation between two parallel plates, one of which is moving relative to the other and pressure gradient introduced known as generalized Couette flow which is motivated by several important problems in engineering and industries. Nanotechnology has been widely

⁴This chapter is based on the paper:

Mkwizu, M. H., Makinde, O. D., and Nkansah-Gyekye, Y. (2015). Effects of Navier slip and wall permeability on entropy generation in unsteady generalized Couette flow of nanofluids with convective cooling. *University Politehnica of Bucharest (U.P.B) Scientific Bulletin, Series D*, Vol. 77, Iss. 4, ISSN 1454-2358.

used in engineering and industry since nanometer size materials possess unique physical and chemical properties. The addition of nanoscale particles into the conventional fluids like water, engine oil, ethylene glycol, etc., is known as nanofluid and was firstly introduced by Choi (1995). Nanofluid may be considered as a single phase flow in low solid concentration because of very small sized solid particles. Among many experimental and theoretical studies on flow of nanofluids in different geometries are Choi (2001) and Abu-Nada (2008). The nanofluid in the enclosure was assumed to be in single phase. It was found that for any given Grashof number, the average Nusselt number increased with the solid volume concentration parameter.

Hydromagnetic blood flow through a uniform channel with permeable walls covered by porous media of finite was done by Ramakrishnan and Shailendhra (2013). They found that the axial velocity of the fluid is reduced by porous parameter and Hartmann number. As expected from physical consideration, it was observed that the shear stress was small for small values of the porous parameter and it exhibited an increasing trend with increasing porous parameter.

Theuri and Makinde (2014) considered thermodynamic analysis of variable viscosity MHD unsteady generalized Couette flow with permeable walls. They found that the decrease in fluid viscosity increases Bejan number while an increase group parameter decreases Bejan number. As Reynolds number increases, Bejan number rises at the lower fixed plate and it falls at the upper moving plate. The situation is reversed with increasing magnetic field.

Makinde and Osalusi (2006) did a research on MHD steady flow in a channel with slip at the permeable boundaries. The results revealed that the fluid velocity is reduced by both magnetic field and wall slip. They also noticed the presence of flow reversal near the wall due to wall slip. Generally, wall skin friction increases with suction and decreases with injection, however, both wall slip and magnetic field also have great influence on wall skin friction.

Egunjobi and Makinde (2012) studied the effect of Navier slip on entropy generation in a porous channel with suction/injection. Suction/injection plays an important role in the control of flow past an infinite permeable plate or within parallel permeable plates, hence its importance in practical problems involving film cooling, control of boundary layers in industrial, geophysical, biomedical, engineering and environmental applications.

Oztop and Abu-Nada (2008) considered natural convection in partially heated enclosures having different aspect ratio and filled with nanofluid. They found that the heat transfer was more pronounced at low aspect ratio and high volume fraction of nanoparticles. The buoyancy effects on stagnation point flow and heat transfer of a nanofluid past a convectively heated stretching/shrinking sheet with or without magnetic field were considered by Makinde *et al* (2013). Wang and Mujumdar (2007) presented a comprehensive review of heat transfer characteristics of nanofluids. Detail reports on convective transport in nanofluids can be found in Buongiorno (2006), Tiwari and Das (2007).

Meanwhile, in the nanofluids flows, the improvement of the heat transfer properties causes the reduction in entropy generation. The foundation of knowledge of entropy production goes back to Clausius and Kelvin's studies on the irreversible aspects of the second law of thermodynamics. Since then the theories based on these foundations have rapidly developed, see Bejan (1982) and Bejan (1996). However, the entropy production resulting from heat and mass transfer coupled with viscous dissipation in nanofluids has remained untreated by classical thermodynamics, which motivates many researchers to conduct analyses of fundamental and applied engineering problems based on second law analysis with respect to nanofluid. Based on the concept of efficient energy use and the minimal entropy generation principle, optimal designs of thermodynamic systems have been widely proposed by the thermodynamic second law Woods (1975). It is possible to improve the efficiency and overall performance of all kinds of flow and thermal systems through entropy minimization techniques.

The analysis of energy utilization and entropy generation has become one of the primary objectives in designing a thermal system. This has become the main concern in many fields such as heat exchangers, turbo machinery, electronic cooling, porous media and combustion. Several studies have thoroughly dealt with conventional fluid flow irreversibility due to viscous effect and heat transfer by conduction Narusawa (1998) and Sahin (1998). Makinde *et al* (2013) performed numerous investigations to calculate entropy production and irreversibility due to flow and heat transfer of nanofluids over a moving flat surface. They found that the entropy generation in the flow system can be minimized by appropriate combination of parameter values together with nanoparticles volume fraction.

In this chapter, we analyse the effects of convective cooling, Navier slip and permeable walls on entropy generation rate in unsteady generalized Couette flow channel of water base nanofluid. Such flow is very important in engineering and industries especially cooling engines, electronics, heat exchanging devices and transformer oil. Also it is important for improving diesel generator efficiency, heat transfer efficiency of chillers, domestic refrigerator-freezers, cooling in machining and in nuclear reactor. In the following sections the problem is formulated, numerically analysed and solved. Relevant results are displayed graphically and discussed.

5.2 Mathematical Model

Consider unsteady laminar flow of viscous incompressible nanofluids containing Copper (Cu) and Alumina (Al_2O_3) as nanoparticles through a permeable walls Couette flow channel. It is assumed that the fluid is injected uniformly into the channel at the lower plate while the uniform fluid suction occurs at the moving upper plate as depicted in figure 5.1 below;

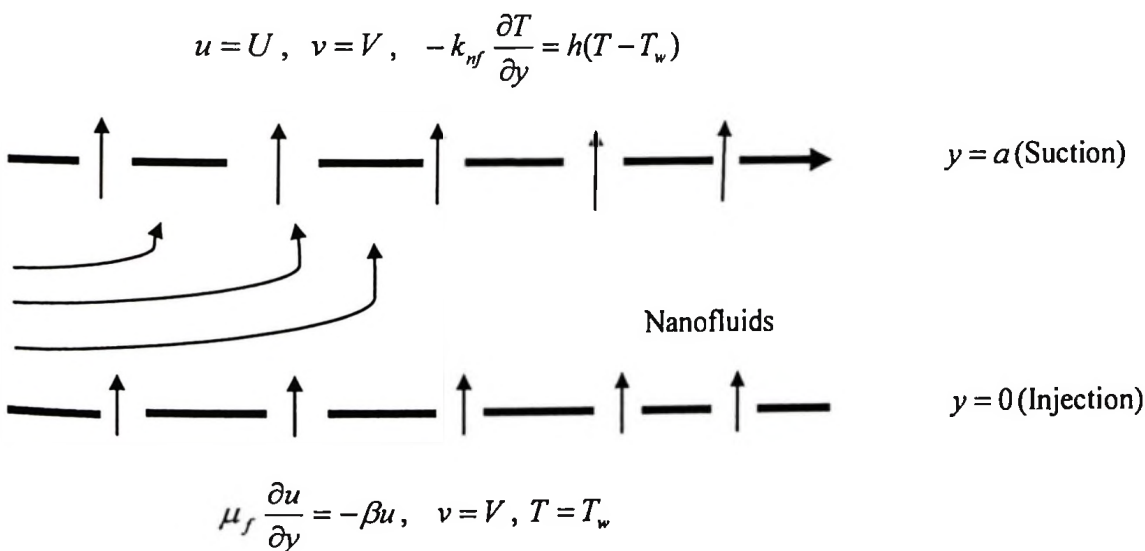


Figure 5.1: Schematic diagram of the problem under consideration

The governing equations for the nanofluids momentum and energy in one dimension with assumption above can be written as follows

$$\frac{\partial u}{\partial \bar{t}} + V \frac{\partial u}{\partial y} = -\frac{1}{\rho_{nf}} \frac{\partial P}{\partial x} + \frac{\mu_{nf}}{\rho_{nf}} \frac{\partial^2 u}{\partial y^2}, \quad (5.1)$$

$$\frac{\partial T}{\partial \bar{t}} + V \frac{\partial T}{\partial y} = \alpha_{nf} \frac{\partial^2 T}{\partial y^2} + \frac{\alpha_{nf} \mu_{nf}}{k_{nf}} \left(\frac{\partial u}{\partial y} \right)^2, \quad (5.2)$$

where u is the nanofluid velocity in the x -direction, T is the temperature of the nanofluid, P is the nanofluid pressure, \bar{t} is the time, a is the channel width, T_w is the lower stationary wall temperature, μ_{nf} is the dynamic viscosity of the nanofluid, k_{nf} is the nanofluid thermal conductivity, ρ_{nf} is the density of the nanofluid and α_{nf} is the thermal diffusivity of the nanofluid which are given by [3, 9]

$$\begin{aligned} \mu_{nf} &= \frac{\mu_f}{(1-\phi)^{2.5}}, \quad \rho_{nf} = (1-\phi)\rho_f + \phi\rho_s, \\ \alpha_{nf} &= \frac{k_{nf}}{(\rho c_p)_{nf}}, \quad \tau = \frac{(\rho c_p)_s}{(\rho c_p)_f}, \quad \frac{k_{nf}}{k_f} = \frac{(k_s + 2k_f) - 2\phi(k_f - k_s)}{(k_s + 2k_f) + \phi(k_f - k_s)}, \\ (\rho c_p)_{nf} &= (1-\phi)(\rho c_p)_f + \phi(\rho c_p)_s. \end{aligned} \quad (5.3)$$

The nanoparticles volume fraction is represented by ϕ ($\phi=0$ correspond to a base fluid), ρ_f and ρ_s are the densities of the base fluid and the nanoparticle respectively, k_f and k_s are the thermal conductivities of the base fluid and the nanoparticles respectively, $(\rho c_p)_f$ and $(\rho c_p)_s$ are the heat capacitance of the base fluid and the nanoparticle respectively. It worth mentioning that the use of the above expression for k_{nf} , is restricted to spherical nanoparticles and does not account for other shapes of nanoparticles. Also, approximation has been employed to approximate the effective viscosity of the nanofluid μ_{nf} as viscosity of a base fluid μ_f containing dilute suspension of fine spherical particles. The initial and boundary conditions are given as follows:

$$u(y,0) = 0, \quad T(y,0) = T_w, \quad (5.4)$$

$$\mu_f \frac{\partial u}{\partial y}(0, \bar{t}) = -\beta u(0, \bar{t}), \quad T(0, \bar{t}) = T_w, \quad (5.5)$$

$$u(a, \bar{t}) = U, \quad -k_{nf} \frac{\partial T}{\partial y}(a, \bar{t}) = h(T(a, \bar{t}) - T_w). \quad (5.6)$$

Table 5.1 below presents thermo physical properties for water, copper and alumina at the reference temperature.

Table 5.1: Thermophysical properties of the fluid phase (water) and nanoparticles

Physical properties	Fluid phase (water)	Cu	Al ₂ O ₃
c_p (J/kg K)	4179	385	765
ρ (kg/m ³)	997.1	8933	3970

The dimensionless variables and parameters are introduced as follows:

$$\left. \begin{aligned} \theta &= \frac{T - T_w}{T_w}, \quad W = \frac{u}{U}, \quad t = \frac{\bar{t}V}{a}, \quad v_f = \frac{\mu_f}{\rho_f}, \quad \bar{P} = \frac{Pa}{\mu_f U}, \\ A &= -\frac{\partial \bar{P}}{\partial X}, \quad X = \frac{x}{a}, \quad \eta = \frac{y}{a}, \quad \text{Pr} = \frac{\mu_f c_{pf}}{k_f}, \quad \text{Ec} = \frac{U^2}{c_{pf} T_a}, \\ \tau &= \frac{(\rho c_p)_s}{(\rho c_p)_f}, \quad m = \frac{(k_s + 2k_f) + \phi(k_f - k_s)}{(k_s + 2k_f) - 2\phi(k_f - k_s)}, \quad \text{Re} = \frac{Va}{\nu_f}, \quad \alpha_f = \frac{k_f}{(\rho c_p)_f}, \quad f = \frac{\mu_f}{\beta a} \end{aligned} \right\} \quad (5.7)$$

The dimensionless governing equations together with the appropriate initial and boundary conditions can be written as:

$$\frac{\partial W}{\partial t} = \frac{A}{\text{Re}(1 - \phi + \phi \rho_s / \rho_f)} + \frac{1}{\text{Re}(1 - \phi + \phi \rho_s / \rho_f)(1 - \phi)^{2.5}} \frac{\partial^2 W}{\partial \eta^2} - \frac{\partial W}{\partial \eta} \quad (5.8)$$

$$\frac{\partial \theta}{\partial t} = \frac{1}{m \text{Pr} \text{Re}(1 - \phi + \phi \tau)} \frac{\partial^2 \theta}{\partial \eta^2} + \frac{\text{Ec}}{\text{Re}(1 - \phi)^{2.5}(1 - \phi + \phi \tau)} \left(\frac{\partial W}{\partial \eta} \right)^2 - \frac{\partial \theta}{\partial \eta} \quad (5.9)$$

with initial and boundary conditions

$$W(\eta,0) = 0, \theta(\eta,0) = 0 \quad (5.10)$$

$$\frac{\partial W}{\partial \eta}(0,t) = -\frac{\beta a}{\mu_f} W(0,t), \theta(0,t) = 0 \quad (5.11)$$

$$W(1,t) = 1 \quad \frac{\partial \theta}{\partial \eta}(1,t) = -mBi\theta(1,t) \quad (5.12)$$

Where, β is the coefficient of sliding friction and f is slip parameter. Other physical quantities of practical interest in this problem are the skin friction coefficient C_f and the local Nusselt number Nu which are defined as

$$C_f = \frac{a\tau_w}{\mu_f U}, \quad Nu = \frac{aq_w}{k_f T_w}, \quad (5.13)$$

where τ_w is the wall shear stress and q_w is the heat flux at the channel walls given by

$$\tau_w = -\mu_{nf} \left. \frac{\partial u}{\partial y} \right|_{y=a}, \quad q_w = -k_{nf} \left. \frac{\partial T}{\partial y} \right|_{y=a} \quad (5.14)$$

Substituting equations (5.14) into (5.13) and using dimensionless variables, we obtain

$$\left. \begin{aligned} C_f &= -\frac{1}{(1-\phi)^{2.5}} \frac{\partial W}{\partial \eta} \\ Nu &= -\frac{1}{m} \frac{\partial \theta}{\partial \eta} \end{aligned} \right\} \text{at } \eta = 1. \quad (5.15)$$

5.3 Entropy Analysis

The second law of thermodynamics is an important tool to scrutinize the irreversibility effects due to flow and heat transfer. Thermodynamic irreversibility is closely related to entropy production. Convection process involving channel flow of nanofluids is inherently irreversible due to the exchange of energy and momentum, within the nanofluid and at solid boundaries. Following Woods [26], the local volumetric rate of entropy generation is given by

$$S'' = \frac{k_{nf}}{T_w^2} \left(\frac{\partial T}{\partial y} \right)^2 + \frac{\mu_{nf}}{T_w} \left(\frac{\partial u}{\partial y} \right)^2 \quad (5.16)$$

The first term in equation (5.16) is the entropy generation due to heat transfer while the second term is the entropy generation due to nanofluid friction. Using dimensionless variables from equation (5.7), we express the entropy generation number in dimensionless form as,

$$N_s = \frac{\alpha^2 S''}{k_f} = \frac{1}{m} \left(\frac{\partial \theta}{\partial \eta} \right)^2 + \frac{Br}{(1-\phi)^{2.5}} \left(\frac{\partial W}{\partial \eta} \right)^2 \quad (5.17)$$

Where $Br = Ec Pr$ is the Brinkman number, the Bejan number Be is define as

$$Be = \frac{N_1}{N_s} = \frac{1}{1 + \Phi} \quad (5.18)$$

where

$$N_s = N_1 + N_2$$

$$N_1 = \frac{1}{m} \left(\frac{\partial \theta}{\partial \eta} \right)^2 \quad (\text{The entropy generation due to heat transfer})$$

$$N_2 = \frac{Br}{(1-\phi)^{2.5}} \left(\frac{\partial W}{\partial \eta} \right)^2 \quad (\text{The entropy generation due to fluid friction})$$

The irreversibility distribution ratio is define as $\Phi = N_2/N_1$. Heat transfer irreversibility dominates for $0 \leq \Phi < 1$ and fluid friction irreversibility dominates when $\Phi > 1$. The contribution of both irreversibilities to entropy generation are equal when $\Phi = 1$.

Equation (5.18) shows that the Bejan number ranges from 0 to 1. The zero value of the Bejan number corresponds to the limit where the irreversibility is dominated by the effect of fluid friction while one value of Bejan number is the limit where the irreversibility due to heat transfer dominates the flow system. The contribution of both heat transfer and fluid friction to irreversibility are the same when $Be = 0.5$.

5.4 Numerical Procedure

Using a semi-discretization finite difference method, the nonlinear initial boundary value problem (IBVP) in equations (5.8)-(5.12) can be solved numerically. We partition the spatial interval into equal parts and define grid size and grid points. The discretization is based on a linear Cartesian mesh and uniform grid on which finite-differences are taken. The first and second spatial derivatives in equation (5.8) and equation (5.9) are approximated with second-order central finite differences.

$$\frac{dW_i}{dt} = \frac{A}{\text{Re} (1 - \phi + \phi \rho_s / \rho_f)} + \frac{(W_{i+1} - 2W_i + W_{i-1}))}{\text{Re} (1 - \phi + \phi \rho_s / \rho_f)(1 - \phi)^{2.5} (\Delta \eta)^2} - \frac{W_{i+1} - W_{i-1}}{2\Delta \eta} \quad (5.19)$$

$$\frac{d\theta_i}{dt} = \frac{(\theta_{i+1} - 2\theta_i + \theta_{i-1}))}{m \text{Pr} \text{Re} (1 - \phi + \phi \tau)(\Delta \eta)^2} + \frac{Ec}{\text{Re} (1 - \phi + \phi \tau)(1 - \phi)^{2.5}} \left(\frac{W_{i+1} - W_{i-1}}{2\Delta \eta} \right)^2 - \frac{\theta_{i+1} - \theta_{i-1}}{2\Delta \eta} \quad (5.20)$$

with initial conditions and boundary conditions

$$W_i(0) = \theta_i(0) = 0, \quad 1 \leq i \leq N+1 \quad (5.21)$$

$$\begin{aligned} W_1 &= \frac{-fW_2}{\Delta \eta - f}, \quad \theta_1 = 0, \\ W_{N+1} &= 1, \quad \theta_{N+1} = \theta_N(1 - m \text{Bi} \Delta \eta) \end{aligned} \quad (5.22)$$

Considering equations (5.19)-(5.22) we can see that, they are first order ODEs with known initial conditions. So they can be easily solved iteratively using Runge-Kutta Fehlberg integration technique implemented on computer using Matlab. From the process of numerical computation, the skin-friction coefficient and the Nusselt number in equation (5.15) are also worked out and their numerical results are presented.

5.5 Results and Discussions

For understanding the dynamics of this physical problem, Figures 5.2-5.23 shows the numerical computations for the representative velocity field, temperature field, skin friction, Nusselt number, entropy generation rate and Bejan number. Some arbitrary chosen specific values to various thermophysical parameters controlling the flow system have been assigned. The Prandtl number (Pr) of the pure water used in this dynamics problem is assigned the

value 6.2 and the effect of solid volume fraction is investigated in the range of $0 \leq \phi \leq 0.3$. The detailed discussion and graphical representation are reported in this section.

5.5.1 Effects of parameter variation on velocity profiles

The effects of various physical parameters on the nanofluid velocity profile are presented on the Figure 5.2-5.6. In general, the velocity increases with time for a given set of parameter values until a steady state profile is achieved as shown in Figure 5.2. The steady state velocity is attained at $t = 1.6$. Figure 5.3 shows an interesting observation that, alumina-water nanofluid tends to flow faster than copper-water nanofluids. This result may be due to the high density of copper nanoparticle as compared to alumina nanoparticle.

Figures 5.4-5.6 show the effects of parameters variation on the velocity profiles using Cu-water nanofluid. An increase in nanoparticles volume fraction causes a slight decrease in the velocity profile see Figure 5.4. This may be due to the density, the dynamic viscosity of the nanofluid which increases with an increasing nanoparticles volume fraction, slip condition, suction and injection of the fluid. The results in Figure 5.5 revealed that the nanofluid velocity increases with an increase in pressure gradient. The opposite effect is observed in Figure 5.6 where increasing Reynolds number causes a decrease in velocity profile. This happens because the viscous force increases within the flow system.

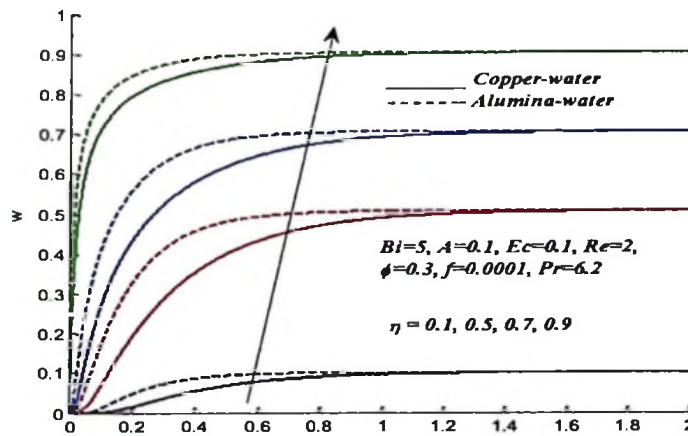


Figure 5.2: Nanofluids velocity profiles with increasing time

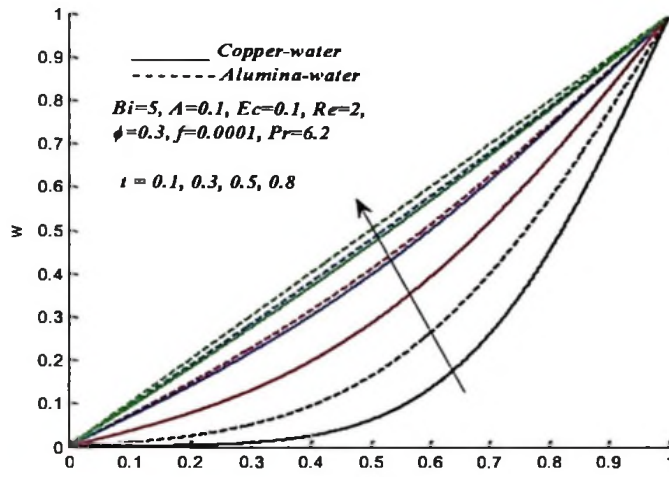


Figure 5.3: Nanofluids velocity profiles across the channel with increasing time

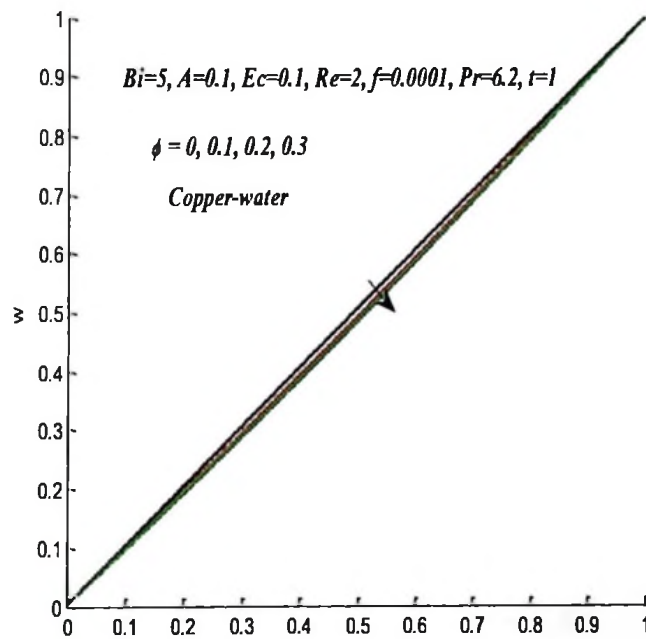


Figure 5.4: Nanofluid velocity profiles with increasing ϕ

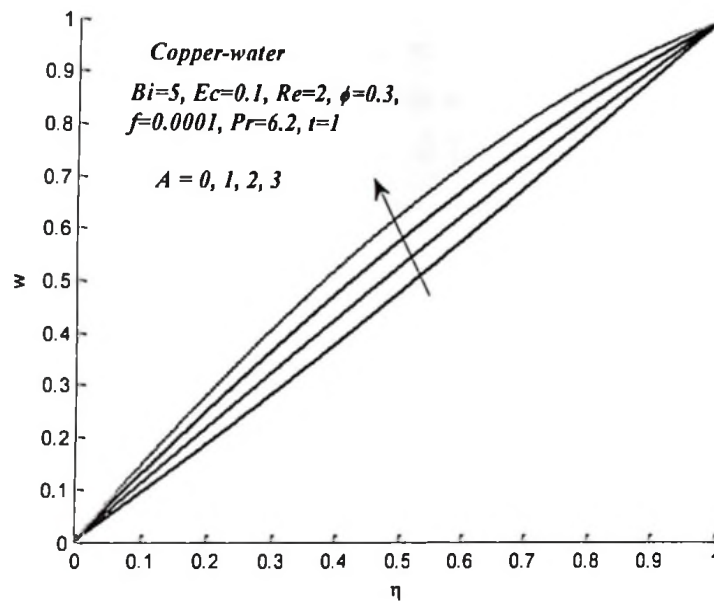


Figure 5.5: Nanofluid velocity profiles with increasing A

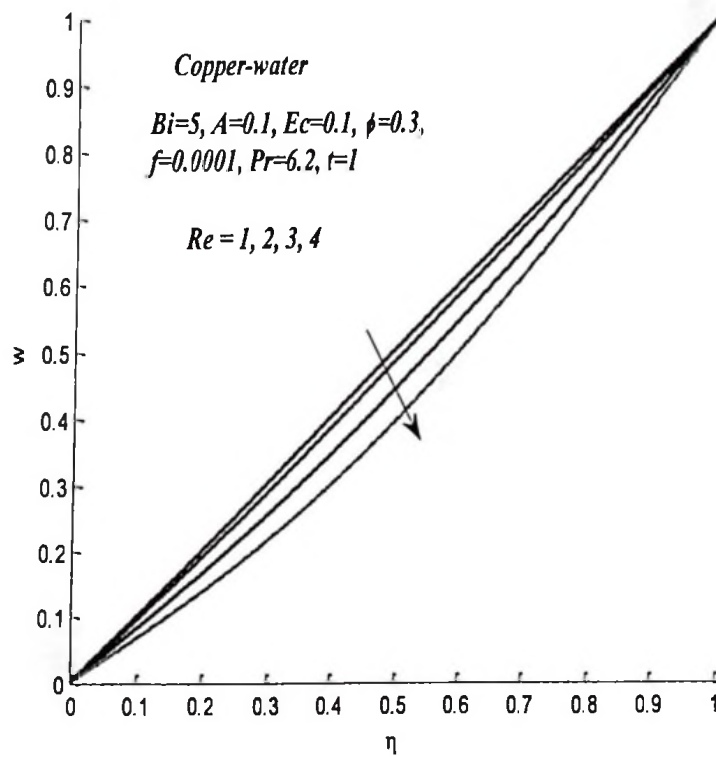


Figure 5.6: Nanofluid velocity profiles with increasing Re

5.5.2 Effects of parameter variation on temperature profiles

The transient effects on the nanofluids temperature profiles are clearly revealed in Figure 5.7-5.12. From Figure 5.7 it is noted that the temperature increases with time near the lower wall it then decreases toward the upper moving wall for a given set of parameter values until a corresponding steady state profile is achieved. This behaviour may be attributed by the slip condition and injection at the lower wall, suction and moving upper wall. Observing clearly it shows that the steady state temperature profile is attained at $t = 2$. Comparing Figure 5.2 and Figure 5.7 it is noteworthy that, the steady state of velocity profile is attained earlier than that of temperature profile. Interestingly, the temperature of Cu-water nanofluid rises higher than that of Al_2O_3 -water nanofluids as shown in Figure 5.8. Moreover, with increase in time the alternating temperature is observed. The temperature profile attains its maximum value at the upper wall and minimum value at the lower wall. Generally this may be due to convective heat loss to the ambient, moving upper wall, slip and permeable walls.

Figures 5.9-5.12 illustrates the effects of parameter variation on the temperature profiles with Cu-water as the working nanofluid. The results showed that the temperature profile increases with an increase in the nanoparticles volume fraction as shown in Figure 5.9. Similar result of increase in temperature is noticed with an increase in slip parameter as shown in Figure 5.10. This behaviour may be attributed by slippery at the walls. Opposite behaviour is observed in Figures 5.11 that, nanofluid temperature falls with an increase in Biot number. It is noted that with an increase in Eckert number the temperature profile rises as shown in Figure 5.12. This increase in temperature may be attributed by viscous dissipation.

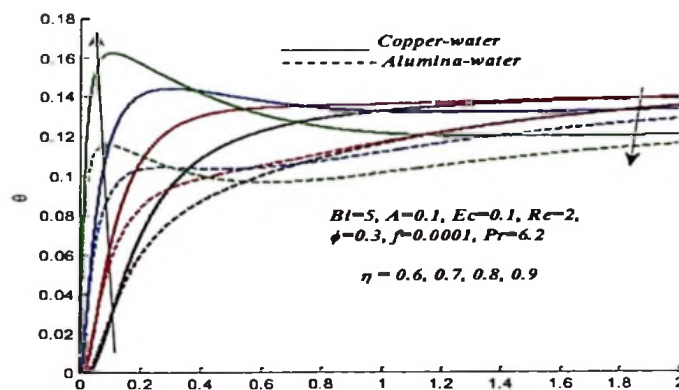


Figure 5.7: Nanofluids temperature profiles with increasing time

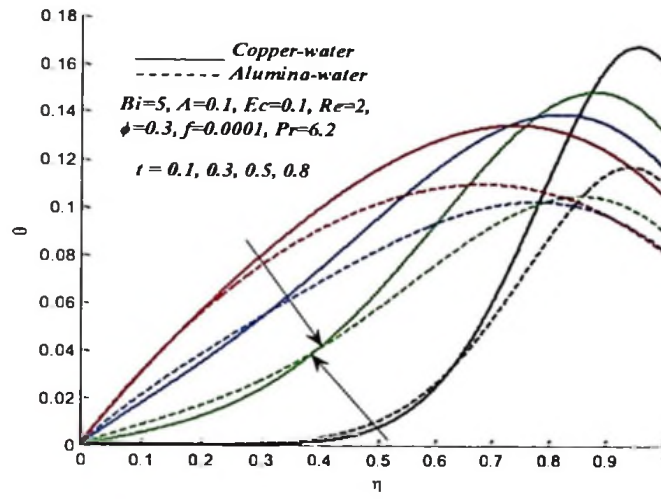


Figure 5.8: Nanofluids temperature profiles across the channel with increasing time

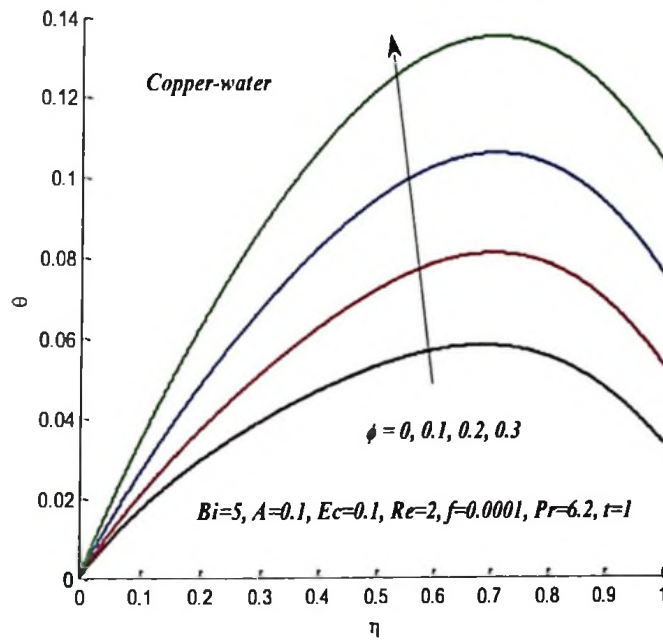


Figure 5.9: Nanofluid temperature profiles with increasing ϕ

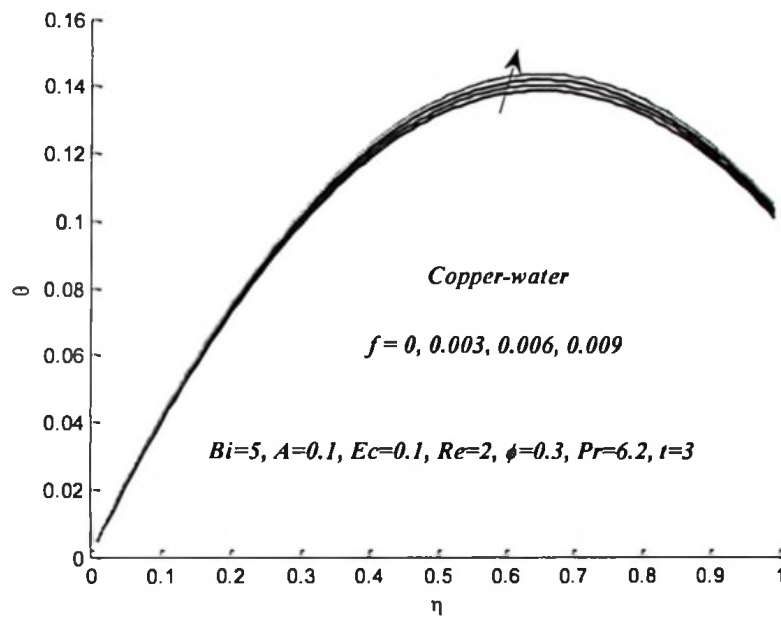


Figure 5.10: Nanofluid temperature profiles with increasing f

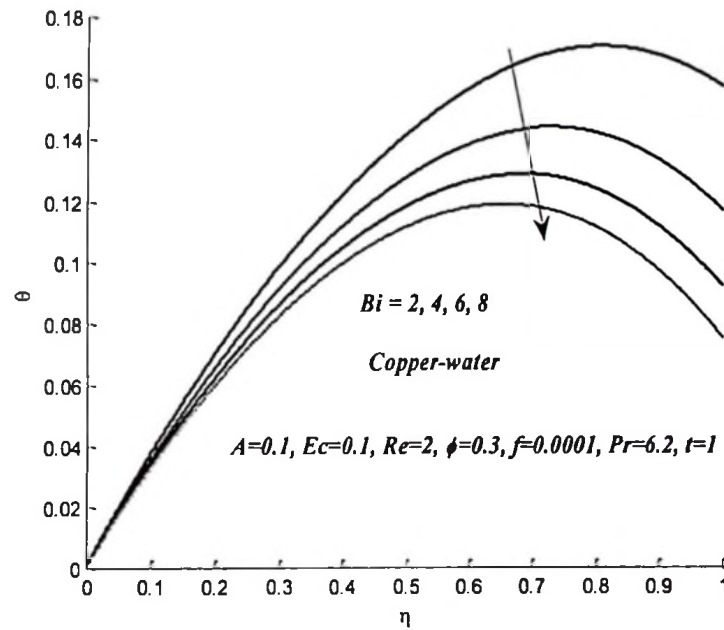


Figure 5.11: Nanofluid temperature profiles with increasing Bi

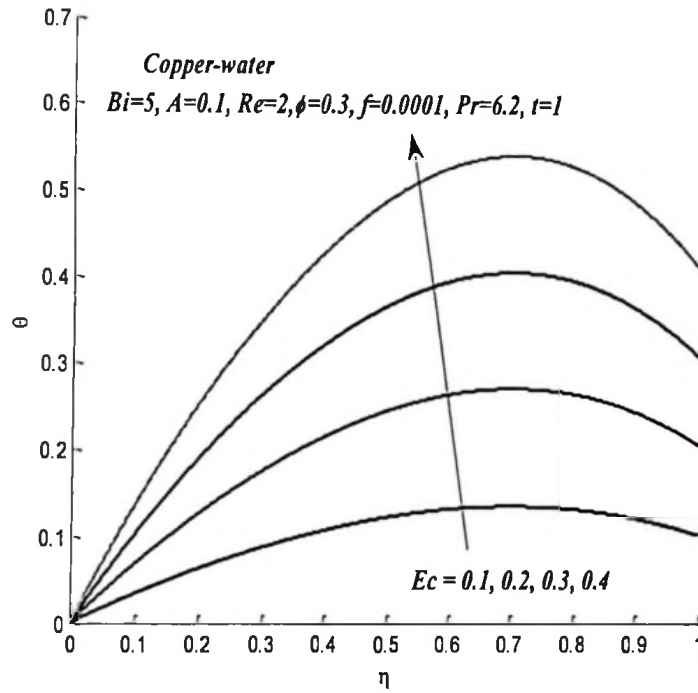


Figure 5.12: Nanofluid temperature profiles with increasing Ec

5.5.3 Skin friction and Nusselt number

Figures 5.13 and Figure 5.14 illustrate the effects of parameter variation on skin friction and Nusselt number using Cu-water as a working nanofluid. In Figure 5.13, the results showed that the skin friction increases with an increase in nanoparticles volume fraction. This is due to movement of the upper wall, injection at the lower wall and suction at the upper wall. The researcher also noted that the skin friction is small at the injection wall and increase toward the suction wall. Moreover interesting result is observed, that the skin friction increases with an increase in Reynolds number and the slight increase is observed when increase in slip parameter but decrease with increase in pressure gradient. Meanwhile, the Nusselt number increases with an increase in nanoparticles volume fraction, Reynolds number and slip parameter but decrease with an increase in pressure gradient as illustrated in Figure 5.14. This may be attributed by Couette flow at the upper wall, injection and suction.

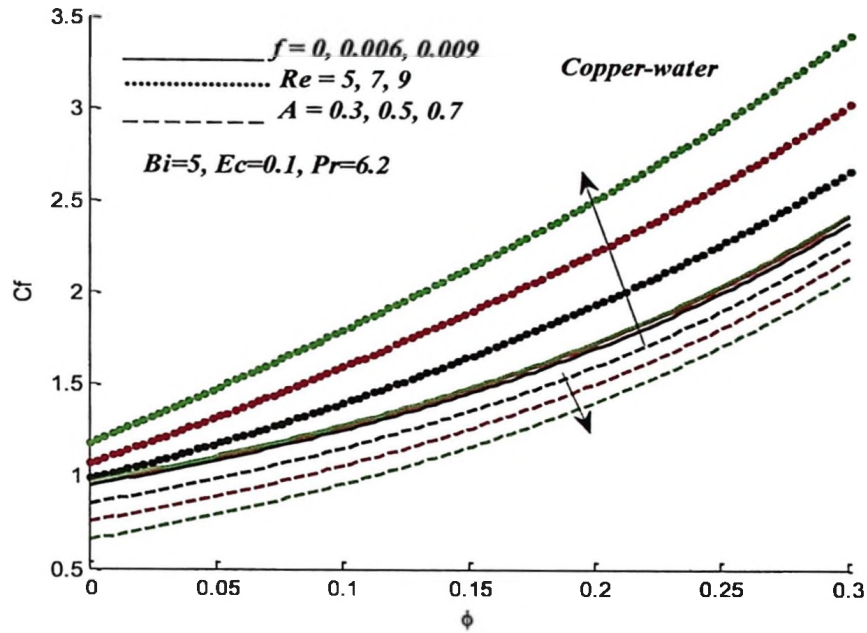


Figure 5.13: Skin friction with increasing ϕ , A , Re and f

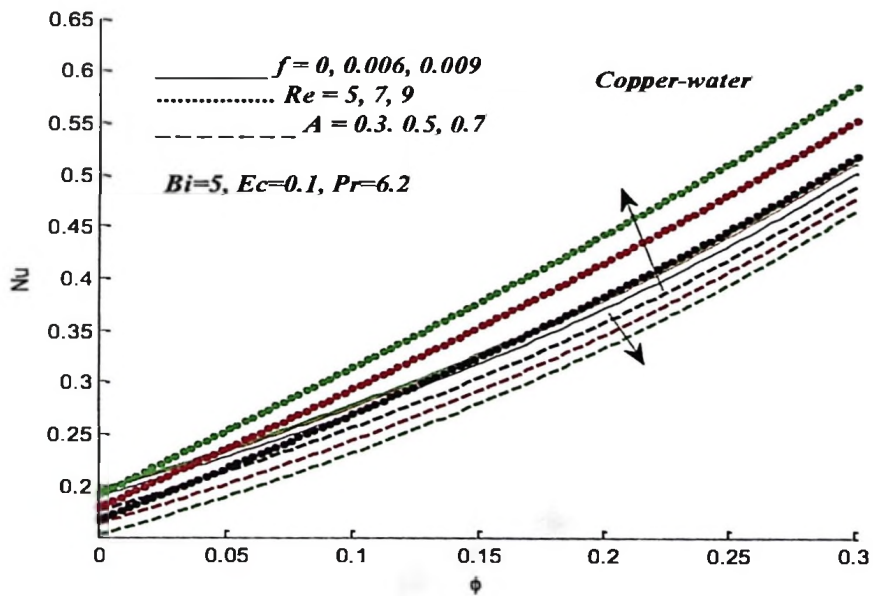


Figure 5.14: Nusselt number with increasing ϕ , A , Re and f

5.5.4 Effects of parameter variation on entropy generation rate

Figure 5.15 shows that the entropy generation rate decreases with time at the lower wall and decrease with time across the upper wall. This behaviour is due to slip and injection at the lower wall, and movement of the upper wall together with suction. The entropy generated by Al_2O_3 -water nanofluid is higher near the lower wall compared with that generated by Cu-water nanofluid and reverse as it approaches the upper wall. A rise in an entropy generation rate is observed at the walls with an increase in nanoparticles volume fraction as illustrated in Figure 5.16. This is due to the fact that temperature gradients at the walls of the channel increase as ϕ increases. Similar observation is noted in Figures 5.17 that, the entropy generation rate rises with increase in slip condition. Furthermore, it is noted in Figure 5.18 that the entropy generation rate decreases at the lower wall with an increase in Biot number and reverse its trend as it approaches the upper wall, this may be attributed by the slip condition at the lower wall and upper moving wall.

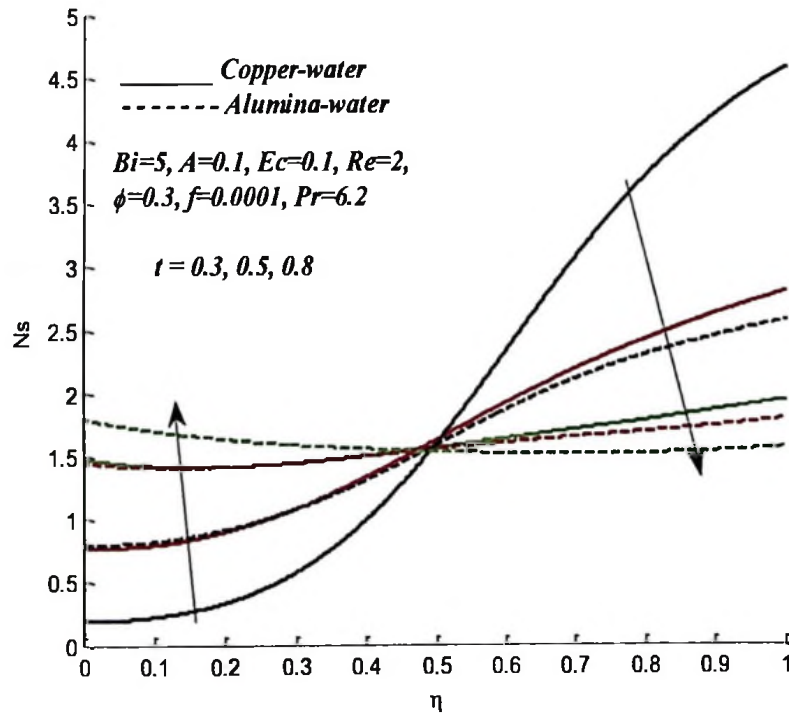


Figure 5.15: Entropy generation rate with increasing time

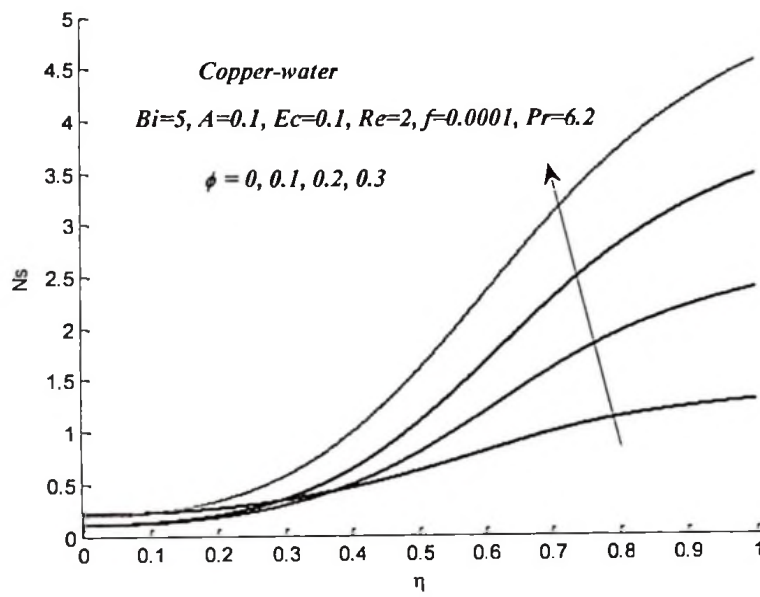


Figure 5.16: Entropy generation rate with increasing ϕ

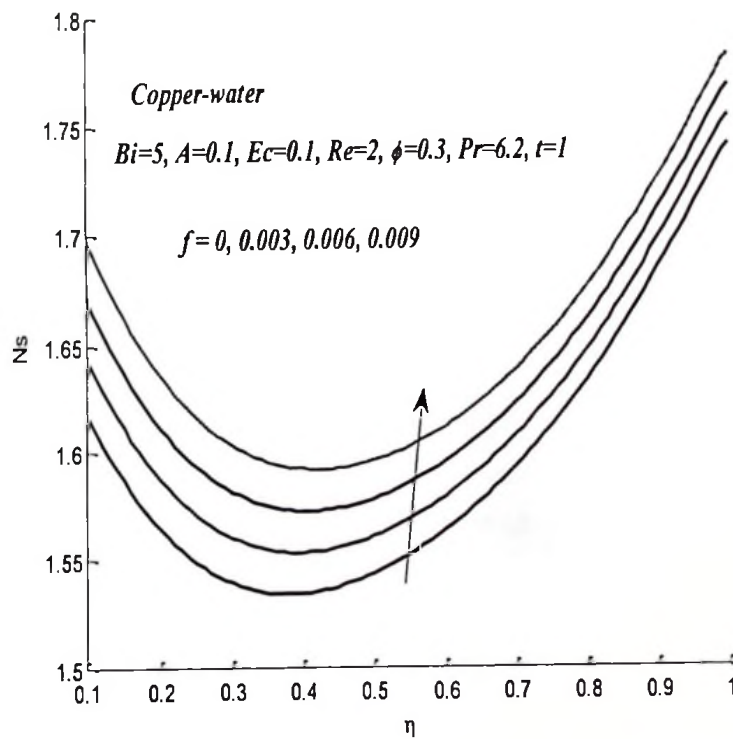


Figure 5.17: Entropy generation rate with increasing f

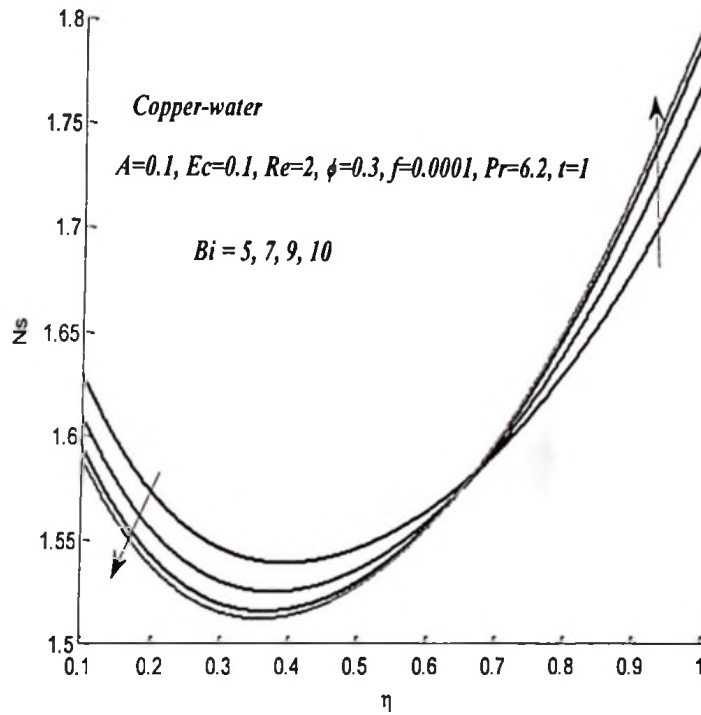


Figure 5.18: Entropy generation rate with increasing Bi

5.5.5 Effects of parameter variation on Bejan number

Figure 5.19 illustrates the transient effect on the Bejan number across the channel. The Bejan number increase with time near the channel lower walls but the slight decreases is noted at the channel centreline. This is because of rise in the dominant effect of fluid friction irreversibility within the channel centreline region, the heat transfer irreversibility at the channel walls, injection, suction, slip condition and the Couette flow. The Bejan number produced by Cu-water nanofluid seems to be higher than that of Al_2O_3 -water nanofluid.

Figure 5.20 shows an increase in the Bejan number at the walls with an increase in nanoparticles volume fraction. This implies that increase in nanoparticles volume fraction causes domination effects of fluid friction irreversibility. Furthermore, the results illustrate in Figure 5.21 that as Biot number increases, the Bejan number decreases at lower wall and at the centreline of the channel, but increases as it approaches the upper wall. Different trend is observed in Figure 5.22 when increasing Eckert number that is Bejan number increases in both walls. Meanwhile, the decrease in Bejan number is observed at the lower wall and centre but increase as it approaches the upper wall with an increase in pressure gradient as

shown in Figure 5.23. Generally, this behaviour may be attributed by slip condition, injection, suction, convective cooling and upper moving wall.

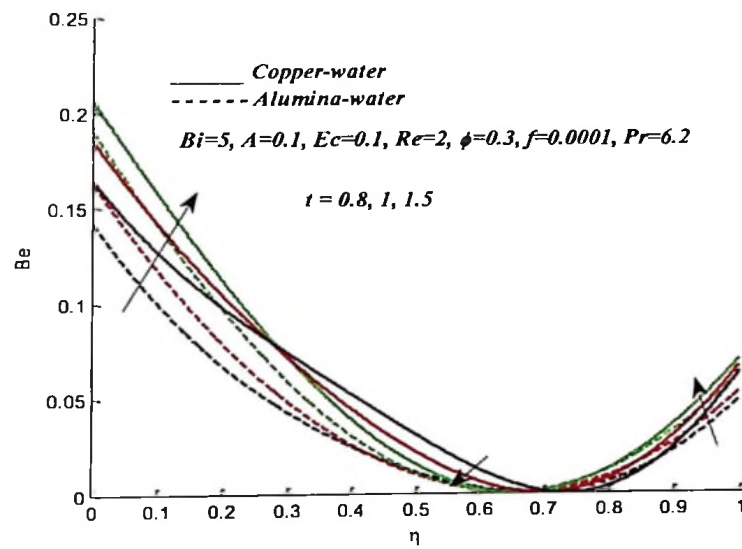


Figure 5.19: Bejan number with increasing time

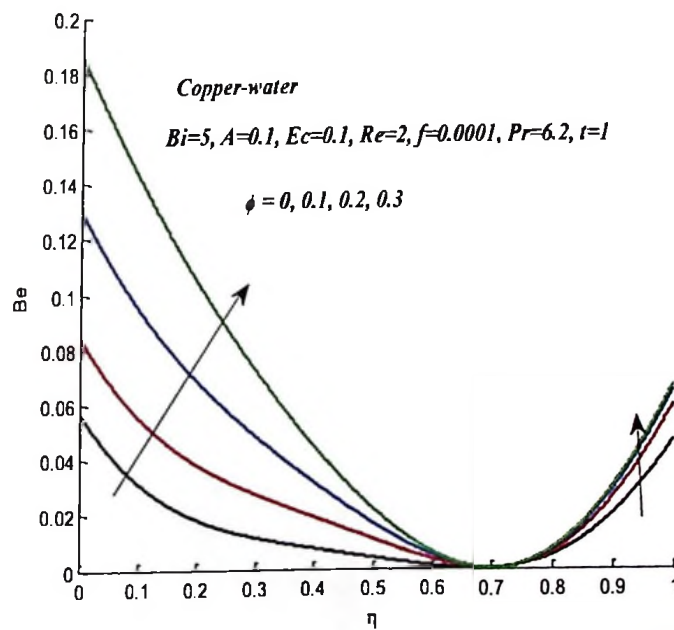


Figure 5.20: Bejan number with increasing ϕ

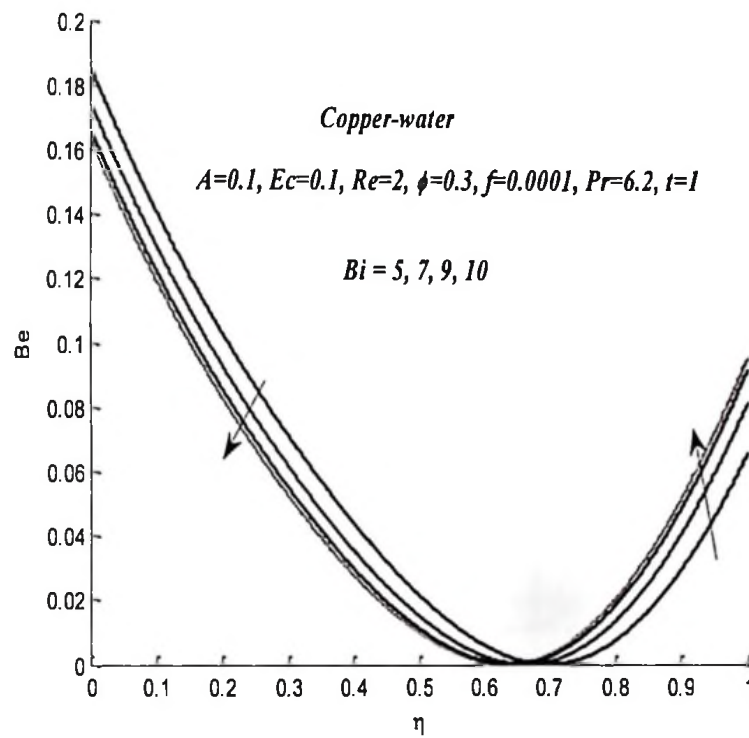


Figure 5.21: Bejan number with increasing Bi

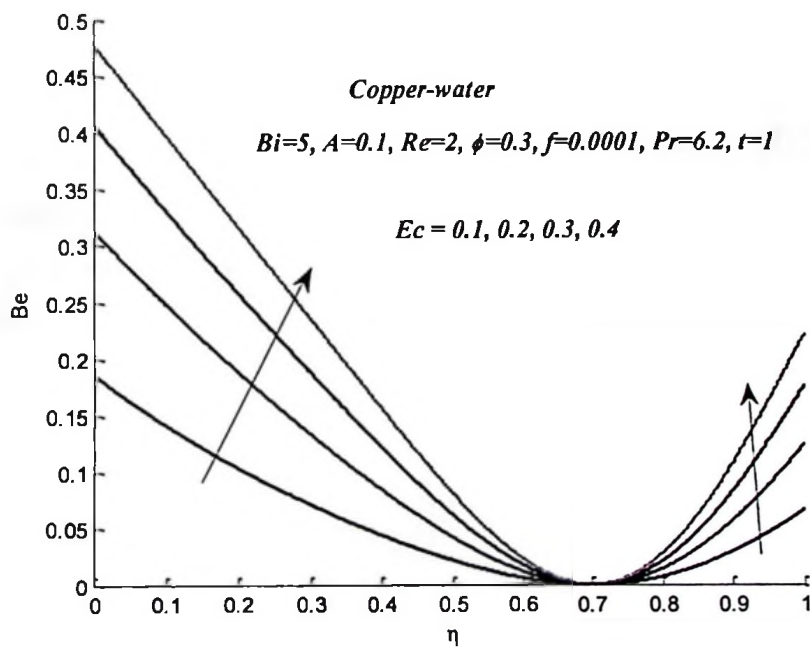


Figure 5.22: Bejan number with increasing Ec

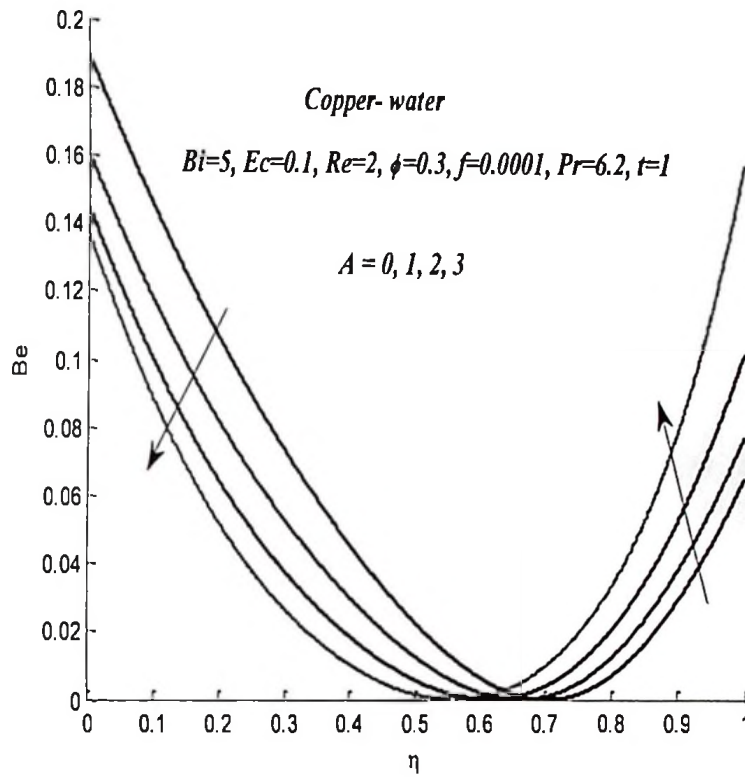


Figure 5.23: Bejan number with increasing A

5.6 Conclusion

Computational model and thermodynamic analysis of the effects of Navier slip and wall permeability on entropy generation in unsteady generalized Couette flow of nanofluids containing Copper (Cu) and Alumina (Al_2O_3) as nanoparticles is presented. Using a semi-discretization method together with Runge-Kutta-Fehlberg integration scheme the transient problem is numerically tackled. Some of the results obtained can be summarized as follows:

- An increase in nanoparticles volume fraction and Reynolds number causes a decrease in the velocity profile. Meanwhile nanofluid velocity profile increases with an increase in pressure gradient.
- The temperature profile increases with an increase in the nanoparticles volume fraction, slip parameter and Eckert number. But a decrease in temperature profile is noticed with an increase in Biot number.
- Skin friction increases with an increase in nanoparticles volume fraction, slip parameter and Reynolds number. But decrease with an increase in pressure gradient. The same results are obtained for the Nusselt number.

- A rise in an entropy generation rate is observed with an increase in nanoparticles volume fraction and slip parameter. It falls near the lower wall and rises near the upper wall with an increase in Biot number.
- The Bejan number increase with time at the lower and upper walls but slight decreases at the channel centreline. It increases at the walls with an increase in nanoparticles volume fraction. As Biot number and pressure gradient increases, Bejan number decreases near the lower wall and at the centre, but increases as it approaches the upper wall. Eckert number causes the increase in Bejan number at the lower and upper walls.

CHAPTER SIX

General Discussion, Conclusion and Recommendations

6.1 General Discussion

In this research flow models have been formulated with the aim of assessing the effects of thermophoresis and Brownian motion on the flow, temperature and concentration of nanofluid, entropy generation, Nusselt number and skin friction. Moreover, the effect of different types of nanoparticles and flow parameters on the flows, buoyancy driven with convective cooling on temperature profile, velocity profile, entropy generation, skin friction and Nusselt number was also assessed. Nanofluid was considered as a single phase flow in low solid concentration because of very small sized solid particles. The next section shows results and general conclusion.

6.2 Conclusion

In chapter two, the flow structure, heat transfer and entropy generation in unsteady channel flow of a variable viscosity water based nanofluids with convective heat exchange with the ambient at the walls are numerically investigated. Using a semi discretization finite difference method together with Runge-Kutta Fehlberg integration scheme, the model nonlinear initial boundary value problem is tackled. Some of the results obtained can be summarized as follows. The nanofluid velocity and temperature profiles increase with an increase in t , β , Ec but decreases with an increase in Bi . The nanoparticles concentration increases along the centreline region and decrease near the walls with an increase in t , β , Ec , Nt . However, an increase in Bi and Nb causes a decrease in nanoparticles concentration along the centreline region and concentration increase near the walls. The skin friction increases with t , β , Ec , Nt and A but decreases with Ec and Nt . The Nusselt number increases with t , Ec , Bi and β . Entropy generation rate generally increases with t , Ec , β , A , Nt . Increase in Bi increase entropy generation at the walls but decreases entropy generation within the channel. Bejan number within the centreline region and at the walls increases with t , Ec , β , A , Nt and λ , consequently, the dominant effects of heat transfer and nanoparticles mass transfer irreversibilities increase.

In chapter three, the combined effect of buoyancy force and convective cooling on the unsteady flow, heat transfer and entropy generation rate in water based nanofluids containing

Copper (Cu) and Alumina (Al_2O_3) as nanoparticles was investigated. The nonlinear governing partial differential equations are solved numerically using a semi discretization finite difference method together with Runge-Kutta Fehlberg integration scheme. The Al_2O_3 -water nanofluid tends to flow faster than Cu-water nanofluid and the velocity profile increases with Ec , Gr , A , but decreases with ϕ . The temperature of Al_2O_3 -water nanofluid rises higher than Cu-water nanofluid and the temperature profile increases with Ec , Gr , A , but decreases with ϕ and Bi . The Cu-water nanofluid produces higher skin friction than Al_2O_3 -water nanofluid and the skin friction increases with Ec , Gr but decreases with ϕ and Bi . The Cu-water nanofluid produces higher Nusselt number than Al_2O_3 -water nanofluid and the Nusselt number increases with Ec , Gr but decreases with ϕ and Bi . The Al_2O_3 -water nanofluid produces higher entropy than Cu-water nanofluid and the skin generation increases with Ec , Gr , A , but decreases with ϕ and Bi . Fluid friction irreversibility dominates the channel centreline region while the effects of heat transfer irreversibility near the walls increases with Gr , Ec , A , but decreases with ϕ and Bi .

In chapter four, the flow structure, heat transfer and entropy generation in unsteady generalized Couette flow of a water-based nanofluid with convective cooling are numerically investigated. The nonlinear governing partial differential equations are solved numerically using a semi discretization finite difference method together with the Runge-Kutta Fehlberg integration scheme. The observed results in this paper can be summarized as follows: The Al_2O_3 -water nanofluid tends to flow faster than Cu-water nanofluid and the velocity profile increases with A but decreases with ϕ and Re . The temperature of Cu-water nanofluid rises higher than Al_2O_3 -water nanofluid and the temperature profile increases with ϕ and Ec but decreases with Bi . Moreover temperature profile increases near the lower wall and decreases as it approaches the upper wall with an increase in A , the opposite situation is observed with an increase in Re Cu-water nanofluid produces higher skin friction than Al_2O_3 -water nanofluid and the skin friction increases with Re and ϕ but decreases with A . Cu-water nanofluid produces higher Nusselt number than Al_2O_3 -water nanofluid and the Nusselt number increases with Re and ϕ but decreases with A . The Al_2O_3 -water nanofluid produces higher entropy generation rate than Cu-water nanofluid near the lower wall, but as it approaches the upper wall, Cu-water nanofluid produces higher entropy generation rate than Al_2O_3 -water nanofluid. The entropy generation increases with ϕ and Ec , it decreases with A . With an increase in Bi the entropy generation rate decreases and reverse its behaviour near

the upper wall. The Bejan number produced by Cu-water nanofluid is greater than Al_2O_3 - water nanofluid. The Bejan number increases with time at the walls but decreases at the centre of the channel. It increases with an increase in ϕ . But as Bi increases, Bejan number decreases near the lower wall and at the centre of the channel, and increases as it approaches the upper wall. An increase in Ec causes the increase in the Bejan number. It is low at the lower wall, high at the centre of the channel and at the upper wall as A increases.

In chapter five, computational model and thermodynamic analysis of the effects of Navier slip and wall permeability on entropy generation in unsteady generalized Couette flow of nanofluids containing Copper (Cu) and Alumina (Al_2O_3) as nanoparticles is presented. Using a semi-discretization method together with Runge-Kutta Fehlberg integration scheme the transient problem is numerically tackled. An increase in nanoparticles volume fraction and Reynolds number causes a decrease in the velocity profile. Meanwhile nanofluid velocity profile increases with an increase in pressure gradient. The temperature profile increases with an increase in the nanoparticles volume fraction, slip parameter and Eckert number. But a decrease in temperature profile is noticed with an increase in Biot number. Skin friction increases with an increase in nanoparticles volume fraction, slip parameter and Reynolds number. But decrease with an increase in pressure gradient. The same results are obtained for the Nusselt number. A rise in an entropy generation rate is observed with an increase in nanoparticles volume fraction and slip parameter. It falls near the lower wall and rises near the upper wall with an increase in Biot number. The Bejan number increase with time at the lower and upper walls but slight decreases at the channel centreline. It increases at the walls with an increase in nanoparticles volume fraction. As Biot number and pressure gradient increases, Bejan number decreases near the lower wall and at the centre, but increases as it approaches the upper wall. Eckert number causes the increase in Bejan number at the lower and upper walls.

Generally, base fluid produce more entropy compared to nanofluid which is very useful as better heat transfer fluid. However, entropy can be reduced by mixture of nanoparticles and base fluid with careful combination of parameters controlling the flow and geometry in consideration. From the graphs we observe that, flow geometry affect the rate of entropy production. For example figures of entropy generation with an increase in Biot number shows, different results. Alumina- water nanofluid produces more entropy compared to Copper- water nanofluid.

Thus, with careful combination of parameter values controlling the flow, the entropy production within the channel flow water base nanofluid in the presence of convective cooling can be minimised.

6.3 Recommendations

In order to minimize or possibly eliminate entropy generation, the study recommends the use of the combination of nanoparticles and base fluids. Although the combination may be expensive compared to just base fluid, but it will be useful and efficient in industries, engineering and medicine, specifically in cooling process, nuclear reactors, transportation, electronics, automotive, as well as biomedicine and food. Moreover, the use of the combination of nanoparticles and base fluid reduces entropy generation in a nanofluid flow as observed in this study, makes the fluid to be much more effective in cooling machines, engines such as automobile engines, welding equipment, high heat flux devices and other.

Bejan number tells us which factor contributes more to entropy production. $Be = 0$ or close to zero means the contribution of fluid friction (viscous dissipation) is the highest (in this case is at the wall, wall lubrication may be applied to reduce friction and entropy production). $Be = 1$ or close to one means the entropy production is dominated by heat transfer (in this case materials for thermal insulation may be used if the system requires heat conservation like hot water geyser, to reduce entropy for efficient operation) .

REFERENCES

- Abu-Nada, E. (2008) 'Application of nanofluids for heat transfer enhancement of separated flow encountered in a backward facing step', *International Journal of Heat Fluid Flow*, 29, 242-249.
- Anoop, K.B., Sundararajan, T., Das, S. K. (2009) 'Effect of particle size on the convective heat transfer in nanofluid in the developing region', *International Journal of Heat and Mass Transfer*, Vol. 52, pp.2189-2195.
- Bejan, A. (1982) 'Second-law analysis in heat transfer and thermal design', *Advance Heat Transfer*, 15, 1–58.
- Bejan, A. (1996) *Entropy Generation Minimization*, CRC, Boca Raton, NY.
- Buongiorno, J. (2006) 'Convective transport in nanofluids', *Journal of Heat Transfer*, vol. 128, pp. 240-250.
- Brinkman, H. C. (1952) 'The viscosity of concentrated suspensions and solutions', *J. Chem. Phys.* 20, 571-581.
- Chinyoka, T and Makinde, D. (2013) 'Numerical Investigation of Entropy Generation in Unsteady MHD Generalized Couette Flow with Variable Electrical Conductivity', *Hindawi Publishing Corporation. The Scientific World Journal*
- Choi, S.U.S. (1995) 'Enhancing thermal conductivity of fluids with nanoparticles', *In: Proc. ASME Int. Mech. Engng. Congress and Exposition, San Franciscos, USA*, ASME, FED 231/MD 66, 99–105.
- Choi, S.U.S., Zhang, Z.G., Yu, W., Lockwood, F.E., Grulke, E.A. (2001) 'Anomalously thermal conductivity enhancement in nanotube suspensions', *Appl. Phys. Lett.*, 79, 2252– 2254.
- Choi, S.U.S. (2009) 'Nanofluids: from vision to reality through research', *Journal of Heat Transfer*, vol. 131, no. 3, pp. 1–9.
- Eegunjobi A.S., Makinde O.D. (2012) 'Effects of Navier slip on entropy generation in a porous channel with suction/injection', *Journal of Thermal Science and Technology*, 7(4), 522 – 535.
- Grosan, T and Pop, I. (2012) 'Fully developed mixed convection in a vertical channel filled by a nanofluid', *Journal of Heat Transfer*, Vol. 134, 082501-1.

- Hwang, K.S., Lee, Ji-H., Jang, S.P. (2007) 'Buoyancy-driven heat transfer of water-Based Al_2O_3 nanofluids in a rectangular cavity', *International Journal of Heat Mass Transfer*, 50, 4003–4010.
- Ibrahim, W and Makinde, O. D. (2013) 'The effect of double stratification on boundary-layer flow and heat transfer of nanofluid over a vertical plate', *Computers & Fluids*, 86, 433–441.
- Ibrahim, W., Shankar, B., Nandeppanavar, M (2012) 'MHD Stagnation Point Flow and Heat Transfer due to Nanofluid towards a Stretching Sheet', *International Journal of Heat and Mass Transfer*, 56, 1-9.
- Jha, B. K and Ajibade, A. O. (2010) 'Transient natural convection flow between vertical parallel plates: one plate isothermally heated and the other thermally insulated', *Journal of Process Mechanical Engineering*, 224(4), 247-252.
- Khalifa A. J. (2001) 'Natural convective heat transfer coefficient – A review II, Surfaces in Two and three dimensional enclosures', *Energy Conversion and Management*, 42, 505-517.
- Khanafer, K., Vafai, K., Lightstone, M. (2003) 'Buoyancy-driven heat transfer enhancement in a two-dimensional enclosure utilizing nanofluids', *International Journal Heat Mass Transfer*, 46, 3639-3653.
- Lee, A., Timchenko, V., Yeoh, G. H., Reizes, J. A. (2012) 'Forced Convection in micro channel with synthetic jet: effect of operating frequency', *ASME, 10th Int. Conf. on Nanochannels, Microchannels, and Minichannels, Rio Grande, Puerto Rico, USA*.
- Mahmoudi, A. H., Shahi, M., Talebi, F. (2012) 'Entropy generation due to natural convection in a partially open cavity with a thin heat source subjected to a nanofluid', *Numer Heat Transfer A*, 61, 283–305.
- Makinde, O. D. (2013) 'Computational modelling of nanofluids flow over a convectively heated unsteady stretching sheet', *Current Nano science*, Vol.9, 673-678.
- Makinde, O. D. (2008) 'Entropy-generation analysis for variable-viscosity channel flow with non-uniform wall temperature', *Applied Energy* 85 (2008) 384–393

- Makinde, O. D and Aziz, A. (2010) 'Second law analysis for a variable viscosity plane Poiseuille flow with asymmetric convective cooling', *Computers and Mathematics with Applications*, 60,3012–3019.
- Makinde, O. D., Chinyoka, T., Eegunjobi, A. (2013) 'Numerical investigation of entropy generation in an unsteady flow through a porous pipe with suction', *International Journal of Exergy*,.
- Makinde, O.D and Eegunjobi, A.S (2013) 'Analysis of inherent irreversibility in a variable viscosity MHD generalized couette flow with permeable walls', *Journal of Thermal Science and Technology*, Vol. 8, No. 1.
- Makinde, O.D., Khan, W.A., Aziz, A. (2013) 'On inherent irreversibility in Sakiadis flow of nanofluids', *International Journal of Exergy*, 13(2), 159-174
- Makinde, O. D., Khan, W. A., Khan, Z. H. (2013) 'Buoyancy effects on MHD stagnation point flow and heat transfer of a nanofluid past a convectively heated stretching/shrinking sheet', *International Journal of Heat and Mass Transfer*, 62, 526-533.
- Makinde, O.D and Osalusi, E. (2006) 'MHD Steady Flow in a Channel with Slip at the Permeable Boundaries' *Rom. Journ. Phys.*, Volume 51, Nos. 3–4, p. 319–328
- Makinde, O.D and Theuri, D. (2014) 'Thermodynamic analysis of variable viscosity MHD unsteady generalized Couette flow with permeable walls', *Applied and Computational Mathematics*, 3(1), 1-8
- Maxwell, J. C. (1904) 'A treatise on electricity and magnetism', 2nd ed. Cambridge: *Oxford University Press*, 435–41.
- Mkwizu, M.H and Makinde, O.D. (2015) 'Entropy generation in a variable viscosity channel flow of nanofluids with convective cooling', *Comptes Rendus Mecanique* 343 38-56.
- Mutuku-Njane, W. N and Makinde, O. D. (2014) 'MHD nanofluid flow over a permeable vertical plate with convective heating', *Journal of Computational and Theoretical Nanoscience*, 11(3), 667-675.
- Na, T.Y. (1979) '*Computational methods in engineering boundary value problems*, Academic press, New York.

- Narusawa, U. (1998) 'The second-law analysis of mixed convection in rectangular ducts', *Heat Mass Transfer*, 37, 197–203.
- Nasrin, R., Alim, M.A., Chamkha, J. (2012) 'Buoyancy- Driven Heat Transfer of Water Al_2O_3 Nanofluid in a Closed Chamber: Effect of Solid Volume Fraction, Prandtl Number and Aspect Ratio', *International Journal of Heat and Mass Transfer*, 55, 7355-7365.
- Natarajan E., Basak T., Roy S. (2008) 'Natural convection flows in a trapezoidal enclosure with uniform and non-uniform heating of bottom wall', *International Journal of Heat Mass Transfer*; 51:747–56.
- Nield, D. A and Kuznetsov, A.V. (2009) 'The Cheng–Minkowycz problem for natural convective boundary-layer flow in a porous medium saturated by a nanofluid', *International Journal of Heat Mass Transf.*, 52, 5792–5795.
- Oztop, H.F and Abu-Nada, E. (2008) 'Numerical study of natural convection in partially heated rectangular enclosures filled with nanofluids', *Internal Journal Heat Fluid Flow*, 29, 1326–1336.
- Ostrach, S. (1972) 'Natural convection in enclosures', *Advances in Heat Transfer*, 8, 161-227.
- Ramakrishnan, K and Shailendhra, K. (2013) 'Hydromagnetic Blood Flow through a Uniform Channel with Permeable Walls Covered by Porous Media of Finite', *Journal of Applied Fluid Mechanics*, Vol. 6, No. 1, pp. 39-47.
- Routbort, J.L., Wu, Y., France, D.M, Singh, D., Timofeeva, E.V. and Smith, D.S.:Argonne (2009) National Lab, Michellin North America, St. Gobain Corp., <http://www1.eere.energy.gov/industry/nanomanufacturing/pdfs/nanofluids>
- Sahin, A. Z. (1998) 'Second law analysis of laminar viscous flow through a duct subjected to constant wall temperature', *Journal of Heat Transfer*, 120, 76–83.
- Shahi, M., Mahmoudi, A. H., Honarbakhsh, R. A. (2011) 'Entropy generation due to natural convection cooling of a nanofluid', *International Communication Heat Mass Transfer*, 38, 972–83.

- Tiwari, R. K and Das, M. K. (2007) 'Heat transfer augmentation in a two-sided lid-driven differentially heated square cavity utilizing nanofluids', *International Journal Heat Mass Transfer.*, 50, 2002–2018.
- Wang, X. Q and Mujumdar, A. S. (2007) 'Heat transfer characteristics of nanofluids': a review, *International Journal Thermal Sciences*, vol. 46, pp. 1-19.
- Woods, L. C. (1975) 'Thermodynamics of Fluid Systems', *Oxford University Press, Oxford*.
- Yang, M. H., Yeh, R. H., Hwang, J. J. (2012) 'Forced convection in a channel with transverse fins', *International Journal of Num. Methods for Heat & Fluid Flow*, 22, 3, 306 – 322.
- Yazdi, M et al., (2011). *Entropy Generation Analysis of Open Parallel Microchannel Embedded Within a Permeable Continuous Moving Surface: Application to Magnetohydrodynamics (MHD)*. *Entropy* 14, 1-23; doi: 10.3390/e 14010001.
- Zhen-Hua Lui, Yuan- Yang Li., (2012). 'A New Frontier of nanofluid Research- Application of Nanofluid in Heat Pipes', *International Journal of Heat and Mass Transfer*, 55, 6786-6797.

APPENDIX

Matlab Codes

```
%close all
clear all
clc
%c=['k','g','r'];
tspan = 0:0.001:10; %time interval with observations at every integer
delta_eta=0.01;
n=1/delta_eta-1;
eta=delta_eta:delta_eta:1-delta_eta;
%eta=0:delta_eta:1;
s0 = [zeros(1,n),zeros(1,n)]; %initial values for x,y,z,m
Pr = 6.2; %model parameter 0.4
%a=0;
%c=['k','r','h','g'];
phi=0.3; %model parameter 0.01
f=1;
% if (phi==0)
%     a=0;
% end
% f1=linspace(1,2,3);
% for i=1:length(f1);
%     f=f1(i);

% var1=[0 0.1 0.2 0.3];
% for j=1:4
%     f=var1(j);
Re=2;
Ec=0.1; %model parameter 0.1
A=1;%the pressure gradient parameter
%d=2;
ro2=997.1;%density of water
K2=0.613;%thermal conductivity of water
cp2=4176; %specifis heat of water
%for d=[1,2,3]
% if(d==1)
%     %phi=0.1;

Br=Pr*Ec;
%
% var=linspace(0,0.3);
% for i=1:length(var)
%     phi=var(i);
%     Br=Pr*Ec;
%     ro1=3970; %alu
%     K1=40; %alu
%     cp1=765; %specific of alu
%     t1=(ro1*cp1)*(ro2*cp2)^(-1);
%     m=((K1+2*K2)+phi*(K2-K1))*((K1+2*K2)-2*phi*(K2-K1))^(-1);
% elseif(d==2)
%     phi=0.1;
%     K1=401;%thermal conductivity of solid
%     ro1=8933;%density of solid cu
%     cp1=385;%specific of cu
%     t1=(ro1*cp1)*(ro2*cp2)^(-1);
%     m=((K1+2*K2)+phi*(K2-K1))*((K1+2*K2)-2*phi*(K2-K1))^(-1);
% else
```

```

% phi=0;
% K1=401;%thermal conductivity of solid
% ro1=8933;%density of solid cu
% cpl=385;%specific of cu
% t1=(ro1*cpl)*(ro2*cp2)^(-1);
% m=((K1+2*K2)+phi*(K2-K1))*((K1+2*K2)-2*phi*(K2-K1))^(-1);
% end
%ro1=8933;
%K1=400;
%t1=0;%volumetric entropy generation rate
Bi=5;%Biot number
[t,s] =
ode15s(@ode_sys5,tspan,s0,[],delta_eta,Pr,Ec,Re,A,t1,ro1,ro2,phi,K1,K2,Bi,n
,m,f);
w1=s(:,1:n);
thetal=s(:,n+1:2*n);
eta=[0 eta 1];

%ENTROPY AND BEJAN
w1=[w1(:,1) w1 [0;ones(length(w1(:,end))-1,1)]];
thetal=[thetal(1:end,1) thetal thetal(:,end)*(1-Bi*m*delta_eta)];

Ns=zeros(length(t),length(eta));
kk=length(t);
for jj=1:kk

    for ii=2:n+1
%Ns(jj,ii)=(1/m*(thetal(jj,ii+1)-thetal(jj,ii-1))^2+(Br/(1-
phi)^2.5)*(w1(jj,ii+1)-w1(jj,ii-1))^2)/(4*delta_eta^2);
% %
Be(jj,ii)=((1/m*(thetal(jj,ii+1)thetal(jj,ii-1))^2)/(4*delta_eta^2))*((1/m*(
thetal(jj,ii+1)-thetal(jj,ii-1))^2+(Br/(1-phi)^2.5)*(w1(jj,ii+1)-w1(jj,ii
1))^2)/(4*delta_eta^2))^(-1);
% %
    end
%
    Ns(jj,1)=(1/m*(thetal(jj,2)-thetal(jj,1))^2+(Br/(1-
phi)^2.5)*(w1(jj,2)-w1(jj,1))^2)/(delta_eta^2);
%
    Ns(jj,n+2)=(1/m*(thetal(jj,n+2)-thetal(jj,n+1))^2+(Br/(1-
phi)^2.5)*(w1(jj,n+2)-w1(jj,n+1))^2)/(delta_eta^2);
%
    Be(jj,1)=((1/m*(thetal(jj,2)thetal(jj,1))^2)/(delta_eta^2))*((1/m*(thetal(j
j,2)thetal(jj,1))^2+(Br/(1-phi)^2.5)*(w1(jj,2)-w1(jj,1))^2)/(delta_eta^2))^(-
1);
    Be(jj,n+2)=((1/m*(thetal(jj,n+2)-
thetal(jj,n+1))^2)/(delta_eta^2))*((1/m*(thetal(jj,n+2)-
thetal(jj,n+1))^2+(Br/(1-phi)^2.5)*(w1(jj,n+2)-
w1(jj,n+1))^2)/(delta_eta^2))^(-1);
    end
%
%plot(eta,Ns(1000,:), 'k', 'LineWidth',2)
plot(eta,Be(800,:), 'g', 'LineWidth',2)
%end
%plot([eta,1],[Be(3000,:),0],c(:,i), 'LineWidth',2)
hold on
% plot([eta,1],[Ns(800,:),1], 'g', 'LineWidth',2)
% plot([eta,1],[Ns(1000,:),1], 'b', 'LineWidth',2)
% plot([eta,1],[Ns(2000,:),1], 'r', 'LineWidth',2)
% hold on
end
ylabel('Be')
xlabel('\eta')

```



```

%xlim([0 0.9])
%ylim([1.5 1.8])

%SKIN AND NUSL
%nu(i)=-1/m*((thetal(end,end)/(delta_eta*(1-m*Bi*delta_eta)))-
thetal(end,end)/delta_eta);
%nu(i)=Bi*thetal(end,end);
%sk(i)=((1-phi)^(-2.5))*(1-wl(end,end))*(delta_eta)^(-1);
%end
%plot(var,nu,'k','LineWidth',2)
%hold on
%plot(var,sk,'k','LineWidth',2)
%plot(var,sk,'ro-','LineWidth',1)
%ylabel('Nu')
%xlabel('\phi')
%ylim([100 200])
%xlim([0 0.3])
%end
%ylim([0.8 0.9])
%[ETA T]=meshgrid(eta,t);
%%%%%%%%%%%%%%%%%%%%%%%%%%%%%%%%%%%%%%%%%%%%%%%%%%%%%%%%%%%%%%%%%%%%%%%%
% surf(T,ETA,wl);colorbar;shading flat, caxis([0, 1]);
% xlabel('Time ( t )', 'FontSize', 10,'LineWidth',2);
% ylabel('Distance ( \eta )','FontSize', 10,'LineWidth',2);
% zlabel('Velocity ( w )','FontSize', 10,'LineWidth',2);
% figure
% surf(T,ETA,thetal);colorbar;shading flat, caxis([0, 1]);
% xlabel('Time ( t )', 'FontSize', 10,'LineWidth',2);
% ylabel('Distance ( \eta )','FontSize', 10,'LineWidth',2);
% zlabel('Temperature ( \theta )','FontSize', 10,'LineWidth',2);
% figure
% surf(T,ETA,H1);colorbar;shading flat, caxis([0, 1]);
% xlabel('Time ( t )', 'FontSize', 10,'LineWidth',2);
% ylabel('Distance ( \eta )','FontSize', 10,'LineWidth',2);
% zlabel('Nanoparticles volume fraction distribution( H )','FontSize',
10,'LineWidth',2);
%figure

%%%%%%%%%%%%%%%%%%%%%%%%%%%%%%%%%%%%%%%%%%%%%%%%%%%%%%%%%%%%%%%%%%%%%%%%
% plot(t,wl(:,0.5*(n+1)),'k--','LineWidth',2)
% hold on
% plot(t,wl(:,0.6*(n+1)),'r--','LineWidth',2)
% plot(t,wl(:,0.7*(n+1)),'b--','LineWidth',2)
% plot(t,wl(:,0.8*(n+1)),'g--','LineWidth',2)
% %title('Solution Curves for the Model')
% ylabel('w')
% xlabel('t')
%ylim([0 1.2])
% figure
% plot(t,thetal(:,0.5*(n+1)),'k--','LineWidth',2)
% hold on
% plot(t,thetal(:,0.6*(n+1)),'r--','LineWidth',2)
% plot(t,thetal(:,0.7*(n+1)),'b--','LineWidth',2)
% plot(t,thetal(:,0.8*(n+1)),'g--','LineWidth',2)
% %title('Solution Curves for the Model')
% ylabel('\theta')
% xlabel('t')
%ylim([0 0.3])
% figure
% plot(t,H1(:,0.1*(n+1)),'LineWidth',1)
% hold

```

```

% plot(t,H1(:,0.3*(n+1)),'LineWidth',1)
% plot(t,H1(:,0.6*(n+1)),'LineWidth',1)
% plot(t,H1(:,0.9*(n+1)),'LineWidth',1)
%title('Solution Curves for the Model')
%ylabel('Nanoparticles volume fraction distribution ( H )')
%xlabel('Time ( t )')
%figure
%%%%%%%%%%%%%%%%%%%%%%%%%%%%%%%%%%%%%%%%%%%%%%%%%%%%%%%%%%%%%%%%%%%%%%%%%%

% plot([eta],[w1(100,:)],'k--','LineWidth',2)
% hold on
% plot([eta],[w1(300,:)],'r--','LineWidth',2)
% plot([eta],[w1(500,:)],'b--','LineWidth',2)
% plot([eta],[w1(800,:)],'g--','LineWidth',2)
% %title('Solution Curves for the Model')
% ylabel('w')
% xlabel('\eta')
%ylim([0 0.2])
%xlim([0 2])
% figure
% plot([eta],[thetal(100,:)],'k','LineWidth',2)
% hold on
% plot([eta],[thetal(300,:)],'g','LineWidth',2)
% plot([eta],[thetal(500,:)],'b','LineWidth',2)
% plot([eta],[thetal(800,:)],'r','LineWidth',2)
% %title('Solution Curves for the Model')
% ylabel('\theta')
% xlabel('\eta')
% figure
% plot([eta],[H1(10,:)],'LineWidth',1)
% pause
% hold
% plot([eta],[H1(30,:)],'LineWidth',1)
% pause
% plot([eta],[H1(60,:)],'LineWidth',1)
% pause
% plot([eta],[H1(90,:)],'r','LineWidth',1)
% %title('Solution Curves for the Model')
% ylabel('Nanoparticles volume fraction distribution ( H )')
% xlabel('Distance ( \eta )')
% title('Solution Curves for the Model')

% plot([eta],[w1(1000,:)],c(:,j),'LineWidth',2)
% plot([eta],[thetal(1000,:)],c(:,j),'LineWidth',2)
% hold on
% end
% ylim([0 4])
% xlim([0 1])
% title('Solution Curves for the Model')
% ylabel('\theta')
% xlabel('\eta')
% xlim([0 0.995])
% legend ('Alumina','Copper','Water only')

```

SPE
QC 318
• E57
M4